

The Palomar/MSU Nearby Star Spectroscopic Survey III: Chromospheric Activity, M-dwarf Ages and the Local Star Formation History ¹

John E. Gizis

Department of Physics & Astronomy, University of Delaware

`gizis@udel.edu`

I. Neill Reid

Space Telescope Science Institute, 3700 San Marin Drive, Baltimore, MD 21218

and

*Department of Physics and Astronomy, University of Pennsylvania, 209 South 33rd Street,
Philadelphia PA 19104-6396*

`inr@stsci.edu`

Suzanne L. Hawley

Department of Astronomy, Box 351580, University of Washington, Seattle, WA 98195-1580

`slh@astro.washington.edu`

ABSTRACT

We present high-resolution echelle spectroscopy of 676 nearby M dwarfs. Our measurements include radial velocities, equivalent widths of important chromospheric emission lines, and rotational velocities for rapidly rotating stars. We identify several distinct groups by their H α properties, and investigate variations in chromospheric activity amongst early (M0-M2.5) and mid (M3-M6) dwarfs. Using a volume-limited sample together with a relationship between age and chromospheric activity, we show that the rate of star formation in the immediate Solar Neighbourhood has been relatively constant over the last 4 Gyr. In particular our results are inconsistent with recent large bursts of star formation. We use the correlation between H α activity and age as a function of colour to set constraints on the properties of L and T dwarf secondary components in binary systems. We also identify a number of interesting stars, including rapid rotators, radial velocity variables, and spectroscopic binaries.

Subject headings: Solar neighborhood — stars: low mass, brown dwarfs — stars: chromospheres — Galaxy: star formation history

¹Observations were made at the 60-inch telescope at Palomar Mountain which is jointly owned by the California Institute of Technology and the Carnegie Institution of Washington

1. Introduction

M dwarfs are the dominant stellar component of the Galaxy by both number and mass. With main sequence lifetimes much longer than the age of the universe, they are a fair tracer of the overall properties of the Galactic disk. Their chromospheric activity decays on timescales of billions of years, providing an age indicator that is relevant for studies of Galactic evolution. By relating the activity levels in M dwarfs to age, we can measure the local star formation history. The latter parameter is one of the major requirements in modelling the local substellar mass function (Reid et al. 1999). Moreover, M dwarf components in multiple systems provide constraints on the age of the system. Finally, an extensive sample of young, low-luminosity stars in the field can furnish a prime hunting ground for imaging surveys designed to find young, luminous brown dwarf and giant planet companions.

As with other low luminosity objects, detailed observations are only possible for M dwarfs in the immediate Solar Neighbourhood. The most extensive source for such objects remains the preliminary version of the third Nearby Star Catalogue (Gliese & Jahreiß 1991, hereafter pCNS3). Papers I (Reid, Hawley & Gizis 1995) and II (Hawley, Gizis & Reid 1996) in this series describe our moderate resolution ($\sim 3\text{\AA}$), red ($6200 - 7500\text{\AA}$) spectroscopic observations of candidate M dwarfs in the pCNS3. We have used those spectra, together with data from the literature, to estimate distances and spectral types. In Paper I we defined a volume-limited sample of northern ($\delta > -30^\circ$) stars, and investigated the luminosity function and kinematics of low-mass stars in the Galactic disk. Paper II presented data for the southern stars and investigated various aspects of the chromospheric behaviour of the whole sample using the $H\alpha$ line as a diagnostic.² In this paper, we present echelle observations of M dwarfs from the volume-limited sample defined in Paper I.

Our echelle spectra are of high ($\sim .2\text{\AA}$) resolution and cover the wavelength range $\lambda\lambda 4800 - 9400\text{\AA}$ for all stars, with data extending to 3700\AA for a subset of the brighter stars. These observations encompass chromospheric emission lines due to hydrogen, helium, and ionised calcium. Previous surveys of activity in M dwarfs have generally concentrated on earlier spectral types ($\leq M4$), as in the $H\alpha$ surveys of 202 stars by Stauffer & Hartmann (1986), or have been limited to relatively small samples, such as the 24 late-type M dwarfs observed by Giampapa & Liebert (1986). The only published analysis based on a volume-limited sample is the recent work by Delfosse et al. (1998, 1999a), who present observations of field M dwarfs within eight parsecs. Their spectroscopy has higher resolution than our data, but their sample includes only 118 stars. Our survey therefore provides a more detailed study than heretofore possible of the distribution of chromospheric activity amongst late-type dwarfs, and, combined with an age-activity relation calibrated by M dwarfs in open clusters, the first opportunity to use those stars to probe the Galactic disk star formation history.

²In both these papers, the tables were printed incorrectly. Combined tables are available in electronic form at the ADC and CDS as Hawley et al. (1997).

The following section presents the basic analysis of our spectroscopic data, including radial velocity and rotational velocity measurements and line strength determinations. Since we have multiple observations of many stars, we have used our data to search for velocity variations, and Section 3 identifies several previously-unrecognised binary systems. Chromospheric activity is discussed in Section 4, where we investigate the H α properties of the sample, describe an age-activity relation calibrated with open cluster observations, and use that relation to probe the recent star formation history of the Galactic disk. Section 5 summarises our main conclusions.

2. Observations

2.1. The sample

Our primary sample consists of the volume-complete sample of 499 single M dwarfs and M dwarf primaries defined in Paper I. We refer to this as the VC sample. The stars have absolute magnitudes in the range $8 \leq M_V \leq 16$, declinations north of -30° and distances within completeness limits ranging from 22 parsecs at $M_V = 8.5 \pm 0.5$ to 5 parsecs at $M_V = 15.5 \pm 0.5$. The latter values were derived based on photometric and trigonometric data available in late 1995, coupled with the $(M_V, \text{TiO5})$ relation derived in paper I. Since then, Hipparcos-based trigonometric parallaxes Perryman et al. (1997), accurate to ~ 1 milliarcsecond, have become available for approximately two-thirds of those systems. As will be discussed in Paper IV of this series (Reid *et al.*, in preparation), the addition of the new astrometric data affects the inclusion/omission of only $\sim 15\%$ of the stars in the Paper I sample. While the new distance determinations should be taken into account in analysis of the kinematics of the local stars (Paper IV) they are of little importance for the analysis of chromospheric activity and age that is undertaken in this paper. Thus, we retain the VC sample as our reference here.

2.2. Echelle spectroscopy

Our data were obtained with the echelle spectrograph (McCarthy 1985) on the Palomar 60-inch telescope, which has a 2-pixel resolution of 19,000. Observations between May 1994 and February 1995 used the original quartz 60° cross-dispersing prisms, giving wavelength coverage from 3700Å to 9500Å. Beyond 7000Å there are gaps in wavelength coverage where the orders extend off the CCD. Because our targets are all red stars, very few counts were obtained in the blue ($\lambda < 4800\text{\AA}$) except for the very brightest stars. The result was that the useful part of the spectrum was squeezed into the lower quarter of the CCD, leading to partial overlap between the reddest adjacent orders. To solve this problem, beginning in June 1995, a new set of cross-dispersing prisms (with SF3 glass and a 42° apex) was used. This setup gives wavelength coverage from 4800 to 9500Å and has complete order separation, although the gaps in wavelength coverage remain. For both setups, the exposure time was 600 seconds per star, except for the faintest ($V > 13$) stars for which the exposure times

were increased to as much as 1800 seconds.

Data were extracted using the FIGARO echelle software (Tomaney & McCarthy, private communication). Wavelength calibration was determined from a 300-second exposure of a Th-Ar lamp taken at the beginning of each night. After each observation of a target star, a short (45 second) exposure of the arc lamp was taken at the same telescope position in order to remove instrumental flexure. The spectra were not flux calibrated.

2.3. Radial Velocities

Radial velocities were determined by cross-correlation against reference M dwarfs from Marcy & Benitz (1989 - MB89). The latter velocities are accurate to better than 0.23 kms^{-1} , a factor of five higher than the accuracy of our own observations (as discussed further below). For the bright, early M dwarfs ($\text{TiO5} > 0.5$) we used the standard echelle FIGARO cross-correlation program. Each order was correlated with the velocity standards, and the average radial velocity from all the orders was determined. The arc lamp exposures, taken adjacent to each program star observation, were also cross-correlated, providing a correction for flexure.

This procedure did not provide reliable velocities for faint, late-type M dwarfs. The lower signal-to-noise at blue wavelengths led to a higher potential for bias from the effects of telluric absorption and night sky lines. We were able to obtain reasonable results for those stars by individually computing the cross-correlation for each order and combining those measurements to find the median radial velocity. This procedure was used for all stars with $\text{TiO5} \leq 0.5$. Figure 1 plots the rms dispersion about the mean radial velocity for all M dwarfs with at least four measurements. The distribution suggests a typical internal accuracy of $\lesssim 1.5 \text{ kms}^{-1}$.

We can determine our external errors by comparison with previous high accuracy velocity studies of M dwarfs. The results are shown in Table 1, where σ_{ref} is the formal uncertainty of the reference sample. We note that a comparison between Tokovinin (1988, 1992) and MB89 (13 stars) gives an rms of only 0.46 kms^{-1} but a mean difference of 0.78 kms^{-1} , consistent with the offset derived from our observations, which are tied to the MB89 system. Similarly, Stauffer & Hartmann (1986) adopt a velocity of 14.1 kms^{-1} for the velocity standard G1 526, while MB89 measure a velocity of 15.7 kms^{-1} for this star. Again, the offset is consistent with our measurement. Finally, we list two comparisons with the recent observations by Delfosse *et al.* (1998) since the dominant contribution to the residuals comes from three stars: G1 206 ($V_{Del} = 8.0 \text{ kms}^{-1}$; $\Delta = V_{P60} - V_{Del} = 9.2 \text{ kms}^{-1}$), G165-008 (8.0 ; $\Delta = -15.5$) and G1 268.3B (-6.0 ; $\Delta = -8.4$). All three stars are known binaries, while G165-008 is also a very rapid rotator (see further below). In general, the comparison indicates that the velocities derived from our echelle spectra are accurate to $\sigma < 1.5 \text{ kms}^{-1}$.

We can also examine the quality of the radial velocities found from our previous moderate resolution spectra. Based on an external comparison with the MB89 standards, we estimated an accuracy of $\sim 15 \text{ kms}^{-1}$ (Paper I). After excluding double-lined spectroscopic binaries, velocity

standards, and three stars with anomalously large residuals, we have 582 stars in common. The standard deviation is 17 kms^{-1} , confirming our previous estimate.

The individual velocities and heliocentric Julian data for each observation, together with the mean value and the rms dispersion based on our observations, are given in Table 2. In addition to the star name, we list the ‘NN’ number cited in Papers I and II. While the latter is merely the rank order in pCNS3, and is not an officially recognised designation, it provides a straightforward means of cross-referencing results between tables for this relatively large dataset. We also include measurements of three M dwarfs which are not included in either the pCNS3 or Papers I and II, but which are discussed in Gizis & Reid (1997). Both the primary G 134-035 and the secondary LP 197-12 were on the slit, so the reported measurement is for a blend of the two stars. G 173-018 is a short-period, double-lined dMe system.³

2.4. Line Strengths

To investigate chromospheric activity, we measured the equivalent widths of atomic features using an automated program that counted the flux in rectangular passbands. The adopted line (from F1 to F2) and pseudo-continuum (PC1 to PC2 and PC3 to PC4) regions are given in Angstroms in Table 3, and the average values observed for each star are given in Table 4. The appearance of the emission lines in a strong dMe star are illustrated in Figure 2. For those sufficiently bright stars observed with the old echelle prisms, the bluer Balmer emission lines were also measured. The NaD lines were not measured due to contamination by sky emission and the difficulty in defining a pseudo-continuum. The measurements of the He 6678 line were difficult due to the weakness of the feature and the nearby TiO absorption band. We found that none of the stars had detectable lithium absorption, as expected for M dwarf stars with ages exceeding ~ 50 Myrs.

Figure 3 compares the $H\alpha$ equivalent width measured from the echelle observations with the lower resolution measurements from Paper I. For the early M dwarfs, the higher resolution observations are systematically smaller by $\sim 0.5\text{\AA}$, probably reflecting differences in the placement of the pseudo-continuum. The large scatter for the cooler dwarfs is due to the variability of these stars’s chromospheres.

For most purposes, it is more useful to compare line fluxes rather than equivalent widths. Absolute calibration is not available for all of the stars in our sample, but the continuum flux near $H\alpha$ can be derived from broadband R_C photometry (Reid, Hawley & Mateo 1995). To improve the calibration, and extend it to $H\beta$, we obtained low resolution spectrophotometry of a subset of 105 stars using the McCarthy spectrograph with a 150-line grating. The observations were made under photometric conditions at the Palomar 60-inch on 9 and 10 July 1996. The wavelength coverage

³Tables 2, 4 and 5, together with the data tables from Paper I and Paper II are available from our PMSU website at: <http://www.physics.upenn.edu/inr/pmsu.html>

was 4600Å to 10170Å with resolution 6Å, providing a good match to the echelle observations. In Figure 4, we show that use of the Bessell (1990b) filter response curves with our spectra reproduces the sixth order polynomial relation between $R - I_C$ and $V - I_C$ derived by Bessell (1990a). The deviations seen at the blue end correspond to stars earlier than type M0 and therefore do not effect our results.

Using these low-resolution spectra, we find that the continuum flux at $H\alpha$ and $H\beta$ can be derived from broadband photometry using the following linear relations:

$$-2.5 \log F_{H\alpha} = (21.68 \pm 0.04) + (0.974 \pm 0.038)R_C$$

$$-2.5 \log F_{H\beta} = (21.01 \pm 0.06) + (1.055 \pm 0.055)V_C$$

where the fluxes are measured in $\text{erg s}^{-1} \text{cm}^{-2} \text{\AA}^{-1}$. These relations are applicable for stars with types M0-M6.5. They are used to transform the measured emission-line equivalent widths to the flux values discussed in Section 4.1. We note that differences in continuum placement at low and high resolution might lead to small systematic errors.

V-band photometry is available for all the M dwarfs in our sample. In cases where R_C photometry was unavailable, we estimated the $V - R_C$ color using the TiO5 value:

$$V - R_C = 3.2345 - 8.9529 \times \text{TiO5} + 12.041 \times \text{TiO5}^2 - 5.6274 \times \text{TiO5}^3$$

When $V - I_C$ colors were needed but unavailable, we used:

$$V - I_C = 6.3657 - 14.6706 \times \text{TiO5} + 17.6957 \times \text{TiO5}^2 - 8.0934 \times \text{TiO5}^3$$

Again these relations are applicable for stars with spectral types M0-M6.5.

2.5. Rapid Rotators

Rotational broadening is measurable for a handful of stars in our spectra. For each observing run, we artificially broadened a star of known low rotation ($v \sin i < 2 \text{ kms}^{-1}$) using a rotational broadening function (Gray 1992). We adopted a limb darkening coefficient of 0.6, shown to be an appropriate value by Marcy & Chen (1992). However, measuring $v \sin i$ by cross-correlation against the standards proved ineffective, probably due to small mismatches in spectral type. Instead, we emulated the method of Marcy & Chen (1992) by using χ^2 fitting to determine the best fit to individual atomic lines. Our lower resolution requires that we use relatively strong atomic lines, as in the region 6420 – 6520Å. Detections are limited to $v \sin i > 20 \text{ kms}^{-1}$ (~ 3 pixels). We estimate a measurement accuracy of $\sim 5 \text{ kms}^{-1}$.

Stars with detected rotational broadening are listed in Table 5. Our results are quite repeatable; for example, G188-38 (NN 3453) was observed 6 times, each time yielding $v \sin i$ between 35 and 40 kms^{-1} . The most notable star is G 165-8 (NN 2128), which has thirteen measurements that

are all consistent with $v \sin i = 80 \text{ kms}^{-1}$, similar to the extreme rotator Gl 890 (Pettersen et al. 1987). One of our observations clearly shows $\text{H}\alpha$ emission from a secondary companion, while others show asymmetries in the line profile. The rotational velocity is close to that of the fastest-rotating M dwarfs in the Pleiades (Terndrup et al. 2000), suggesting that the system is relatively young, $\tau \lesssim 10^8$ years.

A caveat to all of our rotation measures is that close binary pairs which happened to have velocity differences of $\sim 20 \text{ kms}^{-1}$ at the time of our observations could be misidentified as rapid rotators. For example, we measure $v \sin i = 30 \text{ kms}^{-1}$ for Gl 735 (NN 2976), but we exclude the star from Table 5 since it is identified as “SB” in the pCNS3. Gl 206 (NN 933) and Gl 829 (NN 3360), both known SB2s, also show significant line broadening in our spectra. Confusion is less likely where multiple measurements are available.

3. Binaries

Table 6 lists 23 dwarfs which are double-lined spectroscopic binaries (SB2). These systems must have relatively short periods, but our data provide insufficient temporal coverage to attempt period determinations. Note that most objects in the present sample were observed only once, so additional double-lined systems which were in an unfavorable configuration at the time of our observation remain undetected. Thirteen of these 23 SB2 systems have published orbits, while the other ten are new discoveries.

A few single lined stars with multiple velocity measurements, both our own and those available in the literature, have velocities spanning a larger range than expected given the individual uncertainties. This may reflect the presence of an unseen companion (i.e. SB1 system). Table 7 lists stars where the overall rms dispersion of the observations exceeds 4 kms^{-1} . Other stars listed in Table 2 with $\sigma > 3 \text{ kms}^{-1}$ may also merit additional observations. Table 8 lists other candidate SB1 systems where a significant velocity difference exists between our observation and the literature data. With potential velocity amplitudes of a few kms^{-1} and periods of a few years, these systems are likely to have separations of $\sim 1 \text{ AU}$, equivalent to ~ 0.1 arcseconds for stars in this sample. These are therefore good candidates for high-resolution imaging (speckle, adaptive optics, or interferometry) and radial velocity monitoring at higher resolution. Several stars have known companions which may be responsible for the observed velocity differences.

Poveda et al. (1994) have published a catalog of candidate wide binary or multiple systems in the pCNS3 catalog. We have radial velocity measurements for several of their candidates, including two with separations exceeding 0.1 parsec and therefore of potential interest for Galactic dynamics. At such separations, orbital velocities are less than 1 kms^{-1} , so we expect the radial velocities of the components to agree within our measuring uncertainties. Table 9 shows the comparison, where the final column gives the observed velocity difference in terms of our measuring uncertainty, which we take as 1.5 kms^{-1} . Of the two wide systems, Gl 469 and Gl 471 are clearly not associated

(unless one has an unseen companion), but our data show only a 3σ difference between Gl 48 and the Gl 22 system. Except for Gl 140 A/C, where orbital motion might affect the velocity of the brighter star, the remaining candidate binaries have velocity differences consistent with our measuring uncertainties.

4. Chromospheric Activity, Age and the Star Formation History

The chromospheric age-activity correlation amongst main-sequence stars has been studied extensively for solar-type dwarfs, where it is usually parameterised in terms of the ‘t to the half’ law (Skumanich 1972),

$$F(Ca) = At^{-1/2}$$

where $F(Ca)$ is the Ca II K emission-line flux, A is a constant and t the age. Based on that calibration and observations of local G dwarfs, several groups have attempted to reconstruct the recent star formation history in the disk. In particular, both Barry (1988) and Rocha-Pinto et al. (2000) claim that the data indicate several significant bursts of star formation over the last 4 Gyrs. On the other hand, Soderblom, Duncan, & Johnson (1991) argue that these ‘bursts’ are the result of a more complicated activity/age relation than that implied by a simple Skumanich type power law. Our goal is to use our observations of M dwarfs in the VC sample to address the local star formation history. To that end, we first investigate the range of activity and the correlation of activity with age for the low-mass M dwarfs. In particular, we do not require that the M dwarfs follow the same age-activity relation used for the G dwarfs.

4.1. Activity

The primary indicator of chromospheric activity in M dwarfs is H α emission. In Figure 5 we plot the equivalent width of H α as a function of TiO5 (spectral type/effective temperature). Figure 6 is an expanded view of the absorption (negative) equivalent width portion of Figure 5. Active stars known to be short-period binaries (Tables 6 and 7) are shown as open circles while members of the VC sample are shown as solid triangles. Additional stars from this paper which are not in the VC sample are shown as open triangles. To aid discussion, we have labelled five groups (A-E).

Group A: The majority of M dwarfs show H α absorption, with larger average absorption equivalent widths at early spectral types. H α absorption does not necessarily indicate an absence of chromospheric activity, as discussed by Cram & Mullan (1979) and Cram & Giampapa (1987). These authors showed that the presence of a weak to moderate chromosphere induces H α absorption in M dwarfs, which enhances the photospheric absorption. Only a rather strong chromosphere will produce H α emission. Thus, M dwarfs with the strongest H α absorption probably have moderate chromospheres, while those with no chromosphere will exhibit only weak (or perhaps no) absorption

– see discussion of Group E. The observed width of the absorption sequence in Figure 6 is larger than our measuring uncertainty, and therefore probably reflects real star-to-star variations at a given effective temperature. These variations are presumably correlated with the level of chromospheric activity. Also, the fraction of stars per spectral type bin which are in Group A decreases towards later spectral types, which is probably related to the increase in the lifetime of strong chromospheric activity for lower mass stars (see discussion in Section 4.2).

Groups B and C: Most of the early (M0-M2.5) dwarfs with emission, including all the early-M active binaries (BY Dra class) in the VC sample, cluster near the upper envelope of observed activity. We have marked these dwarfs as Group B. There is a striking lack of early-M dwarfs with weaker emission, indicated as Group C. This behavior was noted by Herbst & Miller (1989), who point out a similarity with the Vaughn-Preston gap in the CaII emission of G dwarfs (Vaughan & Preston 1980; Henry et al. 1996). Such a gap can be interpreted either as a stellar population (age) or a stellar chromosphere effect. In the former case, one assumes that age and $H\alpha$ emission have a simple relationship, and the distribution reflects a lack of intermediate age (Group C) stars compared to younger (Group B) and older (Group A) stars. In the latter interpretation, some aspect of chromospheric physics makes it unlikely that a star is observed with intermediate-strength emission lines. For example, stars may remain in the Group B state for a long time, then rapidly evolve through the Group C region.

Group D: The observed distribution of $H\alpha$ equivalent width changes at $TiO5 \sim 0.5$ (spectral type M2.5/3). Amongst earlier spectral types, emission is limited to $\sim 2.5\text{\AA}$ above the mean level of absorption; for the mid-M (M3-M5.5) dwarfs, the emission-line equivalent widths are distributed roughly uniformly between 0\AA and a maximum value of $6\text{-}10\text{\AA}$. This change in properties was also noted by Herbst & Miller (1989) on the basis of data for fewer stars. Little structure is evident, although there is a suggestion of a clump at $H\alpha \sim 4.5\text{\AA}$, $TiO5 \sim 0.4$. According to the empirical mass-spectral type relations derived by Kirkpatrick & McCarthy (1994), spectral type M3 corresponds to $0.26M_{\odot}$, while M2 corresponds to $0.37M_{\odot}$. This range encompasses the mass where M dwarfs are expected to become fully convective ($\sim 0.3M_{\odot}$, Burrows et al. (1997)). The change in the distribution of activity strengths may be related to changes in the magnetic dynamo generation mechanism and/or the atmospheric structure amongst fully-convective stars (Hawley et al. 2000).

Group E: A few dM stars have unusually weak $H\alpha$ absorption. They are sometimes called dM(e) stars, since they appear to be intermediate between the dMe and dM stars. Two different states contribute to this group. Some stars may have extremely weak, or possibly no, chromospheres. The absorption line, or lack thereof, then simply reflects the weak photospheric absorption which disappears at later types. Others have moderately strong chromospheres that have begun to produce enough emission to fill in the absorption line, but not enough to produce a full-fledged emission line. Examples of both types are known (Byrne 1993; Doyle et al. 1994). Two of the stars in Group E, GJ 1062 (NN 647) and LHS 64 (NN 3308) are old, metal-poor M subdwarfs (Gizis 1997), and as such are likely to have weak, if any, chromospheres. Further study of Group E stars may be useful

to characterize this rare, inactive state amongst M dwarfs.

An interesting question raised by our analysis is whether there is an evolutionary pattern through the groups we have identified. Thus, for example, an early type M dwarf might start out quite active (group B). As the chromosphere begins to weaken with age, the $H\alpha$ emission may fade rapidly according to the particulars of the line radiative transfer leading to a quick passage through Groups C and E. Further chromospheric weakening may lead to a slower evolution from the top (less absorption) of Group A to the bottom of Group A, and finally, as the stars age even further (approaching the age of the Galactic disk?) the chromosphere begins to disappear altogether, with the evolutionary path progressing back through Group A to an endpoint in Group E. For later type stars, it may be that the radiative transfer in the $H\alpha$ line is such that it is easier to drive the line into emission. Thus those stars start, and remain, in Group D throughout most of their evolution, at least to their current ages. We are pursuing these ideas by searching for other chromospheric indicators that would allow us to distinguish between moderate activity (filled-in $H\alpha$) and no activity (weak or no $H\alpha$ absorption), and by developing chromospheric models that predict the behavior of the $H\alpha$ (and other) emission lines depending on parameters that characterize the strength of the chromosphere (Hawley et al., in preparation).

We obtained monitoring observations of the nearest M dwarfs as part of this program. These allow us to examine variability in the emission line strength. Figure 7 plots the observed standard deviation in equivalent width as a function of emission line strength for stars with at least 4 observations. For dMe dwarfs with $H\alpha \lesssim 5\text{\AA}$ (including all early M dwarfs and the weaker mid-M dwarfs), variations are $\lesssim 0.5\text{\AA}$, with typical variations at the 15% level. In contrast, stars with stronger emission are significantly more variable, with variability exceeding 30%, corresponding to changes of several Angstroms in equivalent width.

As discussed extensively elsewhere (e.g. Reid, Hawley & Mateo (1995)), equivalent width measurements are useful in segregating stars within a relatively limited range of effective temperature, as in defining the groups in Figure 5, but do not provide a good measure of the absolute level of activity, due to variations in the continuum flux as the effective temperature changes. We have therefore used the relations defined in Section 2.4 to transform our equivalent width measurements to line fluxes, and formed the ratio of the line luminosity to the bolometric luminosity – an absolute measure of the activity strength for each star. Figure 8 plots the result for $H\alpha$ as a function of TiO5 (equivalently colour, spectral type, effective temperature, mass). The Group B stars are clearly evident at spectral types earlier than M2, while the Group D stars comprise the cooler half (smaller TiO5) of the diagram. It is interesting that binaries (open circles) are found scattered throughout the latter group, with no clear clustering at the most active levels. The discussion of the groups given above is applicable also to this figure, with the Group B stars showing high and rather uniform activity and some evidence for binaries having stronger activity, while the Group D stars have a much larger scatter. The mean level of $\log(L_{H\alpha})/L_{bol}$ is ~ -4.0 , in agreement with the value we found for the Hyades (Reid, Hawley & Mateo 1995) and in our lower resolution survey of these same field stars (Paper II). Figure 8 makes it clear however, that the scatter among the

Group D stars (later types) is not uniform. There are more stars that show activity above the mean level (between -3.5 and -4), but the stars below the mean level have a larger range (between -4 and -5). With reference to our previous speculative discussion about chromospheric evolution, this could be evidence that the younger, most active stars cluster around $\log(L_{H\alpha}/L_{bol}) \sim -3.8 \pm 0.2$, while the older, less active stars spread out according to their age and initial activity level. It is notable that the difference in scatter between Group B and Group D is still very striking, which may mean that some change in the dynamo generation at the fully convective boundary is also required (along with evolution and the particulars of $H\alpha$ line transfer) for a full physical explanation of these phenomena.

Figure 9 shows the Balmer decrement, the ratio of $H\alpha$ to $H\beta$ flux. A typical value in the Hyades is ~ 4 , somewhat larger than the mean found here of ~ 2.5 (which does agree with our result in Paper II). There is a slight downward trend toward later types among the Group B stars and again a notable increase in the scatter, particularly toward larger values of the decrement, among the Group D stars. It may be significant that this scatter is apparently restricted to the later spectral types among Group D. The scatter is reminiscent of that seen in Figure 7 in $\sigma_{H\alpha}$. There are 8 stars shown with $\sigma_{H\alpha} > 1.5 \text{ km s}^{-1}$, and three of these (NN 1702, 1724, 1326) have the three highest values of the Balmer decrement, while four of the remaining five (NN 204, 230, 1398, 1934) have decrements well above the average, between 4 and 10. A very strong Balmer decrement and significant variability probably indicate that we have observed flaring activity in these stars; the decrement actually *decreases* in flares on earlier M dwarfs (e.g. AD Leo, Hawley & Pettersen (1991)), but is known to increase strongly during flares on later M dwarfs (e.g. VB 10, Herbig (1956); 2MASSJ0149, Liebert et al. (1999)). The final star, LHS 1723 (NN 855) is anomalous in both figures, lying at $\sim (1, 1.7)$ in Figure 7 and at $\sim (0.4, 1.2)$ in Figure 9. This star has very weak $H\alpha$ emission compared to $H\beta$ and also shows far more variability than other weak $H\alpha$ emitters. It will pose an interesting challenge for chromospheric models.

Finally, our observations comprise the most extensive available set of Helium D3 ($\lambda 5876\text{\AA}$) emission line data for active M dwarfs. Figure 10 shows that there is a strong correlation between the He D3 and $H\alpha$ emission equivalent widths, with the slope of a simple linear fit ~ 0.12 . Alternatively, the flux in the He D3 line may be predicted from the $H\alpha$ flux by $F_{HeD3} = 0.048 \times F_{H\alpha}$. The good correlation suggests that both features probably originate from the same region within the chromosphere. This is in contrast with previous observations and modelling of Ca II, Mg II and $H\alpha$ emission in M dwarfs which implied that the emission in those lines was coming from different chromospheric regions (Mauas & Falchi 1994; Giampapa, Worden & Linsky 1982). An extensive study of He D3 in G and K stars by Saar et al. (1997) suggested formation in the upper chromospheres of those stars, and good correlation of the He D3 flux with those of Ca II and C IV (similar to our result here for $H\alpha$). Andretta & Giampapa (1995) have outlined a method using He D3 observations to infer the filling factor of active regions in F and G stars. It would be of great interest if such a technique was applicable also for M dwarfs.

4.2. An age-activity calibration for M dwarfs

Calibrating age-dependent relations obviously demands stars with well determined ages. In the Galactic disk, open clusters give an independent age determination, and observations of chromospheric activity levels of cluster members provide the calibration. The traditional approach, as in Barry (1988), is to determine a relationship between the activity level (e.g., equivalent width or other measure) and the age. By applying this law to each field star, unique ages can be derived. While we have proposed above a possible qualitative evolutionary sequence that might eventually allow a unique age determination for each M dwarf in our sample, we are far from certain that our proposal is correct, and have not even begun to determine a calibration. Also, observations of clusters show that there is some spread in activity at a given age. Moreover, as demonstrated in Figure 7, variability is clearly present in individual M dwarfs, complicating any effort to determine an exact activity level. Finally, the appearance of Figure 5 suggests potential inconsistencies in applying this method: If the lack of Group C stars is interpreted as a lull in star formation, where is the corresponding gap in Group D? If the concentration of stars in Group B is a burst of star formation, why is there no corresponding concentration at the top of Group D?

Hawley et al.’s (1999) analysis of M dwarfs in open clusters suggests a different approach. While the activity levels of stars in a given cluster exhibit considerable scatter, there is a well-defined $V - I_C$ colour at which activity becomes ubiquitous. All stars redder than this colour are dMe (defined as $EW_{H\alpha} \geq 1.0\text{\AA}$), while the bluer stars are dM without emission. This effect was commented on originally by Stauffer et al. (1994) for the Pleiades. Observations currently exist for M dwarfs in six clusters: IC2602 & IC2391 (30 Myrs, Barnes et al. 1999), NGC 2516 & the Pleiades (125 Myrs, Stauffer, Schultz & Kirkpatrick 1998), the Hyades (625 Myrs, Perryman et al. 1998), and M67 (4.0 Gyrs, Dinescu et al. 1995). Hawley et al. (1999) have used those observations to determine the relationship between the ‘H α limit’ colour and the age in years,

$$V - I_C = -6.91 + 1.05(\log Age) \tag{1}$$

as shown in Figure 11.

We can use this correlation to transform an observed distribution of chromospheric activity as a function of $V - I_C$ colour to an estimate of the cumulative age distribution. We define f_{dMe} as the fraction of dMe dwarfs at a particular colour, $(V - I_C)_i$,

$$f_{dMe} = N(\text{dMe})/N(\text{dM} + \text{dMe}), \quad (V - I_C) = (V - I_C)_i \pm \delta$$

This ratio provides an estimate of the fraction of stars younger than age τ_i , where, from Equation 1,

$$\log \tau_i = ((V - I_C)_i + 6.91)/1.05$$

Thus, for example, the fraction of dMe dwarfs at $V - I_C = 1.0$ is directly proportional to the relative number of stars which have formed in the last $\sim 3 \times 10^7$ years, while f_{dMe} at $V - I_C = 2.6$ corresponds to the relative number of stars with ages of less than 1 Gyr. In this manner, we can determine f_{dMe} for a range of $V - I_C$ colour, and map the cumulative star formation history of the Galactic disk.

4.3. Star Formation History of the Galactic Disk

We have applied the analysis technique outlined in the previous section to data for the M dwarfs in the VC sample. For stars lacking $V - I_C$ measurements, we use the TiO5 index to estimate the colour. The results are plotted in Figure 12, giving f_{dMe} as a function of the inferred age. A constant star formation rate (i.e. f_{dMe} directly proportional to age) is shown for reference as the thick solid line with slope unity in this figure. Two different ways of computing the fraction of dMe stars are illustrated. The long-dashed line (connecting solid triangles) gives the fraction found by weighting all stars equally. The thin solid line (connecting open triangles) shows the fraction found by weighting each star by the inverse of its W velocity, as proposed by Wielen (1974, 1977). The latter approach allows for the increased scale height of higher velocity (older) stars, and consequent shorter residence time in the Solar Neighbourhood. However, this method adds statistical noise by placing significant (undue?) weight on a small number of high velocity stars. In both cases we exclude the SB1 and SB2 (short period binary) systems, since the activity in those stars may be influenced by other effects than age.

Figure 12 indicates that the overall star formation history is broadly consistent with a constant star formation rate. The major feature notable in the distribution is a step at ~ 1 Gyr which, if taken at face value, would indicate that $\sim 10\%$ of the local disk stars formed in a burst at that time. However, this feature is unlikely to be real, since it corresponds with the Group B/D transition in Figure 5 which we discussed at length in Section 4.1. Such a distinct change in activity properties is unlikely to be well described by a simple linear relation. Data for clusters with ages between the Hyades (0.6 Gyr) and M67 (4 Gyr) would be useful in confirming whether this feature has an astrophysical, rather than evolutionary, origin.

The other characteristic of the star formation history illustrated in Figure 12 is a slight deficiency in the number of young (< 1 Gyr) stars relative to the number of older (> 1 Gyr) stars. At ages of less than 1 Gyr, both the weighted and unweighted solutions match the expectation of constant star formation (slope unity), with slopes of 0.92 ± 0.16 and 0.95 ± 0.50 respectively. For the full age distribution, however, we derive best-fit slopes of 1.14 ± 0.09 for the unweighted solution and 1.38 ± 0.19 for the weighted solution. This result implies a slight decrease in the star formation rate in recent times. However, this could reflect incompleteness in the VC sample which, since it is derived primarily from proper motion surveys, may be deficient in young, low space-motion dwarfs.

Figure 12 also compares our analyses with the star formation histories proposed from G dwarf studies by Barry (1988) and Rocha-Pinto et al. (2000). The poor time resolution at large ages, coupled with the lack of calibrating clusters and the relatively small size of the VC sample, limits the utility of comparisons at older ages (> 3 Gyrs). Nonetheless, it is encouraging that all of the models predict similar fractions of stars younger than 4 Gyrs. At younger ages, the M dwarf data are better calibrated. There is no evidence from our analysis for the substantial numbers of young G dwarfs ascribed by Barry (1988) to a recent burst of star formation. Similarly, our data fail to match the details of the Rocha-Pinto et al. (2000) analysis. Indeed, Rocha-Pinto et al. (2000)'s

“Burst A” of young ($\lesssim 0.5$ Gyr) G dwarfs is accompanied by a deficiency of M dwarfs, while their “AB Gap” at 1-2 Gyrs corresponds to an apparent excess of M dwarfs (although, as we noted above, we believe this feature reflects a deficiency in our analysis method rather than a burst of star formation).

The “AB” gap found by Rocha-Pinto et al. (2000) corresponds to the Vaughan-Preston gap Vaughan & Preston (1980). As noted above (Section 4.1), Herbst & Miller (1989) have suggested that the sparse number of early type M dwarfs with weak emission (our Group C) might be an analogous feature. However, observations of Hyades M dwarfs show that the $H\alpha$ limit corresponds to $TiO_5 \sim 0.55$ in that cluster. Thus, the weak emission M dwarfs in Group C must have ages of less than the age of the Hyades (0.6 Gyrs) – i.e. ages which match Rocha-Pinto et al. (2000)’s “Burst A”. As Soderblom, Duncan, & Johnson (1991) and Rocha-Pinto et al. (2000) have discussed, one needs either a complicated G-dwarf age-activity relation to match a constant star formation history, or a complicated star formation history to save the simple G-dwarf age-activity relation. Given the lack of agreement between our M dwarf analyses and the G dwarf analyses, we believe that the complicated G-dwarf age-activity relation explanation is favored. The existence of a large spread in activity in the coeval G dwarfs of M67 (Giampapa et al. 2000) and the large spread in rotation rates in stars of young clusters (Barnes 1997) suggests that any age-activity relation is complex, with stochastic star to star variations. Indeed, M dwarfs show similar behaviour, with a smattering of dMe dwarfs bluer than the $H\alpha$ limit in some clusters. Binarity may well be a contributing factor at both spectral types.

Other measures of the recent star formation history have been made without reference to chromospheric activity. Hernandez, Valls-Gabaud, & Gilmore (2000) have used Hipparcos color-magnitude diagrams to derive the star formation history of the Solar Neighbourhood within the last 3 Gyrs. They find an oscillatory component of star formation with a period of 0.5 Gyr superposed on an underlying constant star formation rate. Their Figure 4 indicates that they see roughly 2.5 times as much star formation from $\sim 1.6 - 2.6$ Gyr as at $\sim 0.3 - 1.0$ Gyr. It is suggestive that this is similar to the deviations from constant star formation seen in our Figure 12 – that is, the possible deficiency of young stars. Neither our data nor Hernandez, Valls-Gabaud, & Gilmore (2000) show the lull in star formation between 1-2 Gyrs seen by Rocha-Pinto et al. (2000).

Our present analysis is only a first step towards using M dwarfs as probes of Galactic star formation. Additional observations of M dwarfs in clusters, particularly clusters older than the Hyades, are required to improve the age-activity calibration during the important 1-4 Gyr time period. Further observations in clusters and the field are needed to quantify the significance and range of star-to-star variations, and (with sufficient resolution) to provide additional information on the evolution of activity at a given spectral type, both among the Group B and Group D stars. Finally, a nearby star sample which is both unbiased kinematically and complete over a larger volume will provide improved statistics for the local field stars. We are currently developing such a sample in a project undertaken under the auspices of the NASA/NSF NStars program (Reid & Cruz, 2001).

4.4. Brown Dwarfs

The ability to constrain the ages of individual M dwarfs can be used to set limits upon the ages of brown dwarf candidates which happen to be in binary systems with M dwarf primaries. This allows an independent test of the predictions of theoretical model isochrones. At the present time, two L dwarfs and two T dwarfs are known to be companions of nearby M dwarfs. In addition, Martín et al. (2000) have shown that Gl 569 A is the companion to a binary system, Gl 569Ba and Bb. In Table 10, we use the presence or absence of H α emission in the primary, together with Equation 1, to constrain the age of each system. The discovery groups have also discussed the limits that chromospheric activity places on the age. In particular, it should be noted that G 196-3 is a very active M2.5 dwarf, so Rebolo et al. (1998) argue that it is likely to be younger than our limit. Based on the lack of emission in Gl 229A, as well as the fact that no rotational broadening is detectable, the young age of 30 Myr advocated by Legget et al. (2002) is ruled out — indicating that the synthetic spectra from model atmospheres are not yet adequate for age determinations. Continued discoveries of L and T dwarf companions to nearby M dwarfs may be expected from both dedicated searches and the 2MASS, DENIS, and SDSS surveys, and improved age determinations will aid in the usefulness of those data.

Our star formation results also apply to the modelling of the substellar mass function. Because age and mass are not directly observable for isolated field brown dwarfs, a mass function can only be derived through simulations. Reid et al. (1999) have modelled L dwarf detections from DENIS and 2MASS, assuming a constant star formation rate for the Solar Neighbourhood. Our results show that this assumption is largely consistent with our analysis of the local low-mass stars, and therefore is likely to be appropriate for the local brown dwarfs as well. However, if there is a slight deficiency in the local density of very young stars (and brown dwarfs), then the numbers of L- and T-type brown dwarfs that we observe is a smaller proportion of the number that actually exist (because they are easier to observe when they are younger/brighter). In this case, the Reid et al. analysis will underestimate both the slope of the mass function and the total number of brown dwarfs in the Galactic disk. A reliable estimate of the local star formation history is critical to determining the contribution made by brown dwarfs to the mass of the Galactic disk.

5. Summary

We obtained high resolution spectra of a large sample of nearby M dwarfs to supplement our earlier moderate resolution survey. The new measurements include accurate radial velocities, H α emission and absorption equivalent widths, and simultaneous observations of several other chromospheric lines, including Helium D3. We discussed several groupings of stars based on their H α activity and speculated on the nature of the chromospheric evolution, including differences between early (M0-M2.5) and mid (M3-M6) dwarfs.

We also argued that the relative numbers of dM and dMe stars as a function of spectral type,

together with an age-activity relation calibrated for M dwarfs, may be used to probe the star formation history of the Galactic disk. We found no evidence for the various recent bursts and lulls in star formation history inferred from G-dwarf activity results. This suggests that the G-dwarf age-activity relationship is complex, and must be better understood before attempting to use it to derive the Galactic star formation history. Finally, we illustrated the use of M dwarf activity levels to constrain the ages of binary systems with brown dwarfs.

Additional study of active M dwarfs in open clusters and the field will allow a better calibration of the M dwarf age-activity relationship, and more accurate determination of the local star formation history, which is crucial for understanding the substellar mass function. When coupled with chromospheric models, we can also hope to attain a better understanding of the underlying physical processes (evolution, atmospheric structure, dynamo generation) that ultimately control the empirical behavior we observe.

We gratefully acknowledge the assistance of Skip Staples and the other telescope operators at the Palomar 60-in. telescope. Jim McCarthy gave helpful assistance with the echelle hardware and software. We would like to thank the staff of Palomar Observatory and Jim McCarthy for their work on making the new cross-dispersing prisms a reality. Tokovinin provided an electronic version of his radial velocity data. JEG was partially supported by Greenstein and Kingsley Fellowships. SLH was partially supported by the NSF through Young Investigator award AST 94-57455. This research has made use of the Simbad database, operated at CDS, Strasbourg, France.

Table 1. Radial Velocity Comparison

Source	N	σ_{ref} kms ⁻¹	$\langle v_{rad} \rangle$ kms ⁻¹	σ kms ⁻¹
Bopp and Meredith (1986)	17	1-2	-1.07	3.58
Delfosse <i>et al.</i> (1998)	93	0.5	0.04	2.38
Delfosse <i>et al.</i> (1998)	90*	0.5	0.12	1.25
Stauffer and Hartmann (1986)	115	0.9	-1.27	1.99
Tokovinin (1988,1992)	51	0.5	-0.75	1.38
Upgren and Caruso (1988)	64	1	-0.11	1.58
Upgren and Harlow (1996)	25	1.2	-0.97	1.83

Note. — * excluding the three stars discussed in the text

Table 2. Radial Velocities

NN	Name	Julian Date	v_{rad}	Julian Date	v_{rad}	Julian Date	v_{rad}	$\langle V_{rad} \rangle$	σ
7	Gl 2	2450008.6917	0.4					0.4	...
11	Gl 4 A	2449561.8691	3.3					3.3	...
12	Gl 4 B	2449561.8780	-1.6					-1.6	...
19	GJ 1002	2450085.6899	-39.5	2450285.9580	-40.7	2450473.6302	-39.5	-40.1	0.6
		2450668.9841	-40.8						
38	G242-048A	2449559.9545	-13.2					-13.2	...
41	GJ 1005 B	2450009.7126	-23.3	2450086.6392	-26.8	2450304.9421	-27.3	-25.5	1.7
		2450473.6410	-23.0	2450668.9975	-26.7	2450670.8852	-26.1		
43	Gl 12	2449560.9415	49.6					49.6	...
54	Gl 14	2449561.8870	3.8	2450286.9933	2.2			3.0	0.8
60	Gl 15 A	2449559.9314	10.8	2450009.6864	12.2			11.5	0.7
61	Gl 15 B	2449559.9437	10.5					10.5	...
76	GJ 1010 A	2449561.9086	-61.4					-61.4	...
83	GJ 2005	2450304.9565	-35.2	2450670.9703	-30.9			-33.0	2.2
87	Gl 21	2450008.7122	-1.1					-1.1	...
89	GJ 1012	2449560.9966	-12.3	2449561.9299	-12.4	2450083.6995	-15.4	-13.4	1.4
92	GJ 22 C	2449561.8961	-3.3	2450008.7326	-4.7	2450083.5709	-2.6	-4.9	1.5
		2450286.9177	-5.2	2450304.0157	-5.0	2450447.7171	-7.4		
		2450468.6446	-4.5	2450502.5976	-3.9	2450670.9142	-7.1		
93	Gl 22 B	2450008.7231	-0.8	2450083.5805	-9.1	2450468.6496	-3.0	-3.4	3.0
		2450502.6065	-2.4	2450670.9232	-1.7				
96	LP525-39B	2450005.7292	-4.6					-4.6	...
115	Gl 26	2450008.7020	-0.8	2450287.0027	-0.5			-0.6	0.1
129	Gl 29.1	2449560.9496	-65.5					-65.5	...
165	LTT10301A	2449559.9738	6.2					6.2	...
168	Gl 38	2449559.9821	-12.9					-12.9	...
171	Gl 40 A	2450005.7378	16.5					16.5	...
185	Gl 44	2449560.9698	-47.5					-47.5	...
187	Gl 46	2449560.9833	14.6					14.6	...
193	Gl 47	2450005.7463	6.6	2450087.6783	8.7	2450286.9834	8.0	8.7	1.9
		2450505.6221	8.0	2450618.9809	12.3				
195	Gl 48	2449561.9393	2.0	2450083.5863	-0.5	2450286.9278	1.1	0.5	0.7
		2450304.0089	0.1	2450447.7388	-0.3	2450468.6561	0.7		
		2450500.6031	0.5	2450505.6029	0.2	2450618.9742	0.9		
		2450670.9295	0.6						
199	Gl 49	2449559.9913	-5.0					-5.0	...
203	Vyss. 3	2449560.9606	8.9					8.9	...
204	Gl 51	2450021.7375	-5.9	2450083.5955	-8.3	2450286.9394	-6.5	-7.3	1.0
		2450303.9504	-8.0	2450447.7311	-6.8	2450468.6656	-9.5		
		2450500.6134	-7.3	2450505.6153	-7.4	2450618.9666	-7.5		
		2450670.9432	-6.3						
210	GJ 1028	2450086.6753	10.0					10.0	...
213	Gl 52	2450005.7533	4.1					4.1	...
230	LP467-16B	2450009.7303	1.7	2450084.5860	1.4	2450285.9653	2.5	2.6	1.1
		2450304.9685	3.0	2450446.6414	2.4	2450467.6466	4.2		
		2450502.6202	4.3	2450670.8977	1.2				
234	Gl 54.1	2450084.5947	27.2	2450085.7453	27.1	2450285.9763	27.1	27.6	0.9
		2450446.6515	26.7	2450473.6518	29.6	2450501.6061	28.1		
		2450670.9794	27.4						

Table 2—Continued

NN	Name	Julian Date	v_{rad}	Julian Date	v_{rad}	Julian Date	v_{rad}	$\langle V_{rad} \rangle$	σ
247	Gl 55.2	2449561.0040	-22.4	2449561.9683	-24.7			-23.6	1.1
260	Gl 56.4	2450005.7594	-18.3					-18.3	...
276	Gl 57.1B	2449731.6102	35.0					35.0	...
296	Gl 63	2449561.9528	-17.0					-17.0	...
301	Gl 65 A	2450085.7025	20.9	2450304.9862	20.3	2450473.6618	24.9	22.0	2.0
316	LHS1289	2449561.9805	-3.6					-3.6	...
319	Gl 70	2449561.9947	-27.1	2450008.7448	-26.0	2450021.7616	-26.2	-26.4	0.4
		2450086.6867	-26.2						
326	G271-149	2450008.7570	54.3					54.3	...
339	Gl 78	2450008.7667	-11.5					-11.5	...
342	Gl 79	2450009.7400	13.0					13.0	...
350	Gl 82	2450005.7837	-8.5					-8.5	...
358	Gl 83.1	2450021.7711	-28.8	2450085.7151	-29.4	2450286.9735	-29.7	-29.5	0.6
		2450304.9947	-29.2	2450446.6640	-30.9	2450467.6580	-29.2		
		2450502.6310	-29.7	2450670.9069	-29.4				
359	G244-047	2450021.7479	-83.8	2450083.6045	-82.2	2450286.9490	-83.5	-83.8	1.4
		2450447.7490	-84.8	2450468.6761	-83.1	2450500.6263	-86.6		
		2450670.9523	-82.9						
363	LHS1326	2450084.6134	20.4	2450303.9653	21.2	2450446.6890	20.7	21.6	0.9
		2450467.6751	22.0	2450502.6415	21.7	2450505.6368	22.1		
		2450670.9904	23.4						
371	Gl 84	2450008.7758	24.7	2450082.5924	24.3	2450285.9934	25.8	25.1	1.4
		2450467.6837	27.3	2450501.6151	25.7	2450670.9984	22.8		
372	Gl 84.1A	2450009.7492	3.6					3.6	...
376	Gl 84.2A	2450009.7681	63.2					63.2	...
381	G173-039	2450005.7984	-10.1					-10.1	...
387	Rob 115	2450085.7248	-69.2	2450285.9837	-71.2			-70.2	1.0
390	Gl 87	2450008.8057	-3.2	2450446.6716	-2.9			-3.1	0.1
398	GJ 1044	2450008.7854	3.6					3.6	...
408	LHS1375	2450084.6314	18.7	2450502.6688	16.7	2450505.6543	15.6	17.0	1.3
427	Gl 96	2450005.8085	-37.9					-37.9	...
435	Gl 98 A	2450008.7959	7.9					7.9	...
453	Gl 102	2450005.8222	-5.4	2450085.7351	-8.0	2450286.9623	-6.4	-6.7	1.2
		2450467.6955	-6.2	2450500.6370	-8.8	2450504.6506	-7.2		
		2450671.0153	-5.2						
460	G173-061	2450467.7068	-61.2	2450501.5988	-60.3			-60.8	0.4
461	Gl 104	2449731.6267	-1.8					-1.8	...
463	Gl 105 B	2450009.7595	24.8					24.8	...
489	Gl 107 B	2450009.7768	27.7					27.7	...
492	Gl 109	2449731.6464	27.4	2450082.6272	31.9	2450086.6980	29.0	29.6	1.5
		2450285.9990	29.9	2450504.6361	29.9				
512	Gl 116	2450005.8309	-49.7					-49.7	...
515	G036-038	2450005.8401	-12.0					-12.0	...
525	Gl 119 A	2450009.7853	78.6					78.6	...
532	LHS1481	2450088.6522	99.1					99.1	...
538	LTT1445 A	2449731.6557	1.9	2450082.6159	-7.3	2450286.0061	-1.4	-3.4	3.8
		2450501.6284	-6.6						
539	LP771-96B	2449731.6646	-8.6	2450286.0104	-5.0	2450501.6374	-2.2	-5.3	2.6
548	Gl 122	2450005.8465	33.8					33.8	...

Table 2—Continued

NN	Name	Julian Date	v_{rad}	Julian Date	v_{rad}	Julian Date	v_{rad}	$\langle V_{rad} \rangle$	σ
550	Gl 123	2450008.8144	-30.0					-30.0	...
556	GJ 1054 A	2450021.7892	93.9					93.9	...
558	LTT1480	2450021.7987	151.5					151.5	...
559	Gl 125	2450005.8673	-2.8					-2.8	...
574	GJ 1057	2450021.7803	25.6	2450084.6457	27.9	2450305.0030	26.8	27.0	0.8
		2450446.7003	26.0	2450446.7094	27.1	2450467.7187	27.4		
		2450501.6512	27.1	2450671.0055	28.0				
579	AC+0641-15	2450021.8095	33.5					33.5	...
582	Gl 130.1A	2450009.7945	21.3					21.3	...
587	Gl 133	2450005.8555	-11.1					-11.1	...
590	Gl 134	2450005.8769	-5.8					-5.8	...
600	G077-046	2449731.6741	29.7					29.7	...
608	Gl 140 A	2450008.8437	24.0					24.0	...
610	Gl 140 C	2450008.8563	19.1					19.1	...
627	Gl 143.1	2450008.8332	14.0					14.0	...
630	Hy207	2450008.8237	25.8					25.8	...
647	GJ 1062	2450009.8207	-85.8					-85.8	...
656	Gl 148	2450021.8189	-25.7					-25.7	...
657	LHS 178	2450088.6367	-54.3					-54.3	...
663	Gl 150.1A	2450005.8962	33.6					33.6	...
664	Gl 150.1B	2450005.8870	33.7					33.7	...
674	Gl 153 A	2450083.6214	2.2					2.2	...
675	Gl 153 B	2450083.6161	1.7					1.7	...
677	Gl 154	2450021.8284	36.0					36.0	...
692	GJ 1065	2449731.7303	-11.6	2450008.8691	-7.6	2450084.6556	-11.6	-10.1	1.4
		2450305.0121	-10.0	2450446.7190	-11.0	2450467.7305	-8.9		
		2450501.6614	...						
699	Step 430	2450008.8786	2.6					2.6	...
701	Gl 156	2450021.8384	62.5	2450088.6636	62.1			62.3	0.2
702	Gl 156.1A	2450083.6309	-18.9					-18.9	...
720	Gl 160.2	2450082.6368	27.3					27.3	...
721	LHS1630	2450082.6526	-2.9					-2.9	...
724	Gl 162	2450008.8880	38.2					38.2	...
732	Gl 164	2450005.9093	-24.6					-24.6	...
742	Gl 166 C	2450082.6641	-41.5					-41.5	...
743	GJ 2033	2450008.8997	47.8					47.8	...
780	Gl 169.1A	2450005.9205	26.7	2450083.6411	27.1	2450303.9915	27.5	26.8	1.4
		2450447.8003	23.7	2450468.6886	27.9	2450500.6503	27.5		
782	Gl 170	2450087.7736	11.0	2450303.9815	14.5	2450502.7029	13.2	12.9	1.5
799	Gl 172	2450005.9283	33.5					33.5	...
802	G039-029	2450009.8692	25.5	2450087.7579	26.7	2450502.6903	28.1	27.6	1.6
		2450504.6707	29.8						
803	Step 497	2450008.9092	20.1					20.1	...
804	Gl 173	2450008.9178	-5.6	2450468.6962	-5.8			-5.7	0.1
811	Wo 9163 B	2450008.9268	-1.5					-1.5	...
817	Gl 176	2450005.9386	26.7	2450083.6617	26.7	2450473.7079	28.2	26.5	1.4
		2450502.6800	24.2						
821	G039-034	2449731.7465	-8.1					-8.1	...
835	GJ 1073	2450009.8811	101.8					101.8	...

Table 2—Continued

NN	Name	Julian Date	v_{rad}	Julian Date	v_{rad}	Julian Date	v_{rad}	$\langle V_{rad} \rangle$	σ
836	G1 179	2449731.7665	-9.1	2450468.7068	-9.1	2450473.6983	-9.1	-9.1	0.0
846	GJ 1074	2450009.8903	17.3					17.3	...
847	G1 181	2450023.8965	-36.0					-36.0	...
849	G1 182	2449731.7563	18.7					18.7	...
853	LP476-207Ab	2450005.9494	18.3	2450084.6772	12.9	2450446.7298	15.6	14.7	3.7
		2450467.7426	13.8	2450473.6797	18.8	2450500.6606	16.4		
		2450504.6857	7.1						
854	G1 184	2450009.8997	66.3					66.3	...
855	LHS1723	2450005.9617	40.8	2450085.7619	42.3	2450446.7386	40.1	41.4	0.8
		2450468.7209	42.0	2450473.6886	42.0	2450500.6697	41.4		
856	G1 185 A	2450005.9713	-15.8	2450085.7710	-15.9	2450446.7453	-10.7	-12.4	2.9
		2450467.7488	-9.1	2450501.6698	-10.4				
859	LHS1731	2450083.6701	13.3					13.3	...
874	Step 546A	2450082.6760	26.6	2450446.7531	21.3	2450467.7682	23.6	23.7	1.7
		2450501.6794	23.7	2450505.6696	23.3				
875	Step 545C	2450082.6849	19.8	2450446.7620	20.3	2450467.7602	22.1	21.2	0.9
		2450501.6880	21.9	2450505.6804	21.9				
876	G085-041	2450083.6812	20.1					20.1	...
882	G1 190	2450008.9357	32.6	2450009.9278	33.8	2450085.7805	33.6	33.9	1.1
		2450446.7762	32.8	2450467.7750	35.5	2450501.6953	35.4		
883	G096-021	2450083.6517	12.9	2450084.6864	14.8			13.9	0.9
888	G1 192	2450023.9066	-25.9					-25.9	...
895	G1 195 A	2450009.9086	32.7					32.7	...
905	G1 199 A	2450082.6938	30.9					30.9	...
919	G1 203	2450009.9188	59.0	2450088.6789	59.3	2450502.7146	59.0	59.4	0.5
		2450504.7019	60.2						
924	GJ 2043 A	2450082.7240	-2.6					-2.6	...
929	G1 204.2	2449764.6472	19.7					19.7	...
930	G1 205	2450446.7690	8.5	2450467.7823	7.1			7.8	0.7
933	G1 206	2450082.7048	17.2					17.2	...
938	G097-052A	2450083.7212	-14.6	2450502.7243	-13.7			-14.1	0.4
939	LTT11679B	2450502.7321	-14.1					-14.1	...
941	G097-054	2450023.9164	35.1					35.1	...
943	LHS5109	2450085.8078	28.4					28.4	...
944	G1 208	2450023.9388	21.6					21.6	...
955	GJ 1083 B	2450088.6960	23.2					23.2	...
956	G1 212	2450009.9369	4.3					4.3	...
959	G1 213	2450005.9806	105.6					105.6	...
961	G1 215	2450084.7000	-19.4					-19.4	...
980	G1 220	2450082.7146	32.3					32.3	...
981	G1 221	2450023.9272	22.0					22.0	...
985	G1 223.1	2450083.6900	27.8					27.8	...
991	G192-011A	2450009.9455	2.0					2.0	...
992	G192-012B	2450009.9576	2.8					2.8	...
998	LHS1805	2450005.9893	1.9	2450086.7293	0.0	2450088.7519	8.7	2.5	2.9
		2450446.7963	0.5	2450468.7473	2.8	2450500.6907	1.0		
999	G099-049	2449731.7774	28.4	2450085.8262	28.3	2450446.7867	28.0	28.7	0.7
		2450467.7929	29.9	2450500.6808	28.2	2450504.7299	29.3		
1004	LHS1809	2450086.7598	19.5	2450473.7202	18.8	2450473.7279	19.4	19.2	0.3

Table 2—Continued

NN	Name	Julian Date	v_{rad}	Julian Date	v_{rad}	Julian Date	v_{rad}	$\langle V_{rad} \rangle$	σ
1005	Gl 226	2450005.9987	-0.5	2450086.7392	-1.3	2450088.7608	-0.1	-1.1	0.5
		2450446.8028	-1.6	2450468.7323	-1.1	2450471.6631	-1.4		
		2450500.7008	-1.4						
1019	Gl 228 A	2450008.9542	57.7	2450085.8356	52.6	2450467.8022	53.5	54.2	2.0
		2450501.7226	53.2						
1021	Gl 229	2449764.6586	4.0	2450008.9441	4.7	2450083.7495	4.8	4.4	0.6
		2450083.7611	3.5	2450088.7271	5.2				
1038	Gl 231.3	2449764.6790	8.9					8.9	...
1041	GJ 2049	2449731.7992	16.2	2450008.9630	17.5			16.9	0.7
1042	Gl 232	2450087.7924	-13.4	2450446.8283	-13.9	2450467.8125	-13.1	-13.5	0.5
		2450501.7356	-14.1	2450504.7171	-12.9				
1048	Gl 234 A	2450085.8448	14.0	2450446.8372	13.4	2450473.7412	15.3	14.3	0.6
		2450501.7455	14.3	2450504.7411	14.3				
1052	Gl 236	2449731.7881	72.5					72.5	...
1057	Gl 239	2449764.6901	-59.2	2450473.7513	-56.9	2450502.7409	-58.7	-58.3	1.0
1068	G108-021A	2449764.7079	81.3					81.3	...
1069	G108-022B	2449764.7404	81.7					81.7	...
1089	LHS 221 B	2450084.7094	-31.0					-31.0	...
1092	Gl 250 B	2449731.8101	-7.6	2450008.9723	-5.5	2450085.8543	-14.8	-8.7	2.9
		2450446.8461	-9.1	2450473.7570	-7.4	2450501.7520	-7.5		
1094	Gl 251	2450006.0082	21.9	2450023.9478	22.7	2450088.7399	21.4	21.7	0.7
		2450502.7643	20.9						
1102	LHS1885	2450086.7790	15.0	2450502.7535	15.4	2450504.7692	16.1	15.5	0.5
1104	Gl 254	2450023.9569	-14.0					-14.0	...
1112	GJ 1093	2450446.8723	-30.4	2450467.8277	-29.9	2450501.7696	-31.5	-30.6	0.7
1120	LHS 224 B	2450086.7700	23.7	2450088.7761	22.3	2450446.8145	23.5	23.2	0.5
		2450468.8064	23.0	2450473.7720	23.2	2450500.7172	23.4		
1126	Gl 263 B	2450008.9813	-5.6					-5.6	...
1130	Gl 265 A	2450009.0164	-19.4	2450502.7841	-22.5			-21.0	1.6
1131	G250-034	2450084.7178	-5.5					-5.5	...
1138	Gl 268 B	2450008.9979	62.4	2450086.7897	-2.4	2450468.7626	50.9	32.7	24.6
		2450471.6737	10.6	2450500.7274	42.1				
1148	Gl 268.3B	2450009.0073	-14.4					-14.4	...
1154	G107-061	2450006.0168	11.2					11.2	...
1160	Gl 270	2450082.7335	-68.1					-68.1	...
1164	Gl 272	2450009.0256	-27.2					-27.2	...
1167	G088-028	2450023.9655	27.1					27.1	...
1168	Gl 273	2450006.0558	18.1	2450502.7743	16.1			17.1	1.0
1175	GJ 1097	2450082.7498	-0.4					-0.4	...
1176	Gl 275.1	2450084.7268	-16.1					-16.1	...
1183	Gl 277 Ab	2449731.8212	-1.3	2450009.0435	1.5			0.1	1.4
1184	Gl 277 B	2449731.8327	-0.3	2450009.0346	1.7			0.7	1.0
1191	Gl 277.1	2449731.8470	-40.7	2450006.0260	-40.8			-40.8	0.1
1193	Vyss. 499	2449731.8590	-15.0					-15.0	...
1196	Gl 278 C	2450009.0528	92.4	2450082.7644	-79.2			6.6	85.8
1201	G089-032	2450085.9113	24.9	2450446.8586	24.9	2450467.8419	24.2	24.6	0.7
		2450501.7835	23.5	2450504.7569	25.5				
1207	LHS1935	2450085.8968	-29.5					-29.5	...
1210	Gl 281	2450082.7736	24.3					24.3	...

Table 2—Continued

NN	Name	Julian Date	v_{rad}	Julian Date	v_{rad}	Julian Date	v_{rad}	$\langle V_{rad} \rangle$	σ
1211	Gl 282 A	2450082.7886	-17.4					-17.4	...
1212	Gl 282 B	2450082.7830	-16.8					-16.8	...
1219	Gl 285	2450084.8246	23.2					23.2	...
1226	GJ 1101	2450009.9708	6.7					6.7	...
1227	Gl 289	2450009.9798	53.5					53.5	...
1233	GJ 1103 A	2450087.8394	34.8	2450088.8477	34.9	2450446.8960	36.2	36.0	1.1
		2450467.8515	36.5	2450501.7967	37.8				
1247	GJ 1105	2450006.0379	-19.3	2450086.7989	-19.4	2450468.7787	-23.0	-21.1	1.8
		2450500.7388	-22.7						
1269	GJ 1107	2450084.7381	-2.7					-2.7	...
1271	Step 681	2450006.0468	-14.4	2450088.8773	-12.6			-13.5	0.9
1278	LHS5133 A	2450084.7479	79.4					79.4	...
1279	LHS5134 B	2450084.7565	87.9					87.9	...
1290	Gl 299	2450085.9207	12.6	2450446.9056	12.3	2450467.8729	12.5	12.6	0.3
		2450501.8171	13.0						
1293	Gl 300	2450087.8519	6.0	2450446.9210	7.0	2450467.8603	8.9	7.6	1.2
		2450501.8066	8.7						
1294	Gl 301 A	2450082.7963	14.1					14.1	...
1299	GJ 2066	2450009.9878	62.6	2450085.9297	63.2	2450446.9129	59.5	62.4	1.5
		2450467.8794	64.6	2450501.8234	62.1	2450505.7373	62.5		
1326	GJ 1111	2450467.8946	8.0	2450500.7566	8.0	2450502.8215	7.4	8.0	0.4
		2450505.7289	8.6						
1328	GJ 2069 D	2450009.9975	-41.2	2450467.9051	41.4	2450502.8920	-63.3	-32.1	43.5
		2450505.7484	-65.3						
1329	GJ 2069 B	2450010.0096	6.7	2450467.9145	5.2	2450502.9043	4.9	5.3	0.8
		2450505.7614	4.4						
1337	LHS 250	2450084.7643	22.1					22.1	...
1340	Gl 310	2450084.7736	11.3					11.3	...
1354	GJ 1113	2450084.7837	53.5					53.5	...
1355	LHS 252	2450086.8334	3.4	2450473.7883	4.5	2450500.7721	5.7	5.1	1.2
		2450504.8077	6.7						
1358	Gl 317	2450085.9412	87.8	2450502.7943	87.8			87.8	0.0
1361	Gl 319 A	2450082.8073	25.2					25.2	...
1377	Gl 322	2450084.7919	-21.4					-21.4	...
1379	Gl 323 A	2450082.8158	-11.8					-11.8	...
1383	Gl 324 B	2450085.9596	25.2					25.2	...
1385	Gl 325 A	2450084.8006	44.9					44.9	...
1391	Gl 328	2450082.8248	0.4					0.4	...
1395	Gl 330	2450010.0275	-8.6					-8.6	...
1398	GJ 1116 A	2450087.8671	12.5	2450467.9267	13.3	2450501.8372	12.2	12.8	0.4
		2450504.7921	13.1						
1405	G041-014B	2450010.0182	18.0	2450087.8773	-4.4	2450230.6429	4.7	-6.4	19.0
		2450446.9316	-7.6	2450467.9447	-34.2	2450501.8448	11.8		
		2450504.8212	-33.1						
1408	GJ 1119	2450087.8916	0.6	2450088.8158	1.7	2450467.9366	1.1	0.8	0.7
		2450502.8046	-0.2						
1417	G234-053	2450084.8133	-22.5	2450473.7978	-26.4	2450502.8398	-26.6	-25.2	1.9
1418	GJ 1120 A	2450082.8437	-10.0					-10.0	...
1419	GJ 1120 B	2450082.8349	-11.9					-11.9	...

Table 2—Continued

NN	Name	Julian Date	v_{rad}	Julian Date	v_{rad}	Julian Date	v_{rad}	$\langle V_{rad} \rangle$	σ
1420	G046-017	2450082.8559	49.0					49.0	...
1426	Gl 334	2450082.8646	40.2					40.2	...
1430	Gl 334.1	2450086.8525	-27.1					-27.1	...
1439	Gl 336	2450084.8336	10.1					10.1	...
1451	Gl 338 A	2450010.0437	12.4	2450086.8399	13.3	2450230.6321	12.5	12.1	0.7
		2450468.7841	11.3	2450473.8038	11.6	2450500.7802	11.4		
1452	Gl 338 B	2450010.0488	13.2	2450086.8450	12.3	2450230.6354	15.2	13.5	1.0
		2450468.7875	13.9	2450500.7859	13.0				
1460	LTT3412	2450085.9680	15.5					15.5	...
1465	Step 762	2450084.8426	6.5					6.5	...
1483	Gl 341.1	2450086.8616	-14.8					-14.8	...
1501	GJ 1125	2450082.8786	43.7	2450502.8320	44.6	2450505.7877	43.9	44.1	0.4
1507	Gl 352 A	2450085.9778	9.5	2450230.6537	11.5	2450446.9373	8.4	9.5	1.0
		2450473.8337	8.9	2450501.8648	9.4	2450505.7720	9.1		
1509	Gl 353	2450086.8730	19.5	2450087.9012	22.1			20.8	1.3
1522	Gl 357	2450082.8872	-33.3	2450230.6619	-33.0	2450467.9645	-30.8	-33.4	1.4
		2450473.8417	-33.9	2450501.8575	-34.4	2450505.7775	-35.1		
1527	Gl 360	2450086.8814	6.0					6.0	...
1528	Gl 361	2450082.8988	12.5					12.5	...
1529	Gl 362	2450086.8905	5.4	2450502.8492	5.1	2450504.8330	5.1	5.2	0.1
1530	Gl 363	2450084.8545	13.0					13.0	...
1535	LHS2181	2450086.0008	32.9					32.9	...
1537	Gl 366	2450086.8996	-26.2					-26.2	...
1541	GJ 1129	2450082.9202	7.9					7.9	...
1550	Gl 369	2450085.9867	60.8					60.8	...
1553	AC03:239	2450082.9308	13.4					13.4	...
1554	Gl 372	2450082.9074	31.1	2450230.6694	35.2	2450446.9521	7.6	24.0	10.6
		2450467.9716	35.0	2450501.8510	13.9	2450505.7959	21.2		
1558	Gl 373	2450086.9095	19.4	2450473.8221	15.5	2450502.8565	15.8	16.9	1.8
1575	Gl 378	2450010.0368	-6.9					-6.9	...
1583	Gl 378.2	2450082.9400	-16.5					-16.5	...
1586	LHS2224	2450084.8703	43.9					43.9	...
1587	Gl 379 A	2450086.9184	-51.6					-51.6	...
1592	Gl 380	2450086.9255	-23.9	2450086.9289	-19.9			-21.9	2.0
1594	Gl 381 B	2450082.9492	25.4	2450230.6844	27.5	2450446.9594	28.1	27.0	0.9
		2450468.8176	27.3	2450473.8518	27.3	2450501.8891	26.4		
1595	Gl 382	2450086.0094	9.8	2450230.6767	9.8	2450446.9648	8.5	8.9	0.9
		2450468.8300	9.6	2450501.8952	8.3	2450505.8123	7.4		
1596	Gl 383	2450231.6723	-2.9	2450502.9147	-2.2			-2.5	0.3
1605	GJ 2079	2450084.8802	4.9					4.9	...
1611	Gl 386	2450086.0277	-8.1	2450502.8819	-10.6	2450504.8646	-11.1	-9.9	1.3
1616	Gl 388	2450084.8891	12.4	2450087.9096	11.1	2450446.9743	9.4	11.1	1.1
		2450467.9534	11.6						
1630	Gl 390	2450084.8971	22.2	2450086.0182	23.1			22.7	0.4
1642	Gl 393	2449496.6487	8.0	2450467.9952	10.0	2450502.9524	8.4	8.8	0.9
1648	Gl 397	2450086.9372	22.4					22.4	...
1649	Gl 397.1A	2450086.9461	-2.9					-2.9	...
1657	LHS 283	2450084.9767	-50.4					-50.4	...
1658	Gl 398	2450084.9099	19.7					19.7	...

Table 2—Continued

NN	Name	Julian Date	v_{rad}	Julian Date	v_{rad}	Julian Date	v_{rad}	$\langle V_{rad} \rangle$	σ
1662	Gl 399	2450084.9189	3.7					3.7	...
1664	GJ 1134	2450084.9328	-0.4	2450502.8710	-3.5			-2.0	1.5
1671	Gl 400 A	2450084.9421	-1.8					-1.8	...
1678	G058-017	2450084.9513	41.6					41.6	...
1679	LHS 292	2450467.9866	-0.6	2450501.8820	0.3			-0.2	0.4
1682	GJ 1138 B	2450087.9220	55.1	2450230.6933	59.3	2450446.9857	57.5	58.2	1.9
		2450468.8459	58.1	2450500.7965	57.9	2450616.6608	61.3		
1687	Gl 402	2449496.6690	-3.0	2450082.9613	-1.9	2450231.6815	-0.5	-2.5	1.0
		2450446.9953	-2.2	2450468.8572	-2.9	2450501.9057	-3.3		
		2450505.8021	-3.7						
1690	Gl 403	2450084.9633	19.2					19.2	...
1692	LHS2320	2450468.0080	0.8	2450504.8914	0.1	2450615.6847	-0.2	0.2	0.4
1702	Gl 406	2450087.9342	16.7	2450231.6909	19.3	2450468.0216	19.7	17.5	1.7
		2450505.8260	15.6	2450505.8372	16.0				
1705	Wo 9342	2450086.9551	0.4					0.4	...
1709	Gl 408	2450082.9720	4.6	2450231.6484	3.8	2450468.0292	2.8	3.2	1.5
		2450501.9264	0.6	2450615.6707	4.4				
1717	Gl 410	2450082.9814	-14.2					-14.2	...
1719	Gl 411	2450082.9886	-85.7	2450230.6995	-86.0			-85.9	0.2
1723	Gl 412 A	2450086.9641	71.8	2450231.7398	68.5	2450468.8659	69.2	69.6	1.2
		2450500.8158	69.0	2450616.6694	69.6				
1724	Gl 412 B	2450086.9767	69.1	2450231.7525	70.4	2450468.8805	67.6	68.9	0.9
		2450500.8091	68.3	2450616.6816	69.2				
1732	Gl 413.1	2450086.0352	-3.1	2450618.6543	-6.0			-4.5	1.5
1736	Gl 414 A	2450084.9924	-18.9					-18.9	...
1737	Gl 414 B	2450084.9866	-13.0					-13.0	...
1742	G119-062	2450085.0041	3.6					3.6	...
1746	Step 928	2449731.9174	30.0					30.0	...
1748	G010-006	2449764.9662	53.5					53.5	...
1751	Gl 420 A	2449881.6531	7.1					7.1	...
1752	Gl 420 B	2449881.6627	13.6					13.6	...
1756	Gl 421 A	2449496.6812	9.1					9.1	...
1757	Gl 421 B	2449496.6900	10.3					10.3	...
1759	Step 932	2449731.9340	48.9					48.9	...
1765	GJ 1145	2450082.9970	-19.1					-19.1	...
1770	Gl 424	2449731.9433	58.2	2450086.9850	62.6	2450231.6392	61.2	61.0	1.3
		2450286.6661	60.8	2450468.8869	60.0	2450500.8222	60.9		
		2450504.8520	62.4	2450616.6510	61.6				
1771	Gl 425 A	2450083.0128	0.4					0.4	...
1772	Gl 425 B	2450083.0071	2.3					2.3	...
1778	GJ 2084 B	2450083.0208	8.2					8.2	...
1784	LHS2405 A	2449881.6834	14.4					14.4	...
1785	LHS2404 B	2449881.6743	15.8					15.8	...
1795	LHS2415	2449731.9606	34.0					34.0	...
1801	Gl 430.1	2450083.0635	-5.9					-5.9	...
1827	GJ 1148	2450085.0171	-7.4	2450502.9255	-11.7	2450505.8559	-10.1	-9.8	1.8
1830	Gl 436	2449731.9714	7.6					7.6	...
1838	Gl 443	2450083.0303	20.8					20.8	...
1845	Gl 445	2450083.0735	-110.6	2450231.6603	-112.8	2450286.6559	-110.3	-112.2	1.5

Table 2—Continued

NN	Name	Julian Date	v_{rad}	Julian Date	v_{rad}	Julian Date	v_{rad}	$\langle V_{rad} \rangle$	σ
		2450468.8946	-112.3	2450500.8302	-114.9	2450504.8432	-113.9		
		2450616.7055	-111.8	2450670.6439	-110.7				
1847	G010-049A	2450085.0329	6.9					6.9	...
1854	GJ 1151	2450086.9940	-33.8	2450231.7229	-32.7	2450447.0153	-36.0	-35.6	1.6
		2450468.9091	-37.2	2450500.8425	-37.1	2450505.8688	-37.2		
		2450616.6961	-35.2	2450618.6967	-35.6				
1855	Gl 450	2449495.6584	0.9	2450231.6547	-0.8	2450285.6621	2.9	1.0	1.3
		2450447.0224	2.7	2450468.0345	2.0	2450500.8509	0.3		
		2450501.9332	-0.9	2450505.8466	1.7	2450615.6634	0.1		
1862	Gl 452 A	2450083.0396	25.6					25.6	...
1866	Gl 452.1	2450085.0496	3.5					3.5	...
1890	Gl 455	2450083.0536	36.7	2450087.0027	55.7	2450088.9094	29.2	41.1	11.4
		2450088.9961	30.3	2450468.0442	53.5				
1894	G237-043	2449881.7024	4.4					4.4	...
1895	Gl 455.1	2449498.6505	18.6					18.6	...
1898	Gl 456	2449495.6714	4.6	2449495.6838	6.9			5.7	1.2
1905	LHS2520	2449764.9793	78.5	2450087.9554	79.7	2450502.9371	79.8	79.5	0.6
		2450617.6632	80.1						
1907	LTT4562 A	2449881.7226	-9.1					-9.1	...
1915	Gl 458 A	2449890.6685	-19.9					-19.9	...
1921	W0 9397	2449493.6675	-15.4					-15.4	...
1923	GJ 1154 B	2450087.9694	-12.2	2450230.7218	-13.6	2450447.0305	-11.5	-13.7	1.6
		2450468.9224	-15.8	2450500.8772	-16.0	2450504.9089	-14.1		
		2450615.7014	-12.9						
1925	Gl 458.2	2449890.6786	-15.7					-15.7	...
1934	GJ 1156	2450086.0819	8.2	2450088.9554	7.2	2450230.7118	5.2	5.1	1.6
		2450285.6739	6.1	2450447.0404	3.4	2450468.9356	3.5		
		2450500.8642	3.5	2450504.9271	3.6	2450615.7146	4.6		
		2450618.7147	6.0						
1935	Gl 459.3	2449731.9806	-2.3					-2.3	...
1937	Gl 461 B	2449498.6602	4.0					4.0	...
1938	Gl 462	2449880.7268	22.6					22.6	...
1942	G237-064	2449880.7397	14.9					14.9	...
1943	Gl 464	2449496.7037	7.6					7.6	...
1945	Gl 465	2449764.9898	52.5	2450087.9784	50.1	2450231.7048	51.3	51.5	1.2
		2450447.0492	51.2	2450468.9570	50.7	2450500.8985	51.1		
		2450505.8934	50.7	2450617.6731	54.2				
1952	LTT4730 A	2449498.6703	-6.9					-6.9	...
1953	LP735-11B	2449498.6791	-5.1					-5.1	...
1954	Gl 469	2449731.9962	-10.2					-10.2	...
1966	Gl 471	2449493.6777	15.1	2449493.6908	15.1			15.1	0.0
1972	Gl 473 A	2450087.9921	6.4	2450230.7313	2.5	2450468.9805	3.2	2.4	2.1
		2450500.8896	0.1	2450504.9445	0.4	2450615.7252	1.9		
1977	Gl 476	2449732.0091	31.6					31.6	...
1988	Gl 480	2449732.0218	-3.7	2450088.0235	-1.3	2450088.9782	-2.0	-2.3	1.0
2009	Gl 486	2449732.0342	20.8	2450088.0013	18.9	2450231.7137	19.1	19.1	0.8
		2450285.6877	19.3	2450468.9900	19.5	2450500.9222	17.5		
		2450615.7353	18.9	2450618.7254	18.5	2450669.6501	19.0		
2010	GJ 1164 A	2449765.0010	-12.4					-12.4	...

Table 2—Continued

NN	Name	Julian Date	v_{rad}	Julian Date	v_{rad}	Julian Date	v_{rad}	$\langle V_{rad} \rangle$	σ
2011	GJ 1164 B	2449764.9979	-14.4					-14.4	...
2017	Gl 487 B	2449890.6882	-23.2	2450083.0823	-19.0	2450501.9390	-11.9	-16.0	4.3
		2450502.9778	-12.8	2450616.7139	-13.4				
2024	Gl 488	2449496.7142	6.7					6.7	...
2035	Gl 490 A	2449495.6937	-9.7					-9.7	...
2042	Gl 493	2449732.0428	-15.8					-15.8	...
2043	Gl 493.1	2450088.0133	-24.1	2450088.9675	-22.9	2450230.7596	-26.5	-25.5	1.5
		2450285.7043	-25.2	2450468.0524	-25.7	2450500.9117	-27.9		
		2450504.9614	-26.8	2450615.7484	-25.1				
2045	Gl 494 B	2449496.7266	-12.2					-12.2	...
2049	G164-042	2449493.7071	-2.1					-2.1	...
2051	Gl 499 A	2449880.7164	1.2					1.2	...
2085	Gl 505 A	2449881.7268	8.7					8.7	...
2086	Gl 505 B	2449881.7336	4.8					4.8	...
2088	G062-028	2449495.7187	4.8					4.8	...
2093	Gl 507 A	2449881.7432	-15.1					-15.1	...
2094	Gl 507 B	2449881.7552	-7.2					-7.2	...
2096	Gl 507.1	2449498.6872	-12.9	2449732.0557	-13.4			-13.2	0.2
2097	Gl 508 Ab	2449880.7503	3.4	2450087.0199	-1.9	2450231.7327	6.5	1.9	5.2
		2450286.6473	9.7	2450502.9691	-6.5	2450505.8788	-3.4		
		2450616.7228	1.9	2450669.6408	5.9				
2100	Gl 508.2	2449493.7185	-39.8					-39.8	...
2102	LHS 350	2449498.7109	-18.4					-18.4	...
2107	Gl 509 A	2449881.7633	-38.3					-38.3	...
2109	Gl 509.1	2449880.7598	-4.2					-4.2	...
2112	Gl 510	2449765.0088	-29.8					-29.8	...
2118	Gl 512 A	2449765.0199	-41.8					-41.8	...
2123	Gl 514	2449496.7374	15.0	2450085.0602	14.9	2450230.7502	16.5	15.2	0.8
		2450285.6953	15.6	2450447.0747	14.2	2450468.9973	14.7		
		2450501.9577	14.1	2450617.6814	16.6	2450668.6527	15.1		
2128	G165-008B	2449732.0679	3.8	2450087.0380	1.8	2450447.0026	-7.4	-7.5	6.5
		2450447.0596	-4.7	2450469.0057	-16.7	2450469.0130	-18.0		
		2450500.9475	-11.4	2450616.7338	-13.3	2450618.7413	-11.8		
		2450618.7467	-10.1	2450618.7718	-2.6	2450618.8186	-1.6		
		2450668.6611	-5.4						
2137	GJ 1172	2449890.7022	13.7					13.7	...
2150	Gl 519	2449732.0779	-17.8	2449880.7715	-11.1			-14.4	3.4
2151	Gl 520 A	2449890.7098	-21.1					-21.1	...
2156	Gl 521	2449880.7805	-60.7					-60.7	...
2157	Gl 521.1	2449495.7306	28.8					28.8	...
2165	Gl 522	2449493.7313	45.7					45.7	...
2168	LHS2784	2449881.7760	5.5	2450087.0284	8.8	2450230.7406	6.9	6.6	1.1
		2450285.7142	6.9	2450447.0692	5.0	2450468.0623	5.7		
		2450500.9379	5.3	2450616.7431	7.1	2450618.7346	6.2		
		2450668.6713	7.8	2450669.6611	7.3				
2173	Gl 525	2449881.7851	18.9					18.9	...
2175	LHS2794	2449765.0286	5.7	2450089.0057	6.4	2450502.9606	3.5	5.0	1.2
		2450617.6921	4.2						
2176	Gl 526	2449493.7400	16.3	2449498.7220	14.8	2449765.0372	17.7	16.0	1.3

Table 2—Continued

NN	Name	Julian Date	v_{rad}	Julian Date	v_{rad}	Julian Date	v_{rad}	$\langle V_{rad} \rangle$	σ
		2450469.0196	17.6	2450500.9279	15.3	2450615.7562	14.4		
2198	Gl 532	2449890.7191	-46.5					-46.5	...
2199	G150-046	2449493.7527	0.9					0.9	...
2201	Gl 533 B	2449496.7472	-10.5					-10.5	...
2204	GJ 1181 B	2449890.7657	13.9					13.9	...
2209	Gl 534.2	2449880.7889	5.4					5.4	...
2211	LHS2830	2449493.7687	-10.8					-10.8	...
2214	LHS2836	2449890.7818	-15.8					-15.8	...
2216	Gl 536	2449496.7640	-24.6	2450089.0169	-25.9	2450502.9859	-27.1	-25.3	1.4
		2450617.6990	-23.5						
2220	Vyss. 150	2449498.7320	-9.0					-9.0	...
2222	Gl 537 A	2449890.7292	-42.2					-42.2	...
2223	Gl 537 B	2449890.7380	-41.2					-41.2	...
2235	Gl 540	2449880.7991	16.2					16.2	...
2242	LTT5580 B	2449890.7914	-4.1					-4.1	...
2256	LHS2887 B	2449890.7542	-23.4	2450088.0350	-20.0	2450502.9957	-26.5	-24.4	2.3
		2450504.9776	-24.6	2450617.7107	-25.1	2450670.6572	-26.9		
2259	Gl 541.2	2449495.7382	4.4					4.4	...
2268	Gl 545	2449890.8073	53.2					53.2	...
2278	Gl 548 A	2449496.7762	8.7					8.7	...
2279	Gl 548 B	2449496.7886	8.6					8.6	...
2281	Gl 549 B	2449495.7507	-9.9					-9.9	...
2295	Gl 552	2449765.0680	6.0					6.0	...
2299	Gl 553	2449497.7417	-21.1	2449765.0580	-24.2			-22.6	1.5
2300	Gl 553.1	2449498.7497	0.5					0.5	...
2310	Gl 555	2449881.7999	-3.2	2450087.0644	0.4	2450230.7716	-1.9	-1.9	1.4
		2450468.0700	-2.5	2450500.9555	-4.4	2450615.7680	-0.9		
		2450618.7580	-0.8	2450668.6839	-1.9				
2316	LHS2952	2449495.7663	-26.6					-26.6	...
2324	Wo 9490 A	2449881.8067	-29.2					-29.2	...
2326	Wo 9490 C	2449881.8139	-26.6					-26.6	...
2329	Wo 9492	2449880.8114	21.1					21.1	...
2335	Gl 562	2449890.8156	42.6					42.6	...
2339	Gl 563.1	2449561.6501	-13.1					-13.1	...
2352	G066-037	2449498.7658	5.7					5.7	...
2356	Gl 568 A	2449890.8312	-34.2	2450089.0308	-35.8	2450504.9868	-38.3	-36.2	1.5
		2450617.7217	-36.4						
2358	Gl 569 Bb	2449561.6599	-7.1	2450230.7808	-8.0	2450501.9670	-5.7	-6.9	0.8
		2450504.9964	-6.9						
2359	LHS2998	2449561.6753	-39.7	2450088.0439	-39.3	2450503.0045	-42.5	-40.4	1.3
		2450616.7540	-40.1						
2367	Gl 570 A	2450087.0673	31.1	2450231.7654	27.1	2450500.9759	28.1	28.8	1.5
		2450615.7993	27.7	2450668.6883	29.8				
2368	Gl 570 B	2449890.8400	34.4	2450087.0728	29.3	2450231.7716	35.9	33.2	2.8
2374	Gl 570.2	2449880.8277	6.9	2450469.0280	8.6			7.8	0.9
2377	Vyss. 734	2449496.7993	-27.0					-27.0	...
2378	Gl 571.1	2449560.6472	14.3					14.3	...
2379	LHS3012	2449765.0480	-17.3					-17.3	...
2380	G015-002	2449560.6633	-6.6					-6.6	...

Table 2—Continued

NN	Name	Julian Date	v_{rad}	Julian Date	v_{rad}	Julian Date	v_{rad}	$\langle V_{rad} \rangle$	σ
2381	Gl 572	2449496.8141	-11.1					-11.1	...
2390	Gl 576	2449548.6459	-83.3	2449548.6514	-83.2			-83.3	0.1
2392	LHS3018	2449495.7758	-24.7					-24.7	...
2397	Gl 579	2449890.8465	-70.7					-70.7	...
2399	LHS3030	2449498.7829	-32.3					-32.3	...
2419	LHS3056	2449493.8015	-29.1					-29.1	...
2420	Gl 581	2449547.6504	-10.4	2449547.6564	-10.7	2450447.0792	-9.4	-10.3	0.5
		2450500.9716	-10.5						
2427	Gl 583	2449890.8541	-19.0					-19.0	...
2428	Wo 9520	2449496.8294	6.4	2450089.0396	5.8	2450505.9116	7.9	7.4	1.4
		2450617.7317	9.9	2450670.6665	7.1				
2453	Gl 589 A	2449561.6935	-43.7					-43.7	...
2456	LHS3091	2449495.8028	-59.9					-59.9	...
2458	Gl 592	2449547.6760	1.5					1.5	...
2464	Gl 595	2449560.6790	80.3	2450088.0505	80.5	2450230.7963	77.0	78.6	2.1
		2450285.7437	79.2	2450500.9850	81.9	2450615.7794	75.9		
		2450618.7688	76.4	2450668.6995	77.3				
2467	Gl 596 A	2449549.6685	2.5					2.5	...
2472	Gl 597	2449890.8723	-42.2					-42.2	...
2477	LHS3117	2449498.7996	1.0					1.0	...
2486	Gl 600	2449493.8254	-10.1					-10.1	...
2504	Gl 606	2449548.6619	-16.6	2450089.0473	-17.2	2450617.7416	-16.4	-17.0	0.6
		2450670.6766	-18.0						
2516	Gl 609	2449549.6852	5.2	2450087.0448	6.2	2450231.7844	6.1	5.7	0.6
		2450285.7271	5.6	2450501.9774	4.6	2450615.7877	6.2		
		2450668.7088	6.0						
2536	Gl 612.1	2449880.8387	2.5					2.5	...
2543	Vyss. 759	2449496.8433	-18.8					-18.8	...
2552	LHS3169	2449561.7197	-50.1					-50.1	...
2563	Gl 616.2	2449548.6688	-27.5					-27.5	...
2566	Gl 617 A	2449493.8313	-20.6	2450089.0672	-16.6	2450617.7527	-16.7	-18.4	1.8
		2450670.6892	-19.5						
2567	Gl 617 B	2449493.8408	-21.9	2450089.0619	-17.6	2450617.7463	-15.8	-19.1	2.5
		2450670.6821	-21.0						
2576	Gl 619	2449880.8463	5.8					5.8	...
2578	Gl 620	2449890.8646	-30.3					-30.3	...
2582	Gl 622	2449547.6876	-63.1					-63.1	...
2583	Gl 623	2449548.6786	-23.7					-23.7	...
2587	LTT14889	2449548.6995	-44.3					-44.3	...
2589	Gl 625	2449560.6871	-10.1	2450087.0564	-12.3	2450231.7896	-14.2	-12.0	1.4
		2450286.6864	-11.4	2450501.0038	-11.4	2450616.7623	-14.3		
		2450618.7801	-11.7	2450669.7167	-10.9				
2599	Gl 628	2449547.6972	-22.8	2450088.0559	-17.3	2450230.8041	-20.4	-21.3	1.7
		2450285.7350	-21.6	2450501.0608	-22.8	2450615.7965	-21.7		
		2450668.7208	-21.3	2450669.6734	-22.6				
2616	Gl 630.1C	2449881.8517	-191.0					-191.0	...
2618	LP275-68	2449549.7018	4.0					4.0	...
2622	Gl 632.1	2449880.8562	-10.1					-10.1	...
2642	Gl 638	2449495.8124	-31.7	2449880.8644	-31.7	2450505.0032	-30.8	-31.1	0.7

Table 2—Continued

NN	Name	Julian Date	v_{rad}	Julian Date	v_{rad}	Julian Date	v_{rad}	$\langle V_{rad} \rangle$	σ
		2450617.7670	-30.1						
2644	LHS3240	2449560.7030	19.5					19.5	...
2647	LP806-8	2449495.8246	-78.9	2449547.7073	-78.0			-78.5	0.5
2656	AG38:152	2449498.8073	-18.4	2450089.0713	-21.4	2450231.7984	-20.9	-18.9	1.6
		2450303.6501	-18.5	2450468.0864	-16.0	2450500.9955	-19.8		
		2450616.7859	-19.5	2450618.7907	-18.2	2450669.7094	-17.8		
2659	Gl 642	2449890.8891	-66.9					-66.9	...
2660	Gl 643	2449495.8370	17.9	2450230.8136	15.9	2450231.8373	15.6	15.2	1.3
		2450285.7545	15.4	2450304.6469	13.2	2450501.9857	14.8		
		2450615.8101	14.9	2450669.6842	14.1				
2661	Gl 644 A	2449495.8463	14.7	2450230.8217	15.1	2450231.8283	8.4	14.2	2.3
		2450285.7617	14.6	2450304.6405	14.9	2450501.9935	15.7		
		2450615.8172	16.1	2450669.6914	14.0				
2665	GJ 1207	2449495.8620	-1.2	2450230.8309	-2.4	2450285.7710	-4.1	-4.2	1.6
		2450304.6560	-6.2	2450502.0030	-6.2	2450505.0152	-5.3		
		2450615.8267	-4.0	2450669.7026	-4.6				
2673	Gl 649	2449498.8175	4.4	2450617.7752	6.7			5.6	1.1
2674	G139-003	2449549.7250	-26.4					-26.4	...
2684	Step 1422	2449548.7115	-21.3					-21.3	...
2688	LHS3262	2450230.8390	36.6	2450286.7534	38.5	2450304.6700	35.6	36.9	1.3
		2450468.0810	36.0	2450501.0261	35.9	2450616.7763	39.6		
		2450618.8021	36.9	2450669.7302	36.2				
2691	Wo 9582 B	2449880.8701	-71.6					-71.6	...
2692	Gl 654	2449548.7209	34.8	2449890.9002	34.2			34.5	0.3
2700	Gl 655	2449498.8308	-50.3					-50.3	...
2708	G203-047A	2449498.8453	-53.6	2450230.8495	-67.5	2450286.7348	-9.5	-42.8	32.0
		2450304.6792	-63.8	2450501.0128	-58.9	2450616.7954	-49.3		
		2450618.8127	-67.7	2450669.7437	27.9				
2712	Gl 660 A	2449548.7368	-6.7					-6.7	...
2714	LTT15087	2449498.8589	-44.5	2450230.8589	-45.2	2450286.7448	-45.7	-45.2	0.6
		2450304.6867	-46.0	2450501.0541	-45.4	2450616.8050	-44.0		
		2450618.8297	-45.8	2450669.7533	-45.4				
2717	Gl 661 A	2449559.6915	-28.5	2450231.8051	-29.5	2450286.7234	-30.5	-29.8	1.1
		2450304.6933	-31.0	2450503.0095	-31.2	2450616.8115	-28.1		
		2450618.8349	-29.0	2450669.7603	-30.5				
2719	GJ 1212	2449549.7426	-1.6					-1.6	...
2727	BP 78844	2449493.8556	-1.9					-1.9	...
2728	Step 1453	2449546.7306	-16.1					-16.1	...
2729	G139-023	2449881.8661	-44.6					-44.6	...
2730	GJ 2128	2449560.7168	-30.4					-30.4	...
2741	Vyss. 791	2449493.8643	-28.9					-28.9	...
2744	Gl 669 A	2449560.7287	-34.2	2449881.8872	-36.8	2450617.7956	-36.7	-35.9	1.1
		2450670.7104	-36.0						
2745	Gl 669 B	2449881.8781	-36.7	2450617.8063	-36.4	2450670.7194	-36.1	-36.4	0.2
2748	Gl 671	2449559.7113	-19.3					-19.3	...
2756	Gl 673	2449561.7779	-21.9	2449881.8953	-24.3			-23.1	1.2
2760	LHS3291	2449560.7543	-15.8					-15.8	...
2768	Gl 677 A	2450615.8297	-7.1					-7.1	...
2772	Gl 678.1A	2449546.7415	-12.9					-12.9	...

Table 2—Continued

NN	Name	Julian Date	v_{rad}	Julian Date	v_{rad}	Julian Date	v_{rad}	$\langle V_{rad} \rangle$	σ
2788	LP920-69	2449495.8733	6.8					6.8	...
2789	Gl 685	2449496.8855	-14.0					-14.0	...
2792	Gl 686	2449498.8702	-9.6					-9.6	...
2797	Gl 687	2449492.8836	-27.2	2449561.7308	-26.8	2450231.8085	-29.1	-28.4	1.2
		2450286.7596	-29.4	2450303.6758	-30.1	2450501.0446	-28.4		
		2450616.8153	-27.4	2450618.8419	-27.5	2450668.7640	-29.7		
2804	Vyss. 796	2449880.8807	-26.1					-26.1	...
2814	G140-009	2449493.8728	-7.1					-7.1	...
2817	Gl 694	2449560.7626	-14.8					-14.8	...
2821	LHS3324	2449547.7295	-78.6					-78.6	...
2824	Gl 695 B	2449548.7460	-13.2	2450231.8449	-14.7	2450286.7720	-13.8	-14.1	0.9
		2450503.0499	-15.2	2450616.8269	-12.7	2450669.7736	-15.2		
		2450670.7367	-14.2						
2830	Gl 696	2449495.8827	-25.4					-25.4	...
2846	G183-013	2449547.7473	-41.2					-41.2	...
2849	Gl 699	2449493.8821	-110.8	2450231.9153	-110.9	2450285.8032	-110.8	-111.1	0.4
		2450304.7027	-110.8	2450503.0416	-111.7	2450505.0214	-111.5		
		2450615.8576	-110.8	2450617.8157	-111.9	2450668.7302	-110.8		
		2450670.7285	-111.1						
2851	LHS3343	2449546.7666	-31.9					-31.9	...
2859	Gl 701	2449495.8920	31.6	2449890.9110	32.8	2450005.5973	33.1	32.5	0.6
2860	G182-037	2449880.8927	-13.1					-13.1	...
2865	GJ 1224	2450231.8566	-33.3	2450285.7901	-33.5	2450304.7230	-35.9	-34.8	1.7
		2450502.0144	-34.7	2450615.8496	-33.5	2450668.7470	-38.0		
2882	Gl 708.2	2449547.7576	7.5					7.5	...
2885	Gl 709	2449548.7671	-36.1					-36.1	...
2888	LHS 462 A	2449548.7583	0.1					0.1	...
2892	Gl 710	2449495.9010	-13.5					-13.5	...
2895	GJ 1226	2449493.9000	-34.0					-34.0	...
2897	LHS3376	2450230.8654	4.6	2450231.9302	5.7	2450286.8050	4.8	5.0	0.8
		2450303.6693	4.5	2450502.0312	4.1	2450616.8365	6.4		
		2450618.8557	5.4	2450668.7569	4.0				
2898	Gl 712	2449547.7785	-44.4					-44.4	...
2901	LTT15435	2449498.8852	-21.8					-21.8	...
2904	GJ 1227	2450230.8753	-13.7	2450286.7828	-14.8	2450303.6941	-14.8	-14.4	0.6
		2450502.0438	-14.8	2450616.8508	-13.4	2450668.7776	-15.0		
2905	G183-041	2450618.8699	-11.7					-11.7	...
2916	G205-028	2449492.9106	-17.7	2449492.9291	-17.6	2449559.7740	-19.3	-18.2	0.8
2917	Gl 717	2449881.9050	-89.8					-89.8	...
2921	LP229-17	2449498.8975	14.6	2450231.8708	12.6	2450286.7947	12.2	12.4	1.1
		2450303.7042	11.3	2450502.0526	10.8	2450616.8626	13.6		
		2450618.8828	12.0	2450668.7888	12.1				
2923	Gl 720 A	2449549.7609	-30.4					-30.4	...
2924	Gl 720 B	2449549.7838	-32.2					-32.2	...
2925	G141-021	2449559.7377	-43.3					-43.3	...
2928	GJ 2138	2449493.9127	-39.7					-39.7	...
2933	Gl 724	2449495.9110	-32.6					-32.6	...
2935	GJ 1230 Ab	2449880.9305	-15.1	2449881.8280	-35.8	2449881.9416	-41.0	-37.6	16.2
		2450231.9449	-49.0	2450304.7445	-13.0	2450617.8509	-57.0		

Table 2—Continued

NN	Name	Julian Date	v_{rad}	Julian Date	v_{rad}	Julian Date	v_{rad}	$\langle V_{rad} \rangle$	σ
		2450668.8126	-52.2						
2936	GJ 1230 B	2450304.7374	-11.8	2450617.8415	-10.8			-11.2	0.5
2937	LP25-02	2449559.7571	10.4					10.4	...
2940	G206-040	2449548.7815	-30.1	2450617.8228	-30.2			-30.1	0.1
2942	G141-029	2449498.9468	-33.2					-33.2	...
2945	Gl 725 A	2449492.9339	-1.6	2449498.9058	0.2	2449561.7634	-2.4	-1.3	1.1
2946	Gl 725 B	2449492.9433	0.2	2449561.7588	-0.8			-0.3	0.5
2947	LTT7434	2449560.7826	-32.2	2450617.8628	-31.7			-32.0	0.3
2953	Gl 726	2449881.9119	12.4					12.4	...
2958	Gl 728	2449546.8036	-22.0					-22.0	...
2960	Gl 729	2449495.9238	-10.6	2450231.8640	-10.5	2450285.7969	-10.9	-10.9	0.9
		2450303.7243	-12.2	2450503.0300	-12.2	2450615.8660	-10.7		
		2450670.7467	-9.4						
2961	Gl 730	2449549.7974	-2.8					-2.8	...
2964	G205-038	2449546.7902	-76.9					-76.9	...
2966	Gl 731	2449548.7919	-10.5					-10.5	...
2974	Gl 734 A	2449547.7903	-24.1					-24.1	...
2976	Gl 735	2449546.8135	-6.2					-6.2	...
2988	Gl 740	2449496.9075	11.2					11.2	...
3004	Gl 745 A	2449493.9312	32.8	2450231.8884	31.6	2450303.7315	32.2	33.0	1.4
		2450618.8927	35.3						
3005	Gl 745 B	2449493.9401	25.3	2450231.8954	31.8	2450303.7387	32.0	31.2	3.7
		2450618.8998	35.5						
3009	Gl 747 A	2449547.8099	-45.4	2450231.8801	-47.7	2450286.8184	-47.3	-47.3	1.3
		2450304.7529	-49.6	2450616.8725	-46.5	2450668.8222	-47.2		
3013	G207-019	2449493.9519	-1.7					-1.7	...
3016	Step 1680	2449880.9155	-24.3					-24.3	...
3017	GJ 1232	2450617.8749	-14.5					-14.5	...
3022	LP336-6	2449548.8003	-24.3					-24.3	...
3024	Gl 748	2449495.9343	-40.4	2450231.9053	-41.2	2450285.8139	-41.6	-41.4	0.8
		2450304.7845	-42.5						
3036	Gl 751	2449497.9418	-72.3					-72.3	...
3037	Gl 752 A	2449498.9267	36.3					36.3	...
3044	Gl 754.1B	2450005.6230	11.4	2450617.9002	14.0			12.7	1.3
3048	GJ 1235	2450615.8737	5.1	2450615.8828	5.4	2450617.8880	3.5	4.7	0.8
3049	GJ 1236	2449495.9502	27.3					27.3	...
3057	G185-022	2449493.9681	-41.1					-41.1	...
3060	GJ 1238	2450618.9044	-20.1					-20.1	...
3068	Gl 761.2	2449495.9603	-48.2					-48.2	...
3074	Gl 763	2449493.9221	-59.8					-59.8	...
3076	Vyss. 811	2449498.9569	-19.5					-19.5	...
3081	Gl 764.1B	2449495.9700	65.1					65.1	...
3100	Gl 766 A	2449881.9256	-5.4	2450617.9110	-5.8			-5.6	0.2
3102	G125-030	2449495.9780	-16.6					-16.6	...
3103	Gl 767 A	2449497.9506	-4.6					-4.6	...
3104	Gl 767 B	2449497.9628	-5.7					-5.7	...
3113	GJ 1243	2449492.9631	-13.1	2449880.9426	-14.5	2449881.8392	-14.6	-14.1	0.6
		2449881.9527	-14.2						
3120	GJ 1245 Ab	2450021.6522	4.2	2450230.8854	5.5	2450286.8301	4.9	5.1	1.1

Table 2—Continued

NN	Name	Julian Date	v_{rad}	Julian Date	v_{rad}	Julian Date	v_{rad}	$\langle V_{rad} \rangle$	σ
		2450303.7536	4.0	2450616.8848	7.3	2450670.7638	4.4		
3121	GJ 1245 B	2450021.6642	3.0	2450230.8941	5.3	2450286.8379	4.6	4.8	0.9
		2450616.9014	5.7	2450670.7794	5.1				
3132	Wo 9677 A	2449547.8304	11.9					11.9	...
3147	GJ 1248	2449493.9848	30.8					30.8	...
3179	Gl 786	2449560.8017	0.7					0.7	...
3181	Gl 786.1	2449560.8145	15.8					15.8	...
3193	Gl 791	2449559.8064	-3.7					-3.7	...
3194	G186-027	2450286.8643	-63.3					-63.3	...
3195	GJ 1253	2450021.6368	-60.2	2450230.9022	-59.5	2450303.7852	-61.6	-60.4	0.7
		2450616.9164	-60.4	2450617.9258	-59.9	2450668.8370	-61.0		
3198	Gl 791.2	2450230.9474	-28.7	2450285.8316	-27.5	2450304.7977	-30.4	-28.6	1.2
		2450615.8954	-27.2	2450668.8546	-29.3				
3203	Gl 793	2449495.9855	12.0	2449498.9723	9.7	2450021.6219	10.5	10.2	1.5
		2450087.5630	8.2	2450087.5704	12.1	2450230.9087	10.9		
		2450286.8421	9.3	2450303.7660	11.8	2450303.7909	10.8		
		2450616.9344	11.6	2450670.7496	7.4	2450670.8239	8.6		
3206	G186-029	2450616.9294	-18.7					-18.7	...
3209	GJ 1254	2449548.8204	-21.5					-21.5	...
3224	GJ 1256	2450088.5906	-57.8	2450230.9210	-59.6	2450285.8406	-60.3	-60.2	1.1
		2450303.8768	-61.5	2450304.7746	-60.5	2450615.9262	-60.9		
		2450668.8674	-60.6						
3231	GJ 1257	2449547.8246	-38.4					-38.4	...
3234	Gl 800 A	2449880.9559	3.8					3.8	...
3242	LTT16064A	2449549.8277	-26.9					-26.9	...
3243	LTT16065B	2449549.8183	-28.3					-28.3	...
3244	Gl 804	2449497.9965	3.9	2449498.9936	4.2			4.0	0.1
3247	Gl 806	2449498.9825	-24.2					-24.2	...
3263	Gl 809	2449498.9628	-15.4	2449880.9858	-20.0	2450008.5902	-17.2	-17.5	1.9
3265	Gl 810 A	2449497.9861	-141.9					-141.9	...
3268	Gl 811.1	2449546.8274	33.5					33.5	...
3269	Gl 812 A	2449546.8400	-42.1					-42.1	...
3278	Gl 815 A	2449547.8417	4.6					4.6	...
3284	Gl 816	2449546.8534	-15.1					-15.1	...
3299	Gl 819 B	2449549.8394	-53.0					-53.0	...
3300	Gl 820 A	2449561.7978	-66.6	2449880.9729	-70.9	2450005.6371	-65.7	-66.0	1.9
		2450086.5557	-64.9	2450088.5643	-63.5	2450230.9865	-67.0		
		2450286.8532	-66.5	2450303.7963	-65.7	2450616.9436	-64.3		
		2450668.8751	-65.2						
3301	Gl 820 B	2449561.8008	-62.8	2449880.9712	-62.7	2450005.6354	-66.3	-64.0	1.3
		2450086.5580	-63.3	2450088.5674	-65.5	2450230.9893	-62.9		
		2450286.8553	-64.4	2450303.7991	-64.9	2450616.9464	-62.5		
		2450668.8775	-64.6						
3307	Gl 821	2449546.8634	-55.6	2450009.6195	-57.7			-56.7	1.1
3308	Wo 9722	2449560.8600	-263.7	2450009.6076	-266.0	2450286.8823	-267.3	-266.2	1.6
		2450303.8145	-267.7						
3312	G187-029	2449547.8584	-10.4					-10.4	...
3323	LTT16240A	2449548.8398	-4.8					-4.8	...
3352	Gl 828.1	2449546.8722	-6.6					-6.6	...

Table 2—Continued

NN	Name	Julian Date	v_{rad}	Julian Date	v_{rad}	Julian Date	v_{rad}	$\langle V_{rad} \rangle$	σ
3356	G188-001	2449880.9640	-69.6					-69.6	...
3360	Gl 829 B	2449547.8688	-20.3	2450086.5623	-25.9	2450230.9265	-25.9	-25.1	2.0
		2450285.8463	-25.7	2450303.8641	-26.2	2450615.9120	-25.1		
		2450668.8735	-26.8						
3361	Gl 830	2449546.8827	-82.9					-82.9	...
3363	Gl 831 A	2449881.9694	-56.2	2450230.9564	-57.5	2450285.8570	-57.5	-57.5	0.6
		2450303.8554	-58.2	2450615.9046	-57.3	2450670.8393	-58.0		
3367	LP397-34B	2449547.8858	1.2					1.2	...
3370	LHS3686 A	2449548.8660	-19.8					-19.8	...
3372	LHS3693	2449549.8504	-14.1					-14.1	...
3375	Gl 834 A	2449549.8611	2.1					2.1	...
3378	Gl 835	2449547.8956	-11.9					-11.9	...
3380	G231-051	2449549.8694	-43.0					-43.0	...
3398	Gl 836.8	2449559.8137	10.4					10.4	...
3403	GJ 1263	2449548.8833	-28.4	2449561.8297	-28.0			-28.2	0.2
3436	Gl 839	2449559.8230	-48.1					-48.1	...
3444	G018-008	2449881.9778	-27.0					-27.0	...
3452	Gl 842.2	2449559.8326	-15.0					-15.0	...
3453	G188-038	2449547.9113	-7.2	2450021.6900	-8.4	2450087.5912	-8.0	-5.4	1.8
		2450230.9351	-3.2	2450231.9198	-5.8	2450231.9871	-3.3		
		2450285.8641	-6.0	2450303.8340	-5.9	2450447.6060	-6.3		
		2450473.5866	-4.0	2450616.9558	-3.4	2450670.8468	-3.6		
3454	Gl 843	2449546.9057	-23.2					-23.2	...
3455	Gl 844	2449547.9220	-12.3					-12.3	...
3458	Gl 846	2449548.8936	19.4					19.4	...
3466	LTT8848	2449546.9160	18.8					18.8	...
3478	Gl 849	2449546.9254	-15.4	2450087.5976	-17.5	2450230.9733	-15.7	-16.2	0.6
		2450285.8719	-16.0	2450304.8289	-16.3	2450617.9789	-16.3		
		2450670.8575	-16.1						
3486	Gl 851	2449881.9866	-53.0					-53.0	...
3489	GJ 1265	2450617.9435	-25.0	2450670.8214	-24.5			-24.8	0.3
3502	Gl 852 A	2450617.9565	34.2	2450670.7957	35.0			34.6	0.4
3503	Gl 852 B	2450617.9724	35.0	2450670.8080	34.3			34.6	0.3
3517	LHS3799	2450008.6096	-4.0	2450230.9655	-1.6	2450231.9635	-1.9	-2.1	1.1
		2450285.8811	-3.0	2450615.9389	-2.0	2450668.8915	-0.4		
3519	Gl 856 A	2449549.9073	-18.2	2450618.9336	-20.1			-19.2	0.9
3526	G232-070	2449549.8912	2.2					2.2	...
3537	Gl 860 A	2450005.6464	-32.7	2450021.6770	-33.7	2450086.5722	-32.6	-34.1	1.1
		2450231.9491	-33.9	2450286.8714	-34.4	2450303.9257	-34.7		
		2450304.8318	-36.3	2450468.5965	-34.6	2450616.9614	-33.6		
3538	Gl 860 B	2450005.6551	-33.2					-33.2	...
3542	GJ 1270	2450005.6717	0.0					0.0	...
3544	Gl 863	2449548.9024	-4.8	2449881.9953	-6.0	2450009.6312	-5.3	-5.4	0.5
3546	Step 2018A	2449546.9420	-4.8					-4.8	...
3553	Gl 864	2449546.9515	8.9					8.9	...
3558	G189-030	2449549.9163	-53.2					-53.2	...
3559	LTT9123 A	2449547.9336	25.7	2450008.6455	26.5			26.1	0.4
3560	LTT9124 B	2450008.6361	25.6					25.6	...
3561	Gl 866 C	2450008.6234	-19.1	2450086.5931	-55.7			-37.4	18.3

Table 2—Continued

NN	Name	Julian Date	v_{rad}	Julian Date	v_{rad}	Julian Date	v_{rad}	$\langle V_{rad} \rangle$	σ
3562	Gl 867 A	2449546.9618	-53.2	2450086.5754	-21.6	2450231.9785	-18.9	-21.2	27.9
		2450285.8878	-52.6	2450304.8424	20.1	2450304.8557	21.5		
		2450616.9902	-46.7	2450668.8989	-18.4				
3563	Gl 867 B	2449546.9743	-6.3	2450086.5842	-28.5	2450231.9730	-27.4	-7.0	19.4
		2450285.8962	-27.7	2450304.8513	9.5	2450616.9845	14.7		
		2450668.9081	16.9						
3576	GJ 1272 A	2449559.8601	-1.0				-1.0	...	
3584	Gl 873	2449559.8447	0.5	2450286.8926	-0.6		0.0	0.5	
3592	Gl 875	2449548.9218	-8.4				-8.4	...	
3604	Gl 876	2449546.9835	-3.3				-3.3	...	
3609	Gl 878	2449549.9308	-28.8				-28.8	...	
3611	G028-024A	2450008.6581	10.4				10.4	...	
3614	Step 2065	2449548.9112	-33.2				-33.2	...	
3616	Gl 880	2449559.8692	-27.6	2450304.8688	-26.6		-27.1	0.5	
3621	Gl 884	2449548.9299	14.1	2450086.5982	16.4	2450231.9945	17.1	16.6	1.1
		2450285.9009	16.7	2450304.8601	17.6	2450616.9957	17.0		
		2450668.9145	17.3						
3629	GJ 1278	2449560.8700	8.5				8.5	...	
3636	LHS 535	2449559.8816	22.5				22.5	...	
3637	Gl 889.1	2450005.6826	31.4				31.4	...	
3641	G028-044	2449548.9459	-7.4				-7.4	...	
3645	Gl 891	2449547.9636	-8.1				-8.1	...	
3653	GJ 2154 A	2449547.9729	2.0				2.0	...	
3672	G067-053	2450005.6946	-3.7				-3.7	...	
3674	V862	2450008.6692	21.2				21.2	...	
3686	LHS 543	2449548.9580	-8.2	2450021.7012	-9.4	2450087.6193	-10.0	-7.6	1.2
		2450230.9803	-6.8	2450285.9085	-6.4	2450303.8933	-6.9		
		2450447.5932	-8.6	2450467.5928	-6.5	2450473.5977	-6.4		
		2450615.9462	-7.3	2450668.9231	-7.4				
3689	Gl 895	2449549.9405	-31.3				-31.3	...	
3693	GJ 2155	2449549.9853	-43.4				-43.4	...	
3699	G190-028A	2449559.8970	-12.5				-12.5	...	
3700	G190-027B	2449559.9128	-13.3				-13.3	...	
3701	GJ 1284	2449547.9855	11.7	2450086.6108	-4.7	2450285.9201	-16.7	5.1	17.6
		2450303.9187	30.1						
3705	Gl 896 A	2449560.8831	0.5	2450021.7107	-2.4	2450085.5878	-1.1	-0.5	1.1
		2450285.9251	0.2	2450303.8997	-0.8	2450447.5816	-2.1		
		2450473.6046	1.2	2450615.9883	0.1	2450618.9401	-0.1		
		2450668.9313	-0.6						
3706	Gl 896 B	2450021.7194	-0.6	2450285.9338	2.7	2450303.9087	2.1	2.2	1.5
		2450473.6127	4.4	2450618.9486	2.8	2450668.9401	1.8		
3708	Gl 897 A	2449546.9923	-0.8				-0.8	...	
3710	Gl 898	2450005.7045	0.7				0.7	...	
3712	Gl 899	2449548.9682	-5.0				-5.0	...	
3713	Gl 900	2449548.9772	-10.1				-10.1	...	
3715	GJ 1286	2450086.6249	-41.4	2450285.9457	-41.9	2450304.8989	-41.7	-41.9	0.6
		2450467.6058	-43.1	2450615.9664	-42.1	2450615.9741	-41.0		
		2450668.9581	-41.9						
3729	G273-093	2449549.9762	19.7				19.7	...	

Table 2—Continued

NN	Name	Julian Date	v_{rad}	Julian Date	v_{rad}	Julian Date	v_{rad}	$\langle V_{rad} \rangle$	σ
3743	G1 905	2450009.6768	-77.5	2450021.7285	-78.5	2450087.6458	-76.8	-77.7	0.7
		2450286.9013	-77.9	2450304.8830	-77.8	2450447.6189	-78.7		
		2450468.6061	-77.6	2450473.6224	-77.3	2450616.9711	-78.4		
		2450670.8636	-76.5						
3748	GJ 1289	2450009.6641	-4.5	2450085.6780	-4.6	2450286.9113	-2.7	-3.7	0.9
		2450303.9434	-4.8	2450446.6274	-4.5	2450468.6349	-2.5		
		2450615.9549	-3.5	2450670.8742	-2.6				
3753	LHS4009	2450087.6595	-3.3	2450304.9120	-3.5	2450467.6191	-3.7	-3.5	0.2
3754	G1 906	2449549.9510	-19.4					-19.4	...
3756	G1 907	2450008.6820	20.1					20.1	...
3757	G1 907.1B	2449560.8940	-10.0					-10.0	...
3759	G1 908	2449548.0035	-71.7	2450446.5903	-71.6	2450668.9678	-72.8	-72.0	0.5
3767	LHS4022	2449547.9938	-7.2	2450085.6668	-8.2	2450304.9216	-6.8	-7.4	1.0
		2450446.6157	-9.2	2450467.6317	-5.6	2450618.9580	-7.8		
		2450669.7982	-7.1						
3775	G1 910	2449549.9609	3.8					3.8	...
3782	G1 912	2449548.9866	17.1					17.1	...
3784	G273-186A	2449560.9265	17.4					17.4	...
3785	G273-185B	2449560.9104	37.9					37.9	...
3786	GJ 1292	2450005.7161	-32.4					-32.4	...
3791	G1 913	2449549.9922	8.4	2449559.9220	6.8			7.6	0.8
3796	GJ 1293	2449548.9960	1.9					1.9	...
	LHS 1169	2450087.7	10.1						
	G 173-18	2450087.7	-17.9	49.9	SB2				
	G 134-15/LP197-12	2450087.7	-73.8		unresolved				

Table 3. Emission Lines

Name	PC1	PC2	F1	F2	PC3	PC4
He D3	5866.6	5872.1	5874.7	5876.7	5877.6	5879.1
He6678	6675.2	6676.1	6677.8	6678.9	6679.1	6680.2
H α	6557.7	6560.0	6561.0	6564.6	6566.2	6568.4
H β	4854.7	4857.5	4860.3	4863.3	4865.0	4870.0
H γ	4335.3	4336.9	4339.4	4341.8	4343.4	4347.4
H δ	4097.2	4100.3	4100.9	4102.5	4102.9	4105.0
H ϵ	3969.2	3969.6	3969.8	3970.9	3971.2	3972.2
H6	3887.0	3887.8	3888.5	3889.5	3890.0	3891.7

Table 4. Equivalent Widths

NN	H α	HeD3	He6678	H β	H γ	H δ	H ϵ	H6	N _{Hα}	$\sigma_{\text{H}\alpha}$	$\sigma_{\text{H}\beta}$
7	-0.396	0.034	-0.057	-0.130	1
11	-0.570	0.054	-0.149	-0.184	1
12	-0.585	0.045	-0.156	-0.208	1
19	0.108	-0.287	0.258	1.701	3	0.190	3.681
38	-0.325	0.075	-0.065	-0.053	1
41	-0.224	-0.020	0.078	1.513	6	0.056	3.511
43	-0.326	-0.011	0.066	-0.223	1
54	-0.569	0.033	-0.187	-0.231	2	0.090	0.037
60	-0.338	0.031	-0.043	-0.096	2	0.035	0.035
61	-0.124	0.039	0.112	0.226	1
76	-0.307	0.093	-0.047	0.036	1
83	10.394	-0.208	0.200	2	9.088	...
87	-0.399	0.022	-0.081	-0.170	1
89	-0.323	-0.035	0.085	-0.257	3	0.021	0.269
92	-0.207	0.021	-0.015	0.060	9	0.048	0.127
93	-0.245	0.045	0.053	0.167	5	0.070	0.299
96	5.226	0.501	0.121	7.315	1
115	-0.369	0.002	0.012	-0.115	2	0.001	0.008
129	2.100	2.300	1
165	4.071	0.461	0.115	6.158	1
168	-0.474	0.041	-0.091	-0.192	1
171	-0.672	0.026	-0.182	-0.313	1
185	-1.058	0.031	-0.151	-0.701	1
187	-0.379	-0.028	0.033	-0.280	1
193	-0.224	0.052	-0.003	0.263	5	0.175	0.596
195	-0.404	-0.010	0.031	-0.051	10	0.038	0.068
199	-0.283	0.045	-0.065	-0.006	1
203	-0.683	0.043	-0.170	-0.257	1
204	10.356	1.410	0.270	14.438	10	2.999	10.837
210	-0.186	0.169	0.173	-0.848	1
213	-0.670	0.038	-0.155	-0.308	1
230	8.270	0.875	0.313	7.289	8	2.651	6.531
234	1.155	0.142	0.162	2.011	7	0.555	0.913

Table 4—Continued

NN	H α	HeD3	He6678	H β	H γ	H δ	H ϵ	H6	N _{Hα}	$\sigma_{\text{H}\alpha}$	$\sigma_{\text{H}\beta}$
247	-0.664	0.065	-0.187	-0.276	2	0.013	0.011
260	-0.661	0.026	-0.181	-0.338	1
276	-0.704	0.098	-0.242	-0.256	-0.559	-0.178	1
296	-0.243	0.035	0.039	0.063	1
301	7.858	1.253	0.226	13.471	3	4.428	10.790
316	-0.624	0.073	-0.157	-0.204	1
319	-0.308	0.029	-0.002	-0.112	4	0.070	0.297
326	-0.319	0.133	0.057	-0.376	1
339	-0.324	0.054	0.021	-0.148	1
342	-0.535	0.043	-0.122	-0.214	1
350	6.652	0.774	0.152	10.494	1
358	1.583	0.218	0.184	2.249	8	0.373	1.179
359	-0.257	-0.004	-0.001	0.067	7	0.067	0.552
363	0.213	-0.066	0.096	0.467	7	0.311	0.987
371	-0.303	0.011	0.009	-0.015	6	0.087	0.233
372	-0.584	0.041	-0.102	-0.275	1
376	-0.413	0.053	-0.098	-0.204	1
381	4.953	0.627	0.098	8.662	1
387	-0.405	-0.162	-0.021	-0.786	2	0.392	0.023
390	-0.410	0.026	-0.037	-0.112	2	0.003	0.067
398	-0.622	0.060	-0.191	-0.222	1
408	2.689	0.038	0.224	-0.410	3	0.621	...
427	-0.488	0.056	-0.116	-0.193	1
435	-0.558	0.071	-0.182	-0.216	1
453	2.531	0.275	0.127	2.936	7	0.359	1.133
460	-0.348	-0.028	0.044	-0.827	2	0.005	0.066
461	-0.442	0.020	-0.028	-0.004	-0.351	-0.241	1
463	-0.252	0.014	0.105	-0.257	1
489	-0.436	0.023	-0.045	-0.145	1
492	-0.296	0.014	0.033	-0.026	-0.211	-0.192	0.168	-0.121	5	0.016	0.061
512	-0.481	0.041	-0.101	-0.219	1
515	-0.496	0.066	-0.080	-0.217	1
525	-0.534	0.041	-0.093	-0.209	1

Table 4—Continued

NN	H α	HeD3	He6678	H β	H γ	H δ	H ϵ	H6	N _{Hα}	$\sigma_{\text{H}\alpha}$	$\sigma_{\text{H}\beta}$
532	-0.199	0.074	-0.005	-0.078	1
538	0.926	0.068	0.101	1.228	1.131	0.130	3	0.474	1.117
539	-0.368	0.005	0.036	-0.292	-0.399	1.586	0.068	-0.297	4	0.104	0.367
548	-0.655	0.048	-0.175	-0.297	1
550	-0.601	0.064	-0.181	-0.295	1
556	1.900	1.600	1
558	1.400	1.000	1
559	-0.485	0.032	-0.055	-0.167	1
574	-0.123	0.150	0.225	-0.068	8	0.085	0.530
579	-1.292	0.048	-0.123	-0.895	1
582	-0.444	0.029	-0.030	-0.184	1
583	-0.400	0.011	-0.025	-0.132	1
587	-0.396	0.044	-0.007	-0.215	1
590	-0.495	0.042	-0.088	-0.145	1
600	0.038	0.095	-0.021	0.582	1
608	0.136	0.115	-0.079	0.349	1
610	-0.076	0.032	-0.004	-0.947	1
627	-0.590	0.053	-0.167	-0.296	1
630	-0.589	0.059	-0.168	-0.332	1
647	-0.186	0.065	-0.007	-0.017	1
656	-0.536	0.068	-0.094	-0.326	1
657	-0.250	0.037	-0.029	-0.282	1
663	-0.532	0.046	-0.133	-0.239	1
664	-0.424	0.029	-0.071	-0.119	1
674	-0.687	0.018	-0.167	-0.284	1
675	-0.389	0.001	-0.030	-0.050	1
677	-0.472	0.048	-0.146	-0.157	1
692	-0.256	0.012	0.097	-0.134	7	0.057	0.400
699	-0.284	0.076	-0.058	-0.060	1
701	-0.653	0.075	-0.198	-0.288	2	0.008	0.033
702	-0.534	0.032	-0.084	-0.141	1
720	-0.714	0.034	-0.225	-0.358	1
721	-0.438	-0.035	0.138	-0.228	1

Table 4—Continued

NN	H α	HeD3	He6678	H β	H γ	H δ	H ϵ	H6	N _{Hα}	$\sigma_{\text{H}\alpha}$	$\sigma_{\text{H}\beta}$
724	-0.415	0.056	-0.077	-0.149	1
732	-0.245	-0.059	0.133	-1.420	1
742	3.466	0.242	0.131	3.860	1
743	-0.390	0.051	-0.046	-0.005	1
780	-0.174	-0.007	0.051	0.036	6	0.073	0.143
782	3.888	0.480	0.168	2.873	3	0.505	1.689
799	-0.490	0.044	-0.152	-0.220	1
802	4.808	0.617	0.121	7.313	4	1.406	2.383
803	1.883	0.159	-0.085	1.983	1
804	-0.406	0.039	-0.023	2.643	2	0.001	3.662
811	-0.451	0.046	-0.080	-0.164	1
817	-0.401	0.023	-0.020	-0.077	4	0.023	0.038
821	-0.440	0.023	-0.030	-0.135	-0.288	-0.201	0.323	-0.274	1
835	-0.057	0.119	0.097	-0.036	1
836	-0.296	-0.004	0.069	-0.157	3.084	3	0.102	0.394
838	-0.372	0.036	-0.014	-0.127	1
846	-0.452	0.039	-0.072	-0.116	1
847	-0.469	0.059	-0.152	-0.180	1
849	1.595	0.210	-0.149	1.618	1.159	1.705	1.570	2.060	1
853	6.033	0.631	0.130	7.972	7	0.488	1.221
854	-0.441	0.042	-0.066	-0.165	1
855	1.158	0.303	0.144	3.856	6	1.686	6.725
856	-0.497	0.037	-0.108	-0.213	5	0.027	0.035
859	-0.355	-0.018	0.056	-0.019	1
874	2.413	0.254	-0.023	3.251	5	0.538	1.059
875	5.775	0.583	0.140	6.827	5	0.552	2.932
876	-0.158	0.051	0.015	-0.020	1
882	-0.259	-0.009	0.059	-0.011	6	0.022	0.067
883	-0.399	0.024	-0.009	0.010	2	0.028	0.112
888	-0.400	0.004	-0.017	-0.287	1
895	-0.426	0.026	-0.064	-0.154	1
905	-0.640	0.023	-0.209	-0.318	1
919	-0.121	0.078	0.080	-0.214	4	0.056	0.147

Table 4—Continued

NN	H α	HeD3	He6678	H β	H γ	H δ	H ϵ	H6	N _{Hα}	$\sigma_{\text{H}\alpha}$	$\sigma_{\text{H}\beta}$
924	-0.531	0.026	-0.102	-0.188	1
929	-0.315	-0.029	0.016	-0.022	1
930	-0.401	0.039	-0.092	-0.040	3	0.029	0.028
933	3.695	0.272	0.081	3.913	1
938	0.093	-0.015	0.023	0.181	2	0.484	0.279
939	0.126	0.084	0.097	-0.151	1
941	-0.268	0.077	0.121	-0.155	1
943	-0.020	-0.049	0.087	0.270	1
944	-0.157	0.056	-0.159	0.007	1
955	2.420	0.059	0.069	-0.400	1
956	-0.391	0.037	-0.080	-0.137	1
959	-0.215	0.002	0.103	-0.220	1
961	-0.572	0.054	-0.171	-0.222	1
980	-0.504	-0.067	-0.062	0.078	1
981	-0.613	0.038	-0.179	-0.263	1
985	-0.783	0.049	-0.184	-0.517	1
991	-0.229	0.055	-0.078	-0.041	1
992	5.696	0.764	0.149	9.222	1
998	-0.155	0.008	0.095	0.026	6	0.142	0.226
999	3.329	0.382	0.135	5.357	4.811	4.116	1.551	...	6	0.481	1.017
1004	-0.231	-0.365	0.183	-0.280	4	0.072	0.872
1005	-0.384	0.036	0.001	-0.110	7	0.057	0.292
1019	-0.324	0.023	0.010	-0.059	4	0.041	0.050
1021	-0.512	0.039	-0.086	-0.137	-0.306	-0.152	0.314	0.064	5	0.007	0.035
1038	-0.325	0.027	0.043	-0.343	0.029	1
1041	-0.604	0.071	-0.135	-0.245	2	0.048	0.108
1042	-0.285	0.040	0.164	-0.501	5	0.139	0.319
1048	3.420	0.385	0.159	5.038	5	0.349	0.953
1052	-0.504	0.089	-0.092	-0.260	-0.491	1
1057	-0.404	0.055	-0.081	-0.140	-0.207	-0.212	0.342	0.001	3	0.027	0.022
1068	-0.306	-0.016	0.055	-0.032	-0.242	-0.123	-0.238	...	1
1069	-0.125	-0.035	0.098	-0.453	-0.558	1
1089	-0.308	-0.018	0.041	-0.048	1

Table 4—Continued

NN	H α	HeD3	He6678	H β	H γ	H δ	H ϵ	H6	N _{Hα}	$\sigma_{\text{H}\alpha}$	$\sigma_{\text{H}\beta}$
1092	-0.292	0.032	-0.010	0.064	-0.276	-0.184	0.206	-0.127	6	0.070	0.155
1094	-0.272	-0.002	0.043	-0.152	4	0.005	0.024
1102	2.237	0.297	0.208	1.175	3	0.983	1.017
1104	-0.601	0.047	-0.169	-0.302	1
1112	0.818	0.428	0.230	1.161	2	0.939	1.466
1120	-0.185	0.299	0.166	-0.455	6	0.198	0.585
1126	-0.071	0.009	0.044	0.129	1
1130	-0.553	0.042	-0.138	-0.284	2	0.021	0.003
1131	-0.414	0.009	-0.048	-0.086	1
1138	1.400	2.500	1
1148	-0.202	0.026	0.020	-0.033	1
1154	-0.389	0.036	-0.066	-0.127	1
1160	-0.456	0.056	-0.121	-0.267	1
1164	-0.250	0.065	-0.069	0.168	1
1167	-0.508	0.043	-0.042	-0.124	1
1168	-0.295	-0.012	0.072	-0.203	2	0.117	0.289
1175	-0.405	-0.023	0.060	-0.221	1
1176	-0.551	0.006	-0.092	-0.126	1
1183	1.250	0.136	0.016	1.719	1.550	1.286	2	0.194	0.392
1184	2.157	0.250	0.106	2.650	2	0.389	1.727
1191	-0.421	0.050	-0.068	-0.135	-0.358	-0.399	0.126	...	2	0.040	0.033
1193	-0.615	0.026	-0.067	-0.449	1
1196	2.200	2.100	1
1201	4.844	0.677	0.231	6.376	5	0.248	1.521
1207	-0.179	0.032	0.047	-0.072	1
1210	-0.646	0.014	-0.131	-0.182	1
1211	-0.883	0.010	-0.190	-0.594	1
1212	-0.461	0.046	-0.176	-0.181	1
1219	8.370	1.270	0.230	14.498	1
1226	3.896	0.717	0.180	6.234	1
1227	-0.290	0.004	-0.016	-0.153	1
1233	-0.309	-0.054	0.085	-0.865	5	0.110	0.661
1247	-0.248	-0.016	0.076	-0.199	4	0.034	0.137

Table 4—Continued

NN	H α	HeD3	He6678	H β	H γ	H δ	H ϵ	H6	N _{Hα}	$\sigma_{\text{H}\alpha}$	$\sigma_{\text{H}\beta}$
1269	-0.699	0.064	-0.217	-0.294	1
1271	-0.422	0.048	-0.126	-0.213	2	0.014	0.002
1278	-0.606	0.060	-0.194	-0.266	1
1279	2.068	0.228	0.015	2.775	1
1290	-0.292	-0.070	0.102	0.143	4	0.077	0.567
1293	-0.192	0.041	0.091	-0.062	4	0.050	0.299
1294	-0.563	0.003	-0.147	-0.182	1
1299	-0.362	0.033	-0.013	-0.104	6	0.025	0.050
1326	6.693	0.867	0.242	4.104	4	5.121	4.273
1328	4.600	6.400	1
1329	4.290	0.742	0.204	4.241	4	0.671	1.184
1337	-0.173	-0.002	0.004	0.151	1
1340	-0.564	0.051	-0.150	-0.230	1
1354	-0.834	0.034	-0.202	-0.495	1
1355	0.312	0.247	-0.063	-0.098	4	0.395	0.466
1358	-0.281	0.001	0.069	-0.005	2	0.052	0.315
1361	-0.568	0.055	-0.133	-0.175	1
1377	-0.555	0.043	-0.172	-0.271	1
1379	-0.359	0.041	-0.163	-0.156	1
1383	-0.249	-0.098	0.167	-0.237	1
1385	-0.577	0.051	-0.159	-0.249	1
1391	-0.616	0.027	-0.153	-0.213	1
1395	-0.325	0.063	-0.063	-0.154	1
1398	6.363	1.101	0.264	9.274	4	1.624	10.715
1405	2.200	3.400	1
1408	1.142	0.095	0.113	1.033	4	0.131	0.373
1417	-0.293	-0.048	0.096	-0.212	3	0.055	0.185
1418	-0.669	0.048	-0.172	-0.299	1
1419	-0.628	0.042	-0.166	-0.257	1
1420	-0.325	-0.011	0.008	-0.056	1
1426	-0.423	0.064	-0.132	-0.064	1
1430	-0.735	0.073	-0.245	-0.384	1
1439	-0.556	0.030	-0.116	-0.191	1

Table 4—Continued

NN	H α	HeD3	He6678	H β	H γ	H δ	H ϵ	H6	N _{Hα}	$\sigma_{\text{H}\alpha}$	$\sigma_{\text{H}\beta}$
1451	-0.559	0.043	-0.140	-0.287	6	0.065	0.173
1452	-0.498	0.047	-0.131	-0.248	5	0.042	0.122
1460	-0.083	0.031	-0.024	0.174	1
1465	-0.658	0.057	-0.207	-0.324	1
1483	-0.736	0.028	-0.214	-0.353	1
1501	-0.331	0.015	0.059	-0.223	3	0.061	0.238
1507	-0.325	-0.005	0.018	-0.455	6	0.049	0.805
1509	-0.401	0.042	-0.097	-0.087	2	0.025	0.029
1522	-0.317	0.037	0.016	-0.336	6	0.042	0.278
1527	-0.040	0.050	-0.005	0.229	1
1528	-0.353	0.031	-0.058	0.041	1
1529	1.087	0.118	0.051	1.586	3	0.205	0.380
1530	-0.301	-0.023	0.060	-0.307	1
1535	-0.279	-0.020	0.065	-0.094	1
1537	-0.414	0.023	-0.040	-0.093	1
1541	-0.143	-0.084	0.084	1.120	1
1550	-0.447	0.053	-0.075	-0.065	1
1553	-0.550	0.043	-0.164	-0.172	1
1554	-0.383	0.062	-0.025	-0.016	6	0.048	0.227
1558	-0.452	0.060	-0.134	-0.127	3	0.010	0.037
1575	-0.505	0.025	-0.062	-0.189	1
1583	-0.559	0.077	-0.199	-0.219	1
1586	-0.253	-0.005	0.081	-0.128	1
1587	-0.521	0.049	-0.148	-0.231	1
1592	-0.611	0.064	-0.195	-0.276	2	0.001	0.006
1594	-0.370	0.031	-0.003	-0.197	6	0.035	0.087
1595	-0.302	0.044	-0.040	-0.026	6	0.053	0.087
1596	-0.553	0.043	-0.147	-0.211	2	0.011	0.009
1605	0.834	0.105	-0.156	0.829	1
1611	-0.365	0.002	0.050	0.068	3	0.017	0.397
1616	3.399	0.374	0.075	4.353	4	0.174	0.506
1630	-0.411	0.043	-0.067	-0.067	2	0.018	0.006
1642	-0.525	0.009	-0.025	-0.376	-1.026	-0.580	3	0.260	0.419

Table 4—Continued

NN	H α	HeD3	He6678	H β	H γ	H δ	H ϵ	H6	N _{Hα}	$\sigma_{\text{H}\alpha}$	$\sigma_{\text{H}\beta}$
1648	-0.646	0.065	-0.204	-0.291	1
1649	-0.518	0.040	-0.164	-0.215	1
1657	-0.219	-0.017	0.054	-0.065	1
1658	4.399	0.289	0.078	5.797	1
1662	-0.355	-0.035	0.004	0.284	1
1664	-0.297	-0.083	0.097	0.164	2	0.024	1.415
1671	-0.449	0.055	-0.130	-0.217	1
1678	-0.762	0.046	-0.222	-0.378	1
1679	1.332	-0.620	0.160	-0.110	2	1.938	0.897
1682	-0.268	0.051	0.106	-0.382	6	0.047	0.320
1687	-0.280	0.021	0.131	-0.166	-0.862	7	0.224	0.254
1690	-0.144	-0.141	0.042	-0.715	1
1692	6.837	0.720	0.164	3.724	4	1.160	3.224
1702	7.877	0.692	0.277	4.501	5	2.135	4.195
1705	-0.623	0.065	-0.208	-0.257	1
1709	-0.307	0.024	0.015	-0.090	5	0.045	0.192
1717	0.002	0.069	-0.103	0.277	1
1719	-0.197	0.046	-0.018	-0.014	2	0.021	0.077
1723	-0.255	0.051	-0.054	-0.088	5	0.009	0.033
1724	6.143	0.577	0.309	3.083	5	2.420	1.286
1732	-0.591	-0.043	-0.022	-0.600	3	0.223	0.508
1736	-0.646	0.074	-0.192	-0.246	1
1737	-0.432	0.039	-0.058	-0.121	1
1742	4.196	0.254	0.078	5.744	1
1746	-0.503	0.036	-0.062	-0.094	-0.273	-0.242	0.283	-0.555	1
1748	-0.532	0.057	-0.127	-0.240	-0.348	1
1751	-0.851	0.002	-0.224	-0.642	1
1752	-0.212	-0.015	-0.060	-0.537	1
1756	-0.719	0.050	-0.205	-0.328	-0.489	1
1757	-0.649	0.039	-0.162	-0.323	1
1759	3.400	3.100	1
1765	-0.580	0.063	-0.159	-0.187	1
1770	-0.441	0.035	-0.060	-0.176	-0.332	-0.209	0.157	0.117	8	0.025	0.121

Table 4—Continued

NN	H α	HeD3	He6678	H β	H γ	H δ	H ϵ	H6	N _{Hα}	$\sigma_{\text{H}\alpha}$	$\sigma_{\text{H}\beta}$
1771	-0.164	0.054	-0.175	-0.038	1
1772	1.858	0.137	-0.042	0.350	1
1778	-0.027	0.065	-0.171	0.064	1
1784	-0.328	-0.024	-0.012	-0.329	1
1785	-0.166	-0.057	0.010	-0.538	1
1795	-0.293	-0.085	0.014	-0.657	1
1801	-0.311	0.045	-0.108	-0.013	1
1827	-0.274	-0.006	0.079	-0.131	3	0.031	0.302
1830	-0.370	0.023	0.020	-0.066	-0.346	-0.096	0.125	0.012	1
1838	-0.324	0.010	-0.017	-0.184	1
1845	-0.226	0.001	0.086	-0.107	8	0.040	0.203
1847	4.664	0.536	0.320	6.517	1
1849	-0.181	-0.015	0.126	-0.342	1
1854	-0.131	-0.013	0.182	-0.323	7	0.088	0.378
1855	-0.261	0.052	-0.053	0.062	-0.226	-0.070	0.356	0.024	9	0.154	0.334
1862	-0.367	0.007	-0.036	-0.107	1
1866	1.248	0.131	0.038	1
1890	1.200	1.000	1
1894	-0.176	-0.077	0.084	-0.207	1
1895	-0.414	0.060	-0.180	-0.287	-0.660	-0.484	0.149	-0.305	1
1898	-0.579	0.060	-0.131	-0.216	-0.442	-0.526	2	0.015	0.076
1905	-0.261	0.025	0.093	-0.322	4	0.040	0.301
1907	-0.300	-0.049	0.029	-0.554	1
1915	-0.580	0.062	-0.120	-0.285	1
1921	-0.464	0.004	-0.063	-0.118	-0.607	-0.365	-0.179	-0.002	1
1923	5.409	0.366	0.228	3.307	7	0.770	1.758
1925	-0.459	0.060	-0.158	-0.295	1
1934	6.114	0.544	0.229	3.602	10	1.903	2.267
1935	-0.586	0.060	-0.149	-0.191	-0.479	-0.421	-0.013	0.421	1
1937	-0.351	0.037	-0.101	-0.043	-0.240	-0.064	0.612	0.138	1
1938	-0.594	0.034	-0.190	-0.350	1
1942	-0.225	0.026	0.030	-0.336	1
1943	-0.724	0.034	-0.169	-0.636	-0.474	-0.833	1

Table 4—Continued

NN	H α	HeD3	He6678	H β	H γ	H δ	H ϵ	H6	N _{Hα}	$\sigma_{\text{H}\alpha}$	$\sigma_{\text{H}\beta}$
1945	-0.280	0.047	0.022	-0.213	-0.457	8	0.081	0.145
1952	0.566	0.037	-0.009	1.178	1
1953	0.575	0.092	-0.010	1.202	1
1954	-0.326	-0.006	0.109	-0.014	-0.378	1
1966	-0.382	0.045	-0.043	-0.142	-0.350	-0.181	0.310	0.023	2	0.176	0.065
1972	4.783	0.576	0.173	6.945	6	0.790	2.099
1977	-0.400	0.001	0.024	-0.020	-0.393	1
1988	-0.274	0.004	0.046	0.094	3	0.061	0.033
2009	-0.278	-0.015	0.096	-0.104	-0.358	9	0.023	0.260
2010	-0.867	0.042	-0.205	-0.430	-0.873	0.111	1
2011	-0.661	0.061	-0.133	-0.302	-0.639	1
2017	0.200	0.600	1
2024	-0.653	0.054	-0.176	-0.307	-0.760	-0.651	1
2035	1.360	0.153	-0.101	1.522	1.303	1.873	2.418	1.925	1
2042	-0.824	0.037	-0.192	-0.378	-0.626	-0.220	1
2043	4.592	0.441	0.194	3.690	7	0.855	1.511
2045	1.087	0.119	-0.066	0.986	0.159	0.533	1
2049	-0.290	0.044	-0.043	-0.108	-0.265	-0.100	1
2051	-0.325	0.057	-0.178	-0.166	1
2085	-0.967	0.000	-0.167	-0.712	1
2086	-0.390	0.073	-0.096	-0.121	1
2088	-0.251	-0.007	0.087	-0.238	-0.173	1
2093	-0.467	0.037	-0.082	-0.207	1
2094	-0.255	0.001	0.034	-0.136	1
2096	-0.543	0.049	-0.061	-0.134	-0.451	-0.235	0.405	0.175	2	0.006	0.033
2097	-0.458	0.029	-0.074	-0.155	8	0.036	0.042
2100	-0.461	0.046	-0.064	-0.103	-0.375	-0.264	0.206	-0.053	1
2102	-0.254	-0.030	0.097	0.109	-0.034	1
2107	-0.591	0.058	-0.188	-0.315	1
2109	-0.174	0.056	-0.213	-0.113	1
2112	0.006	0.083	-0.031	0.511	-0.948	1
2118	-0.316	-0.017	0.052	0.127	-0.521	-0.010	1
2123	-0.425	0.039	-0.066	-0.080	-0.482	-0.227	9	0.046	0.112

Table 4—Continued

NN	H α	HeD3	He6678	H β	H γ	H δ	H ϵ	H6	N _{Hα}	$\sigma_{\text{H}\alpha}$	$\sigma_{\text{H}\beta}$
2128	9.000	11.200	1
2137	-0.574	0.072	-0.172	-0.260	1
2150	-0.530	0.046	-0.148	-0.223	-0.404	-0.252	0.251	0.101	2	0.006	0.055
2151	-0.491	0.060	-0.162	-0.247	1
2156	-0.442	0.055	-0.047	-0.209	1
2157	-0.560	0.052	-0.146	-0.198	-0.386	-0.201	0.129	0.072	1
2165	-0.665	0.060	-0.204	-0.303	-0.622	-0.336	0.166	-0.105	1
2168	-0.212	-0.047	0.106	-0.012	11	0.056	0.252
2173	-0.440	0.040	-0.092	-0.162	1
2175	-0.281	-0.034	0.075	-0.589	4	0.028	0.465
2176	-0.453	0.028	-0.038	-0.116	-0.251	-0.176	0.227	0.035	6	0.031	0.022
2198	-0.582	0.054	-0.202	-0.314	1
2199	-0.386	0.041	-0.028	0.022	-0.351	-0.258	1
2201	-0.764	0.016	-0.176	-0.396	-0.792	1
2204	-0.620	0.049	-0.158	-0.401	1
2209	-0.530	0.038	-0.149	-0.350	1
2211	-0.296	0.020	0.061	-0.075	-0.249	-0.278	0.156	0.237	1
2214	4.010	0.521	0.168	4.383	1
2216	-0.512	0.023	-0.062	-0.248	-0.827	-0.725	0.155	-0.486	4	0.098	0.133
2220	-0.492	0.041	-0.109	-0.070	-0.370	-0.165	-0.233	0.201	1
2222	-0.300	0.052	-0.070	-0.079	1
2223	-0.376	0.062	-0.083	-0.135	1
2235	-0.489	0.050	-0.063	-0.252	1
2242	1.000	0.600	1
2256	4.516	0.531	0.156	5.991	6	0.333	2.247
2259	-0.508	0.057	-0.132	-0.154	-0.439	-0.243	-0.665	0.126	1
2268	-0.229	-0.139	0.129	-0.120	1
2278	-0.602	0.066	-0.142	-0.248	-0.535	-0.315	0.368	-0.064	1
2279	-0.539	0.052	-0.109	-0.133	-0.409	-0.224	0.098	0.078	1
2281	-0.372	-0.026	0.008	-0.050	-0.159	-0.121	1
2295	-0.435	0.018	-0.018	-0.083	-0.183	-0.078	1
2299	-0.700	0.060	-0.192	-0.288	-0.608	-0.348	0.245	0.243	2	0.076	0.074
2300	-0.284	-0.021	0.088	-0.261	1

Table 4—Continued

NN	H α	HeD3	He6678	H β	H γ	H δ	H ϵ	H6	N _{Hα}	$\sigma_{\text{H}\alpha}$	$\sigma_{\text{H}\beta}$
2310	-0.177	-0.017	0.108	0.017	8	0.060	0.335
2316	0.900	1.100	1
2324	-0.603	0.042	-0.211	-0.342	1
2326	-0.620	0.058	-0.192	-0.320	1
2329	-0.357	0.028	-0.028	-0.242	1
2335	-0.585	0.053	-0.200	-0.335	1
2339	-0.795	0.043	-0.237	-0.377	1
2352	-0.381	-0.007	-0.002	0.010	-0.478	-0.404	0.537	0.356	1
2356	0.203	0.012	0.081	0.256	4	0.067	0.153
2358	0.852	0.104	-0.019	1.210	4	0.269	0.377
2359	-0.295	0.023	0.071	-0.112	4	0.106	0.480
2367	-0.859	0.032	-0.217	-0.472	5	0.014	0.018
2368	-0.414	0.031	-0.060	-0.153	3	0.025	0.004
2374	-0.600	0.086	-0.118	-0.320	2	0.118	0.047
2377	-0.706	0.069	-0.216	-0.326	-0.745	-0.208	-0.237	-0.043	1
2378	-0.726	0.066	-0.164	-0.420	1
2379	-0.430	0.071	0.123	-0.111	1
2380	-0.439	-0.031	0.035	-0.238	1
2381	-0.408	0.045	-0.126	-0.127	-0.416	-0.170	0.430	0.062	1
2390	-0.807	0.034	-0.068	-0.607	-0.733	-0.281	-0.013	0.080	2	0.168	0.257
2392	-0.287	0.040	-0.052	0.055	-0.173	-0.161	0.511	0.030	1
2397	-0.603	0.078	-0.152	-0.309	1
2399	-0.392	-0.002	0.035	-0.112	-0.336	-0.238	0.537	-0.277	1
2419	-0.295	0.005	0.105	-0.051	-0.423	1
2420	-0.359	-0.023	0.030	-0.327	-0.728	-0.593	0.023	-0.269	4	0.180	0.194
2427	-0.627	0.051	-0.191	-0.453	1
2428	1.857	0.188	-0.031	2.134	1.449	1.404	5	0.144	0.253
2453	-0.212	0.015	0.043	0.021	1
2456	-0.097	-0.007	0.074	0.040	-0.077	-0.209	0.187	0.155	1
2458	-0.418	-0.057	0.114	-0.404	1
2464	-0.213	0.010	0.069	-0.228	8	0.052	0.253
2467	-0.763	0.083	-0.233	-0.274	-0.804	-0.343	1
2472	-0.187	-0.028	0.001	-0.180	1

Table 4—Continued

NN	H α	HeD3	He6678	H β	H γ	H δ	H ϵ	H6	N _{Hα}	$\sigma_{\text{H}\alpha}$	$\sigma_{\text{H}\beta}$
2477	-0.386	0.002	-0.009	-0.153	-0.359	-0.555	0.784	-0.169	1
2486	-0.533	0.054	-0.152	-0.190	-0.378	-0.217	0.167	0.035	1
2504	-0.339	0.025	-0.055	-0.088	-0.477	-0.237	0.249	-0.032	4	0.129	0.055
2516	-0.201	0.003	0.130	-0.196	-0.148	7	0.086	0.222
2536	-0.731	0.051	-0.243	-0.402	1
2543	-0.380	0.051	-0.124	-0.103	-0.487	-0.332	1
2552	-0.286	-0.049	0.092	0.862	1
2563	1.931	0.202	-0.042	2.164	1.909	2.131	2.155	2.566	1
2566	-0.626	0.058	-0.171	-0.228	-0.512	-0.225	0.213	0.034	4	0.018	0.004
2567	-0.350	-0.009	0.031	-0.042	4	0.022	0.052
2576	-0.674	0.054	-0.187	-0.324	1
2578	-0.494	0.060	-0.106	-0.390	1
2582	-0.428	0.069	-0.134	-0.068	-0.424	1
2583	-0.237	0.011	0.041	0.033	-0.150	-0.175	0.394	...	1
2587	0.026	0.054	0.030	0.275	0.033	0.483	0.334	0.363	1
2589	-0.361	0.021	-0.007	-0.133	8	0.039	0.034
2599	-0.234	-0.026	0.080	-0.013	-0.313	-0.138	8	0.045	0.070
2616	3.400	4.400	1
2618	4.095	0.521	0.121	7.397	1
2622	-0.788	0.036	-0.237	-0.436	1
2642	-0.657	0.060	-0.192	-0.289	-0.441	-0.205	0.268	0.027	4	0.022	0.036
2644	-0.409	0.013	0.024	0.057	1
2647	-0.457	0.107	-0.072	-0.236	2	0.105	0.226
2656	-0.872	0.023	-0.206	-0.453	-0.676	-0.348	0.165	-0.260	9	0.022	0.025
2659	-0.480	0.037	-0.095	-0.267	1
2660	-0.228	-0.014	0.083	-0.108	0.094	8	0.066	0.352
2661	1.708	0.193	0.044	2.257	2.101	1.717	1.338	1.872	8	0.195	0.414
2665	3.295	1.041	0.131	4.226	4.930	2.061	8	0.641	2.212
2673	-0.490	0.027	-0.061	-0.120	-0.337	-0.238	0.395	0.041	2	0.047	0.014
2674	0.995	0.155	0.141	1.999	1
2684	-0.518	0.052	-0.094	-0.193	-0.612	1
2688	-0.067	0.079	0.338	-0.018	8	0.110	0.580
2691	-0.565	0.087	-0.188	-0.333	1

Table 4—Continued

NN	H α	HeD3	He6678	H β	H γ	H δ	H ϵ	H6	N _{Hα}	$\sigma_{\text{H}\alpha}$	$\sigma_{\text{H}\beta}$
2692	-0.395	0.047	-0.012	-0.154	-0.360	-0.177	0.155	0.081	2	0.008	0.110
2700	-0.327	-0.006	0.010	-0.042	-0.501	1
2708	-0.134	-0.027	0.113	0.001	-0.143	-0.282	0.227	0.265	8	0.075	0.229
2712	-0.165	0.020	0.060	0.150	-0.041	-0.310	1
2714	-0.284	-0.019	0.070	-0.156	-0.067	-0.111	8	0.053	0.169
2717	-0.269	-0.005	0.052	-0.130	8	0.026	0.176
2719	-0.308	-0.006	0.060	0.009	1
2727	-0.589	0.077	-0.206	-0.312	1
2728	-0.451	0.038	-0.092	-0.113	-0.435	-0.039	1
2729	-0.458	0.070	-0.053	-0.326	1
2730	-0.385	0.043	0.006	0.026	1
2741	-0.297	0.074	-0.128	-0.034	-0.230	-0.019	0.315	0.168	1
2744	1.764	0.169	0.103	2.942	4	0.295	1.002
2745	5.932	0.946	0.283	8.250	3	0.305	3.737
2748	-0.387	0.021	0.035	-0.068	1
2756	-0.640	0.051	-0.207	-0.273	2	0.067	0.007
2760	-0.243	-0.112	0.160	-1.198	1
2768	-0.894	0.101	-0.190	-0.670	1
2772	-0.455	0.058	-0.099	-0.086	-0.190	-0.096	0.362	0.132	1
2788	-0.638	0.075	-0.163	-0.151	1
2789	-0.401	0.050	-0.114	-0.083	-0.433	-0.250	0.356	0.299	1
2792	-0.384	0.037	-0.058	-0.085	-0.244	-0.204	0.273	-0.052	1
2797	-0.340	0.005	0.045	-0.048	-0.137	-0.158	0.277	0.095	9	0.024	0.046
2804	1.312	0.122	-0.152	0.990	1
2814	0.053	0.081	-0.085	0.339	0.080	0.184	0.985	0.687	1
2817	-0.338	0.024	0.007	0.029	0.024	0.065	0.297	0.095	2	0.144	0.156
2821	-0.212	0.013	0.087	0.065	-0.302	1
2824	-0.283	-0.047	0.105	0.044	-0.015	-0.004	0.308	0.141	7	0.043	0.092
2830	-0.616	0.066	-0.195	-0.236	-0.542	-0.297	0.011	0.041	1
2846	-0.314	0.048	0.064	0.115	-0.259	1
2849	-0.204	0.006	0.102	-0.077	-0.080	-0.220	0.399	0.013	11	0.037	0.056
2851	-0.215	0.010	0.065	0.178	-0.062	-0.169	1
2859	-0.445	0.032	-0.062	-0.157	-0.315	-0.192	0.479	0.060	3	0.015	0.043

Table 4—Continued

NN	H α	HeD3	He6678	H β	H γ	H δ	H ϵ	H6	N _{Hα}	$\sigma_{\text{H}\alpha}$	$\sigma_{\text{H}\beta}$
2860	-0.458	0.061	-0.089	-0.211	1
2865	3.009	0.250	0.246	2.063	6	0.292	1.630
2882	-0.508	0.044	-0.132	-0.169	-0.510	-0.090	1
2885	-0.538	0.055	-0.100	-0.191	-0.370	-0.153	0.315	-0.071	1
2888	-0.289	0.023	0.057	-0.077	-0.263	-0.123	0.468	...	1
2892	-0.595	0.064	-0.169	-0.261	-0.479	-0.283	0.045	0.246	1
2895	-0.215	0.009	0.049	-0.094	-2.102	1
2897	2.136	0.225	0.153	2.434	8	0.426	1.265
2898	-0.375	0.046	0.077	0.132	1
2901	-0.232	-0.009	0.074	-0.150	-0.127	1
2904	-0.173	-0.027	0.156	-0.125	6	0.107	0.748
2905	-0.142	-0.017	0.177	0.791	1
2916	-0.147	0.011	0.051	0.276	-0.042	-0.243	0.216	...	3	0.142	0.208
2917	-0.670	0.063	-0.184	-0.381	1
2921	-0.224	-0.011	0.082	0.062	-0.282	-0.331	0.295	0.194	8	0.073	0.070
2923	-0.509	0.050	-0.111	-0.175	-0.275	-0.223	0.249	0.088	1
2924	-0.253	0.040	0.105	0.003	1
2925	0.473	0.022	0.094	0.851	1
2928	-0.303	0.036	0.008	-0.077	-0.161	-0.265	0.068	-0.115	1
2933	-0.498	0.033	-0.089	-0.170	-0.359	-0.459	1
2935	2.100	4.000	1
2936	0.273	0.259	0.264	-0.851	2	0.018	0.566
2937	2.685	0.244	0.127	4.609	1
2940	-0.319	-0.001	0.052	-0.021	-0.088	-0.264	0.209	-0.285	2	0.039	0.028
2942	4.186	0.401	0.098	6.332	5.806	3.959	2.508	1.569	1
2945	-0.308	0.003	0.041	-0.064	-0.113	-0.167	0.170	0.015	3	0.043	0.006
2946	-0.267	-0.010	0.067	-0.036	-0.118	-0.174	0.381	0.028	2	0.052	0.006
2947	-0.340	-0.015	0.154	-0.458	2	0.036	...
2953	-0.590	0.037	-0.194	-0.323	1
2958	-0.666	0.065	-0.173	-0.238	-0.455	-0.232	0.180	-0.087	1
2960	1.796	0.186	0.117	3.091	2.406	1.463	0.818	0.310	7	0.364	0.653
2961	-0.476	0.085	-0.104	-0.157	-0.525	1
2964	-0.331	-0.018	0.095	0.035	-0.146	1

Table 4—Continued

NN	H α	HeD3	He6678	H β	H γ	H δ	H ϵ	H6	N _{Hα}	$\sigma_{\text{H}\alpha}$	$\sigma_{\text{H}\beta}$
2966	-0.460	0.058	-0.112	-0.138	-0.279	-0.187	0.280	0.067	1
2974	-0.691	0.076	-0.238	-0.257	-0.586	-0.318	0.165	-0.033	1
2976	2.100	3.100	1
2988	-0.614	0.038	-0.107	-0.331	-0.582	1
3004	-0.195	0.021	-0.007	-0.082	-0.111	-0.223	4	0.015	0.082
3005	-0.197	0.023	-0.004	-0.063	-0.302	-0.308	4	0.022	0.073
3009	-0.213	0.004	0.076	-0.004	-0.028	-0.048	6	0.050	0.149
3013	-0.337	-0.012	0.049	-0.075	-0.150	-0.282	0.026	...	1
3016	-0.349	0.017	-0.051	-0.168	1
3017	-0.168	-0.107	0.178	-0.437	1
3022	-0.980	0.077	-0.246	-0.293	-0.994	-0.188	1
3024	-0.257	-0.026	0.071	-0.039	-0.039	-0.062	0.334	0.064	4	0.014	0.094
3036	-0.642	0.059	-0.185	-0.285	-0.559	-0.299	0.192	0.047	1
3037	-0.420	0.001	0.012	-0.103	-0.236	-0.173	0.389	0.021	1
3044	-0.276	0.007	0.041	-0.130	0.037	3	0.061	0.222
3048	-0.252	0.144	0.218	0.198	3	0.110	0.667
3049	-0.251	0.010	0.070	-0.278	-0.509	1
3057	-0.279	-0.010	0.085	-0.152	-0.149	-0.169	0.244	0.099	1
3060	0.278	-0.100	0.425	-0.050	1
3074	-0.550	0.052	-0.146	-0.216	-0.385	-0.212	0.093	0.007	1
3076	-0.514	0.031	-0.106	-0.173	-0.352	-0.196	0.648	0.205	1
3081	-0.754	0.058	-0.220	-0.401	1
3100	-0.190	-0.073	0.104	-0.025	2	0.019	0.074
3102	-0.401	0.030	-0.054	-0.130	-0.223	-0.053	1
3103	-0.451	0.042	-0.083	-0.074	-0.352	-0.198	0.463	...	1
3104	-0.283	0.043	0.008	0.042	-0.054	-0.155	1
3113	4.940	0.520	0.131	5.786	5.494	4	0.725	1.306
3120	2.770	0.417	0.216	4.784	6	0.453	1.996
3121	3.072	0.298	0.272	2.201	5	0.507	0.752
3132	-0.734	0.039	-0.182	-0.232	-0.598	-0.342	-0.089	-0.092	1
3147	-0.276	0.022	0.016	-0.014	-0.293	1
3157	1.210	0.140	-0.026	1.345	27	0.204	0.688
3179	-0.775	0.041	-0.239	-0.303	1

Table 4—Continued

NN	H α	HeD3	He6678	H β	H γ	H δ	H ϵ	H6	N _{Hα}	$\sigma_{\text{H}\alpha}$	$\sigma_{\text{H}\beta}$
3181	-0.735	0.068	-0.231	-0.233	1
3193	-0.410	-0.029	0.014	-0.031	-0.064	-0.200	2	0.057	0.022
3194	-0.312	0.342	0.219	0.036	1
3195	-0.131	0.840	0.231	-0.363	6	0.070	0.335
3198	4.735	0.627	0.148	6.286	5	1.199	1.477
3203	-0.039	0.023	0.028	0.322	0.396	0.204	0.428	0.164	12	0.139	0.260
3206	-0.471	0.041	0.071	1.029	1
3209	-0.133	0.046	0.088	-0.069	0.113	0.066	1
3224	0.137	0.143	0.158	0.857	7	0.138	1.925
3231	0.764	0.080	-0.145	0.522	0.078	1
3234	-0.482	0.009	-0.062	-0.221	1
3242	-0.448	0.055	-0.085	-0.100	-0.239	-0.305	1
3243	-0.334	-0.025	0.070	-0.149	-0.416	1
3244	-0.512	0.039	-0.112	-0.193	-0.374	-0.269	0.238	-0.056	2	0.033	0.018
3247	-0.425	0.021	-0.029	-0.145	-0.319	-0.232	0.155	0.073	1
3263	-0.456	0.044	-0.089	-0.158	-0.332	-0.158	0.235	0.145	3	0.012	0.049
3265	-0.207	-0.082	0.116	0.028	-0.153	0.179	1
3268	-0.422	0.007	0.031	-0.125	1
3269	2.366	0.339	0.144	4.054	3.335	1.951	1.127	0.455	1
3278	2.500	2.500	1
3284	-0.364	0.034	0.025	0.012	-0.200	0.223	0.035	...	1
3299	-1.433	0.107	-0.281	-0.738	0.312	1
3300	-0.739	0.047	-0.184	-0.397	10	0.014	0.043
3301	-0.592	0.059	-0.156	-0.244	10	0.015	0.031
3307	-0.346	0.052	-0.046	-0.153	-0.340	2	0.021	0.039
3308	-0.259	-0.019	-0.022	-0.312	4	0.042	0.239
3312	-0.511	0.046	-0.067	-0.095	0.714	-0.256	0.185	-0.060	1
3323	4.806	0.545	0.135	8.040	1
3352	-0.624	0.073	-0.162	-0.185	-0.473	-0.069	1
3356	-0.361	0.048	-0.065	-0.174	1
3360	-0.267	-0.017	0.037	-0.052	0.056	-0.302	7	0.068	0.195
3361	-0.731	0.084	-0.204	-0.294	-0.598	-0.276	0.206	0.031	1
3363	0.409	-0.156	0.140	0.839	6	0.120	0.399

Table 4—Continued

NN	H α	HeD3	He6678	H β	H γ	H δ	H ϵ	H6	N _{Hα}	$\sigma_{\text{H}\alpha}$	$\sigma_{\text{H}\beta}$
3367	3.097	0.438	0.084	6.200	1
3370	-0.352	-0.296	0.143	-0.796	1
3372	-0.363	0.041	0.040	-0.071	-0.180	1
3375	-0.351	0.058	-0.123	-0.040	-0.323	-0.201	0.340	0.136	1
3378	-0.446	0.061	-0.089	-0.094	-0.239	-0.180	0.261	0.121	1
3380	-0.552	-0.003	-0.174	-0.196	-0.553	-0.274	0.342	-0.095	1
3398	-0.646	0.044	-0.202	-0.251	1
3403	-0.262	-0.025	0.111	-0.189	0.765	2	0.047	0.072
3436	-0.632	0.072	-0.170	-0.235	1
3444	-0.425	0.066	-0.059	-0.227	1
3452	-0.545	0.034	-0.133	-0.147	1
3453	4.844	0.693	0.119	9.242	13.561	6.225	1.215	3.762	12	1.117	2.181
3454	-0.275	-0.033	0.074	-0.088	1
3455	-0.267	0.033	-0.007	0.128	-0.215	1
3458	-0.520	0.054	-0.129	-0.155	-0.373	-0.181	0.317	0.161	1
3466	-0.550	0.064	-0.146	-0.153	-0.363	-0.319	0.137	0.191	1
3478	-0.384	-0.015	0.038	-0.070	-0.190	-0.347	0.285	0.055	7	0.017	0.086
3486	-0.367	0.039	-0.017	-0.138	1
3489	-0.081	0.038	0.211	0.326	2	0.014	0.585
3502	5.155	0.688	0.225	7.505	2	0.433	1.520
3503	2.665	0.275	0.227	5.213	2	0.401	4.114
3517	3.792	0.517	0.189	3.300	6	0.899	1.056
3519	4.260	0.455	0.079	6.078	5.367	2	0.197	0.720
3526	-0.226	0.035	0.060	-0.009	1
3537	-0.122	0.009	0.054	0.095	9	0.130	0.158
3538	1.723	0.126	0.102	2.639	1
3542	-0.191	-0.040	0.141	-0.223	1
3544	-0.387	0.045	-0.067	-0.195	-0.179	-0.248	0.212	0.022	3	0.016	0.103
3546	4.951	0.585	0.091	8.070	7.420	1
3553	-0.534	0.041	-0.110	-0.189	-0.361	-0.273	0.102	0.041	1
3558	-0.662	0.048	-0.193	-0.267	-0.456	-0.216	0.290	0.000	1
3559	-0.355	0.006	-0.012	-0.141	2	0.055	0.003
3560	-0.222	0.143	0.106	-0.291	1

Table 4—Continued

NN	H α	HeD3	He6678	H β	H γ	H δ	H ϵ	H6	N _{Hα}	$\sigma_{\text{H}\alpha}$	$\sigma_{\text{H}\beta}$
3561	1.800	2.700	1
3562	2.200	2.700	1
3563	4.534	0.535	0.142	7.635	4.634	7	0.583	2.309
3576	-0.914	0.028	-0.238	-0.501	1
3584	4.048	0.353	0.101	5.385	2	0.478	0.948
3592	-0.507	0.045	-0.120	-0.188	-0.601	-0.154	0.409	...	1
3604	-0.200	-0.008	0.093	0.001	-0.039	-0.248	1
3609	-0.212	0.044	0.051	0.010	1
3611	-0.486	0.074	-0.076	-0.255	1
3614	-0.468	0.040	-0.086	-0.129	-0.389	-0.355	0.161	0.239	1
3616	-0.418	0.041	-0.060	-0.086	2	0.077	0.013
3621	-0.584	0.033	-0.176	-0.236	-0.600	-0.298	7	0.035	0.033
3629	-0.621	0.045	-0.187	-0.173	1
3636	-0.351	0.011	0.064	-0.103	1
3637	-0.393	0.060	-0.086	-0.177	1
3641	-0.260	-0.011	0.066	0.108	-0.350	1
3645	-0.359	0.033	-0.054	-0.062	-0.509	1
3653	-0.587	0.052	-0.140	-0.174	-0.543	-0.448	1
3672	3.797	0.431	0.097	6.125	1
3674	-0.650	0.013	-0.183	-0.433	1
3686	-0.208	0.026	0.092	0.072	0.162	-0.046	11	0.062	0.164
3689	-0.488	0.045	-0.078	-0.113	-0.452	-0.230	0.078	-0.023	1
3693	-0.476	0.075	-0.131	-0.214	-0.440	-0.269	0.150	0.585	1
3699	4.016	0.357	0.085	5.510	1
3700	6.434	0.815	0.186	11.095	1
3701	2.900	4.100	1
3705	4.428	0.474	0.103	6.468	10	0.551	1.026
3706	5.493	0.625	0.167	9.601	6	0.716	1.427
3708	1.984	0.209	0.015	2.457	2.011	1.812	1.100	1.153	1
3710	-0.589	0.026	-0.209	-0.311	1
3712	-0.371	0.035	0.004	0.252	-0.212	1
3713	-0.082	0.077	-0.197	0.049	-0.284	0.106	0.746	0.465	1
3715	1.228	-0.017	0.192	1.084	7	0.979	1.779

Table 4—Continued

NN	H α	HeD3	He6678	H β	H γ	H δ	H ϵ	H6	N _{Hα}	$\sigma_{\text{H}\alpha}$	$\sigma_{\text{H}\beta}$
3729	-0.382	0.082	0.018	0.197	1
3743	0.092	-0.001	0.178	0.259	10	0.117	0.131
3748	0.534	0.016	0.140	0.942	8	0.342	0.630
3753	3.499	0.359	0.117	1.953	3	0.754	1.779
3754	-0.622	0.043	-0.174	-0.253	-0.526	-0.291	0.318	-0.004	1
3756	-0.275	0.067	-0.026	-0.178	1
3757	-0.094	0.054	-0.221	0.069	1
3759	-0.329	0.053	-0.036	-0.073	-0.225	-0.128	0.092	0.047	3	0.032	0.032
3767	-0.388	0.041	0.026	0.101	-0.273	7	0.121	0.294
3775	-0.559	0.037	-0.204	-0.261	-0.553	-0.216	0.335	0.121	1
3782	-0.371	0.038	-0.005	0.022	-0.267	0.178	0.314	...	1
3784	-0.253	0.007	0.050	-0.144	1
3785	3.100	5.300	1
3786	-0.239	-0.030	0.077	-0.117	1
3791	-0.498	0.043	-0.116	-0.160	-0.355	-0.200	0.338	0.145	2	0.002	0.028
3796	-0.661	0.073	-0.201	-0.218	-0.671	-0.260	0.435	...	1

Table 5. Rapid Rotators

NN	Name	$v \sin i$ (km/s)
381	G 173-039	30
556	GJ 1054A	30
802	G 039-029	30
1279	LHS 5134	35
1759	Steph 932	30
2128	G 165-008	80
3453	G 188-038	37
3198	Gl 791.2	35

Table 6. Double-Lined Binaries

NN	Name	Reference
129	G1 29.1	Strassmeier et al. (1993)
556	GJ 1054A	...
558	LTT 1480	...
656	G1 148	Tokovinin (1991)
1138	G1 268	Strassmeier et al. (1993)
1196	G1 278C	Strassmeier et al. (1993)
1328	GJ 2069A	Delfosse et al. (1999)
1405	G 041-014	Delfosse et al. (1999)
1759	Steph 932	...
1890	G1 455	...
2017	G1 487	Delfosse et al. (1999)
2128	G 165-008	...
2242	LTT 5580	...
2316	LHS 2952	...
2616	G1 630.1A	Strassmeier et al. (1993)
2935	GJ 1230AC	Delfosse et al. (1999)
2976	G1 735	Strassmeier et al. (1993)
3278	G1 815A	Strassmeier et al. (1993)
3561	G1 866A	Delfosse et al. (1999)
3562	G1 867A	Strassmeier et al. (1993)
3701	GJ 1284	...
3785	G 273-185	...
...	G 173-018	...

Table 7. Candidate Single-Lined Binaries: Multiple observations

NN	Name	σ	Reference
853	LP 476-207	4.0	Delfosse et al. (1999)
1554	G1 372	24.0	Harlow (1996)
2097	G1 508 A	5.5	...
2708	G 203-47	34.2	Delfosse et al. (1999)
3563	G1 867 B	20.9	...

Table 8. Candidate Single-lined Binaries: Velocity differences

NN	Name	Δv (km/s)	Source
1019	G1 228 A	-54	Uppgren and Caruso (1988)
1361	G1 319 A	-8	Uppgren and Harlow (1996)
1938	G1 462	-9	Uppgren and Caruso (1988)
2157	G1 521.1	-25	Stauffer & Hartmann (1986)
2235	G1 540	-10	Stauffer & Hartmann (1986)
2486	G1 600	10	Uppgren and Caruso (1988)

Table 9. Candidate wide binaries

Star 1	V_{rad} kms ⁻¹	Star 2	V_{rad} kms ⁻¹	Separation A.U.	$\Delta V/\sigma$
Gl 48	0.5	G 22 C	-4.9	225400	3.1
		Gl 22 B	-3.4		
Gl 49	-5.0	Gl 51	-7.3	3530	1.5
Gl 140 A	24.0	Gl 140 C	19.1	2310	3.3
G 192-11	2.0	G 192-12	2.8	2965	0.5
Gl 469	-10.2	Gl 471	15.1	52170	17
Wo 9490 A	-29.2	Wo 9490 C	-26.6	3538	1.7
Gl 720 A	-30.4	Gl 720 B	-32.2	2312	1.7
Gl 897 A	-0.8	Gl 898	0.7	6068	1.0

Table 10. M and L/T Dwarf Systems

NN	M Dwarf Name	Sp.	V-I	H α (\AA)	L/T Dwarf Name	Sp. Type	Age(Gyr)	Ref
1021	Gl 229A	M0.5	2.01	-0.5	Gl 229B	T	> 0.32	N95
2368	Gl 570BC	M1.0	2.12	-0.4	Gl 570D	T	> 0.40	B00
...	G 196-3	M2.5	2.34	4	G196-3B	L	< 0.64	R98
3	GJ 1001A	M3.5	2.69	< 1	GJ 1001B	L	> 1.4	G99
2358	Gl 569 A	M2	2.24	1.29	Gl 569Ba/Bb	M8/L0?	< 0.52	M00

Note. — References: N95: Nakajima et al. (1995); R98: Rebolo et al. (1998); B00: Burgasser et al. (2000); G99: Goldman et al. (1999); M00: Martín et al. (2000)

REFERENCES

- Andretta, V. & Giampapa, M.S. 1995, ApJ, 439, 405
- Barnes, S.A. 1997, Ph.D. Thesis, Yale University
- Barnes, S.A., Sofia, S., Prosser, C.F., & Stauffer, J.R. 1999, ApJ, 516, 263
- Barry, D.C. 1988, ApJ, 334,436
- Bessell, M.S. 1990a, A&AS, 83, 357
- Bessell, M.S. 1990b, PASP, 101, 1181
- Burgasser, A.J., et al. 2000, ApJ, 531, L57
- Burrows, A., Marley, M., Hubbard, W.B., Lunine, J.I., Guillot, T., Saumon, D. 1997, ApJ491, 856
- Byrne, P.B. 1993, A&A, 272, 495
- Cram, L.E., & Giampapa, M.S. 1987, ApJ, 323, 316
- Cram, L.E., & Mullan, D.J. 1979, ApJ, 234, 579
- Delfosse, X., Forveille, T., Perrier, C., Mayor, M. 1998, A&A, 331, 581
- Delfosse, X., Forveille, T., Beuzit, J.-L., Udry, S., Mayor, M., Perrier, C. 1999a, A&A, 344, 897
- Delfosse, X., Forveille, T., Mayor, M., Burnet, M., & Perrier, C. 1999b, A&A, 341, L63
- Dinescu, D.I., Demarque, P., Guenther, D.B., & Pinsonneault, M.H. 1995, AJ, 109, 2090
- Doyle, J.G., Houdebine, E.R., Mathioudakis, M., & Panagi, P.M. 1994, A&A, 285, 233
- Giampapa, M.S., Worden S.P. & Linsky, J.L. 1982, ApJ, 258, 740
- Giampapa, M.S., & Liebert, J. 1986, ApJ, 305, 784
- Giampapa, M.S., Radick, R.R., Hall, J.C., & Baliunas, S.L. 2000, American Astronomical Society, SPD meeting #32, #02.120
- Gizis, J.E. 1997, AJ, 113, 806
- Gizis, J.E., & Reid, I.N. 1997, PASP, 109, 849
- Gliese, W., & Jahreiß, H. 1991, Preliminary Version of the Third Catalog of Nearby Stars, ADC/CDS Catalog V/70 (pCNS3)
- Goldman, B., et al. 1999, A&A, 351, L5

- Gray, D.F. 1992, *The Observation and Analysis of Stellar Photospheres*, 2nd ed. (Cambridge University Press, Cambridge)
- Harlow, J.B.B. 1996, *AJ*, 112, 2222
- Hawley, S.L. & Pettersen, B.R. 1991, *ApJ*, 378, 725
- Hawley, S.L., Gizis, J.E., & Reid, I.N. 1996, *AJ*, 112, 2799
- Hawley, S.L., Gizis, J.E., & Reid, I.N. 1997, *ADC/CDS Catalog III/198*.
- Hawley S.L., Reid I.N., Gizis J.E. & Byrne P.B. 1999a, "Chromospheric Activity in Low Mass Stars: Observational Results from Clusters and the Field", in *Solar and Stellar Activity: Similarities and Differences*, ed. C.J. Butler and J.G. Doyle, (ASP Conference Series No. 158), 63.
- Hawley, S.L., Reid, I.N., & Tourtellot, J.G. 1999b, "Properties of M dwarfs in Clusters and the Field", in the La Palma Conference on Very Low Mass Stars and Brown Dwarfs in Stellar Clusters and Associations, ed. R. Rebolo, (Cambridge Univ. Press), in press
- Hawley, S.L., Reid, I.N. & Gizis, J.E. 2000, "Magnetic Activity in Low Mass Stars and Brown Dwarfs", in *From Giant Planets to Cool Stars*, ed. C. Griffith and M. Marley (ASP Conference Series No. 212), 252.
- Henry, T.J., Soderblom, D.R., Donahue, R.A., & Baliunas, S.L. 1996, *AJ*, 111, 439
- Herbig, G. 1956, *PASP*, 68, 531
- Herbst, W. & Miller, J.R. 1989, *AJ*, 97, 1989
- Hernandez, X., Valls-Gabaud, D. & Gilmore, G. 2000, *MNRAS*, 316, 605
- Kirkpatrick, J.D., & McCarthy, D.W. 1994, *AJ*, 107, 333
- Leggett, S.K., Hauschildt, P.H., Allard, F., Geballe, T.R., & Baron, E. 2002, *MNRAS*, in press (astro-ph/0112335)
- Liebert, J., Kirkpatrick, J.D., Reid, I.N., Fisher, M.D. 1999, *ApJ*, 519, 345
- Marcy, G.W., & Benitz, K.J. 1989, *ApJ*, 344, 441
- Marcy, G.W., & Chen, G.H. 1992, *ApJ*, 390, 550
- Martín, E.L., Koresko, C.D., Kulkarni, S.K., Lane, B.F., & Wizinowich, P.L. 2000, *ApJ*, 529, L37
- Mauas, P.J.D. & Falchi, A. 1994, *A&A*, 281, 129
- McCarthy, J.K. 1985, *Proc. SPIE*, 554, 155

Nakajima, T., Oppenheimer, B.R., Kulkarni, S.R., Golimowski, D.A., Matthews, K., & Durrance, S.T. 1995, *Nature*, 378, 463

Perryman, M.A.C., et al. 1997, *A&A*, 323, L49

Perryman, M.A.C., et al. 1998, *A&A*, 331, 81

Pettersen, B.R., Lambert, D.L., Tomkin, J., Sandmann, W.H., Lin, H. 1987, *A&A*, 183, 66

Poveda, A., Herrera, M.A., Allen, C., Cordero, G., Lavalley, C. 1994, *RMxAA*, 28, 43

Rebolo, R., Zapatero Osorio, M.R., Madruga, S., Bejar, V.J.S., Arribas, S., & Licandro, J. 1998, *Science*, 282, 1309

Reid, I.N., Hawley, S.L., & Gizis, J.E. 1995, *AJ*, 110, 1838

Reid, I.N., Hawley, S.L. & Mateo, M. 1995, *MNRAS*, 272, 828

Reid, I.N., Kirkpatrick, J.D., Liebert, J., Burrows, A., Gizis, J.E., Burgasser, A., Dahn, C.C., Monet, D., Cutri, R., Beichman, C.A., & Skrutskie, M 1999, *ApJ*, 521, 613

Rocha-Pinto, H.J., Scalo, J., Maciel, W.J., Flynn, C. 2000, *A&A*, 358, 869

Saar, S.H., Huovelin, J., Osten, R.A., Shcherbakov, A.G. 1997, *A&A*, 326, 741

Skumanich, A. 1972, *ApJ*, 172, 565

Soderblom, D.R., Duncan, D.K., & Johnson, D.R.H. 1991, *ApJ*, 375, 722

Stauffer, J.R., & Hartmann, L.W. 1986, *ApJS*, 61, 531

Stauffer, J.R., et al. 1994, *AJ*, 108, 160

Stauffer, J.R., Schultz, G., Kirkpatrick, J.D. 1998, *ApJ*, 499, L199

Strassmeier, K.G., Hall, D.S., Fekel, F.C., Scheck, M. 1993, *A&AS*, 100, 173

Terndrup, D.M., et al. 2000, *ApJ*, 119, 1303

Tokovinin, A. 1988, *Astrophysics*, 28, 173

Tokovinin, A. 1992, *A&A*, 256, 121

Ugoren, A.R., & Caruso, J.R. 1988, *AJ*, 96, 719

Ugoren, A.R., & Harlow, J.J.B. 1996, *PASP*, 108, 64

Vaughan, A.H., & Preston, G.W. 1980, *PASP*, 92, 385

Wielen, R. 1974, *Highlights of Astronomy*, ed. G. Contopoulos, (Reidel Publ. Co., Dordrecht), 3, 395

Wielen, R. 1977, *A&A*, 60, 263

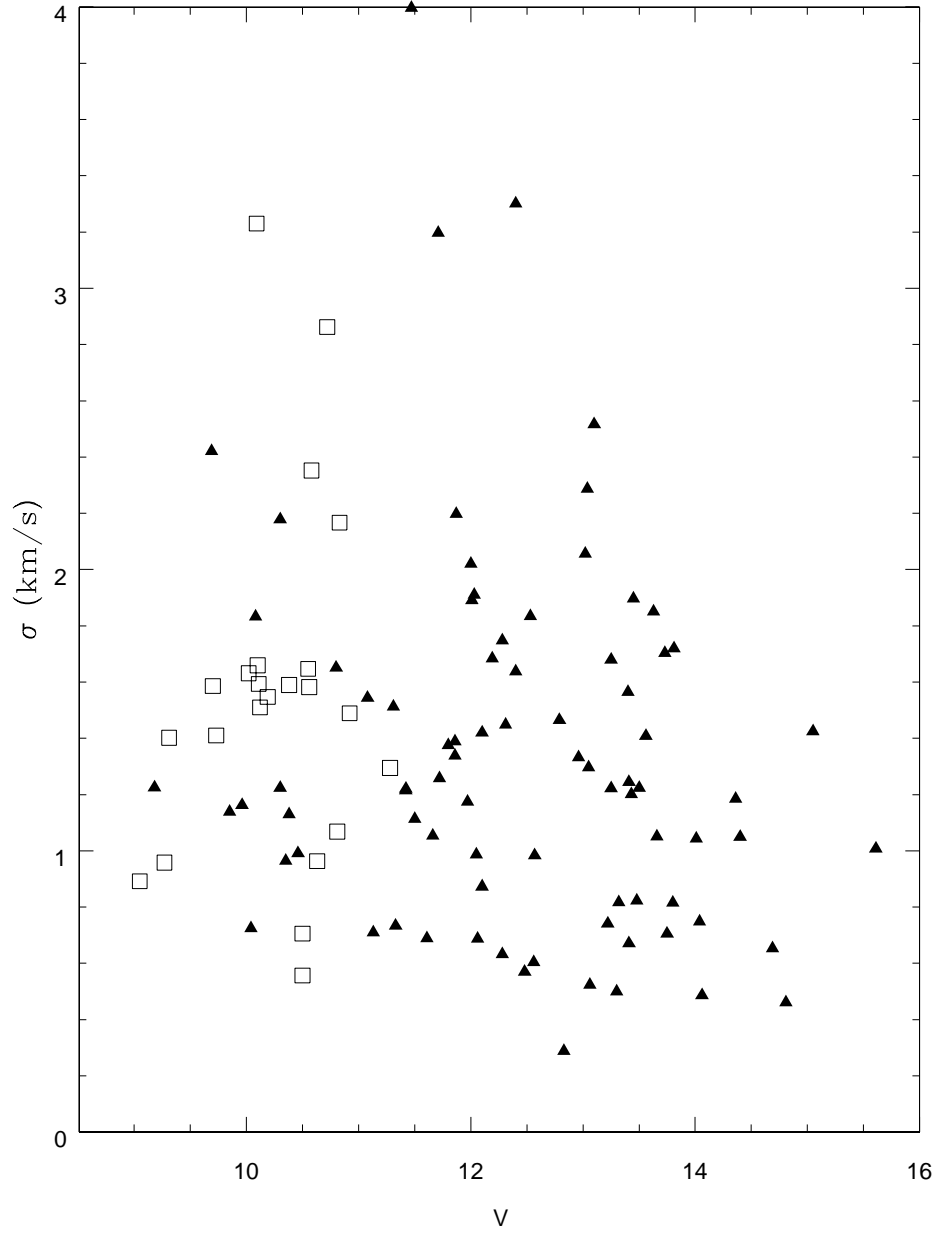
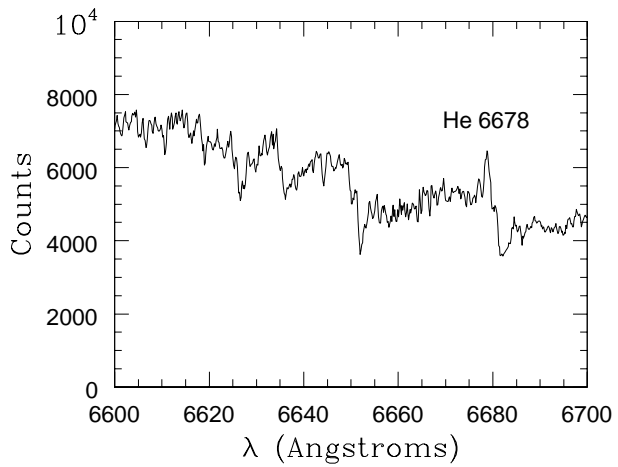
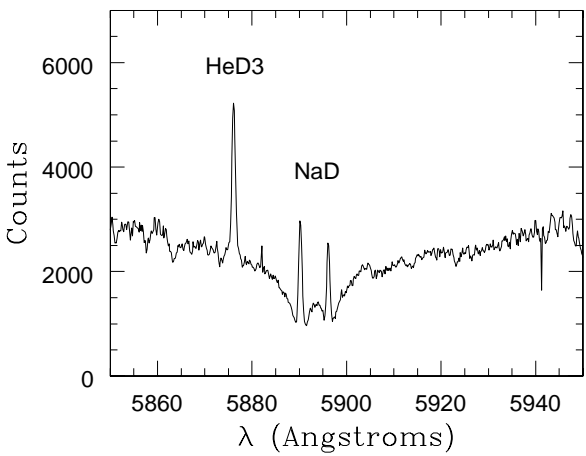
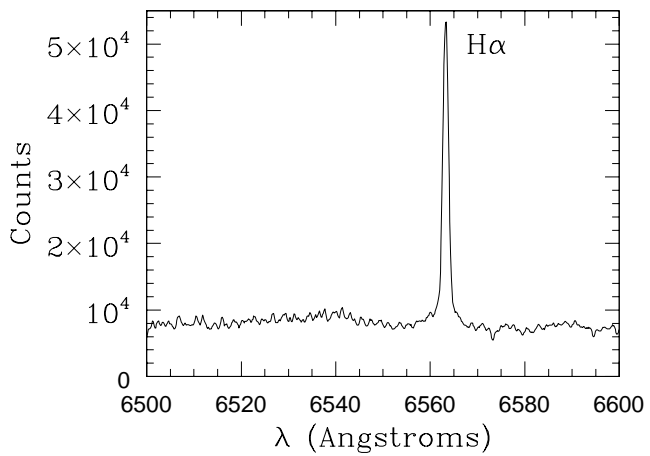
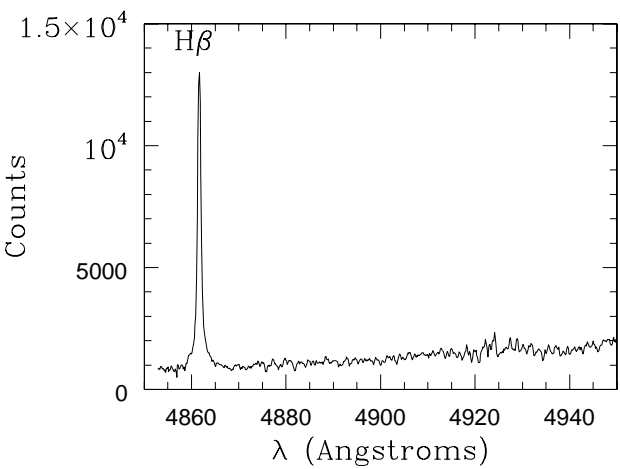


Fig. 1.— The observed σ of the measured radial velocities for stars with multiple observations. Early M dwarfs ($\text{TiO5} > 0.5$) are shown as open squares and mid M dwarfs ($\text{TiO5} \leq 0.5$) are shown as solid triangles. There is no trend with the apparent magnitude of the star.

Fig. 2.— Spectra of G1 285 (NN 1219) showing the $H\alpha$, $H\beta$, He D3, NaD, and He 6678 emission lines.



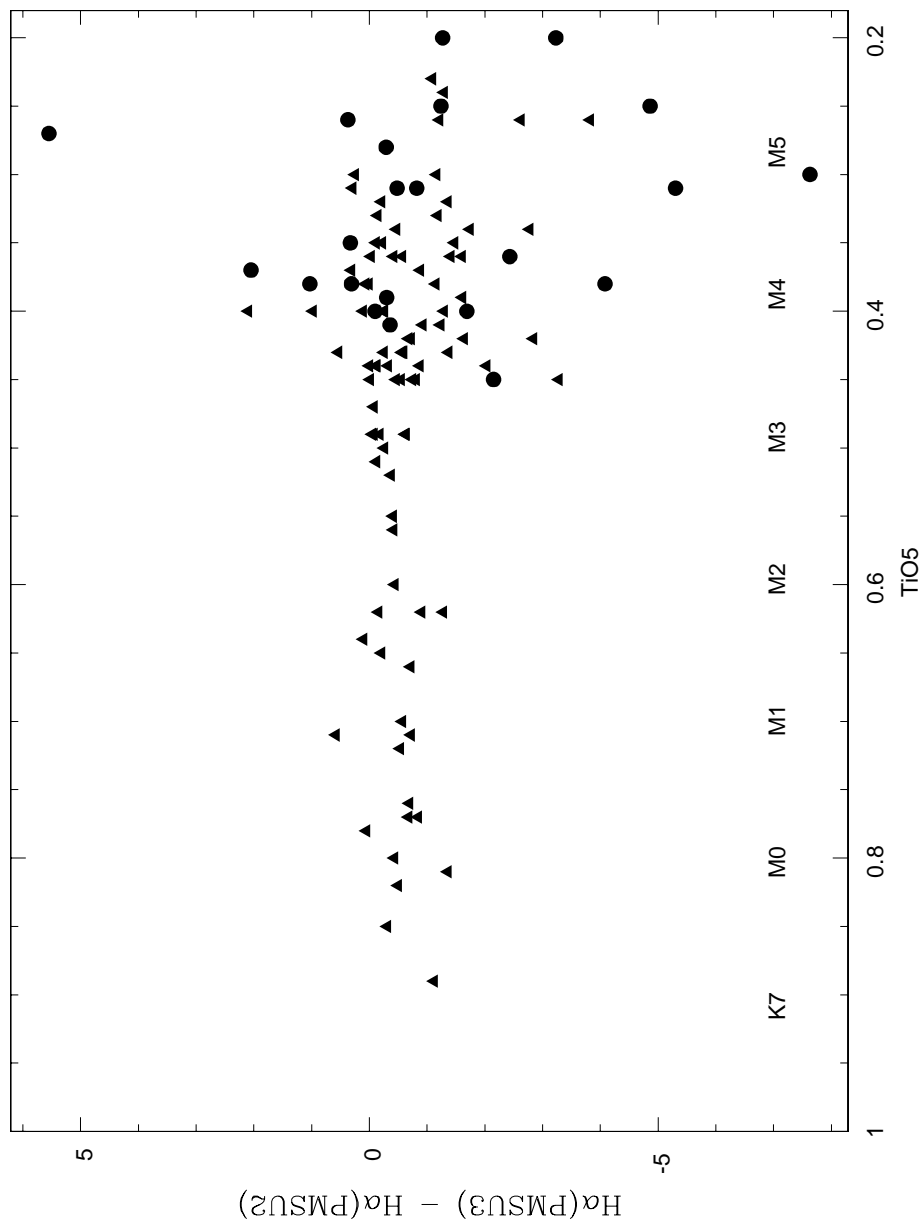


Fig. 3.— A comparison between the $H\alpha$ emission line strength measured at high resolution in this paper (PMSU3) and in our previous, low-resolution work (Paper II). Points where the PMSU3 measurements exceed 5\AA are shown as circles; weaker dMe stars are shown as triangles. A systematic difference of $\sim 0.5\text{\AA}$ is evident, which we attribute to differences in placing the pseudo-continuum. The increased scatter amongst later-type stars is probably due to variability (see Section 4.1 and Figure 7).

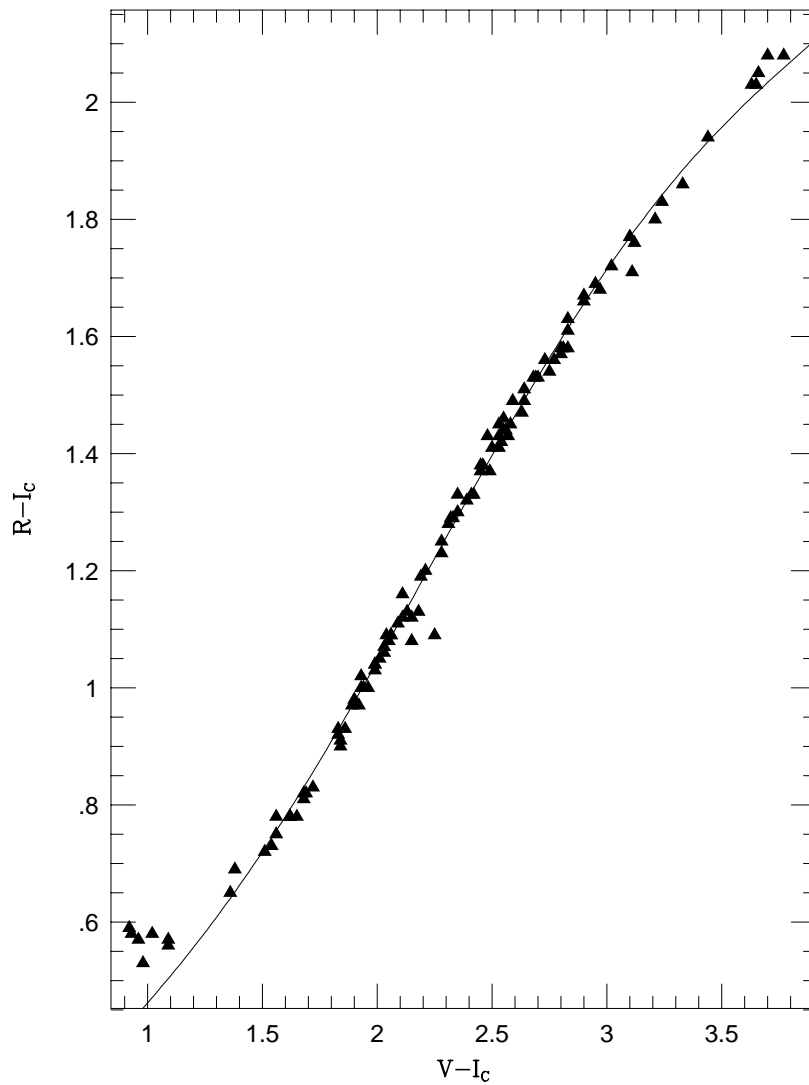


Fig. 4.— Synthetic colors for M dwarfs using our low-resolution spectra and the filter curves of Bessell (1990b). The solid curve is the Bessell (1990a) polynomial fit to actual M dwarf photometry. We conclude that our spectra are correctly flux calibrated.

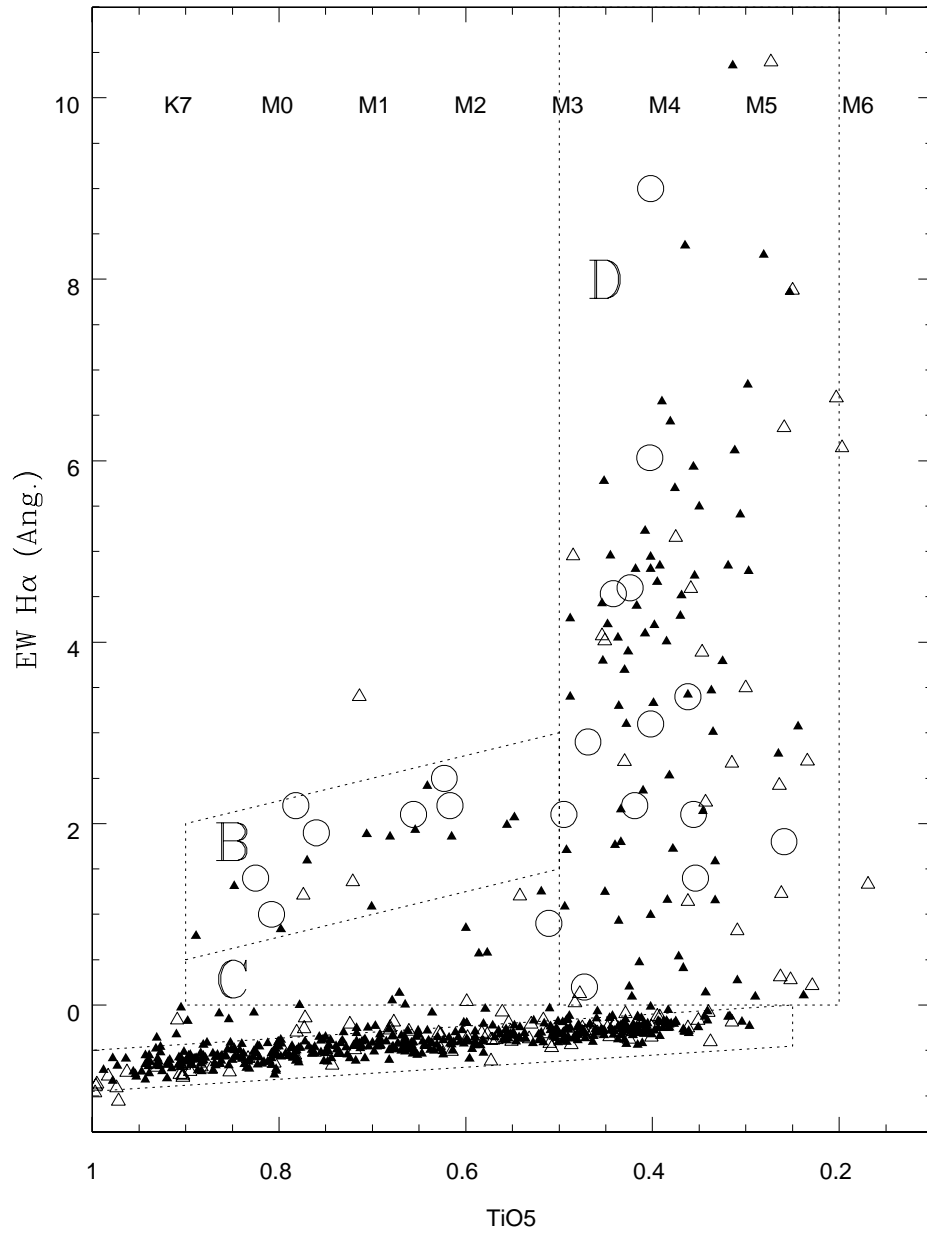


Fig. 5.— The H α equivalent width as a function of TiO5 (spectral type). Stars in the VC sample are shown as solid triangles, stars with emission due to a close companion are shown as open circles, and other non-VC stars are shown as open triangles.

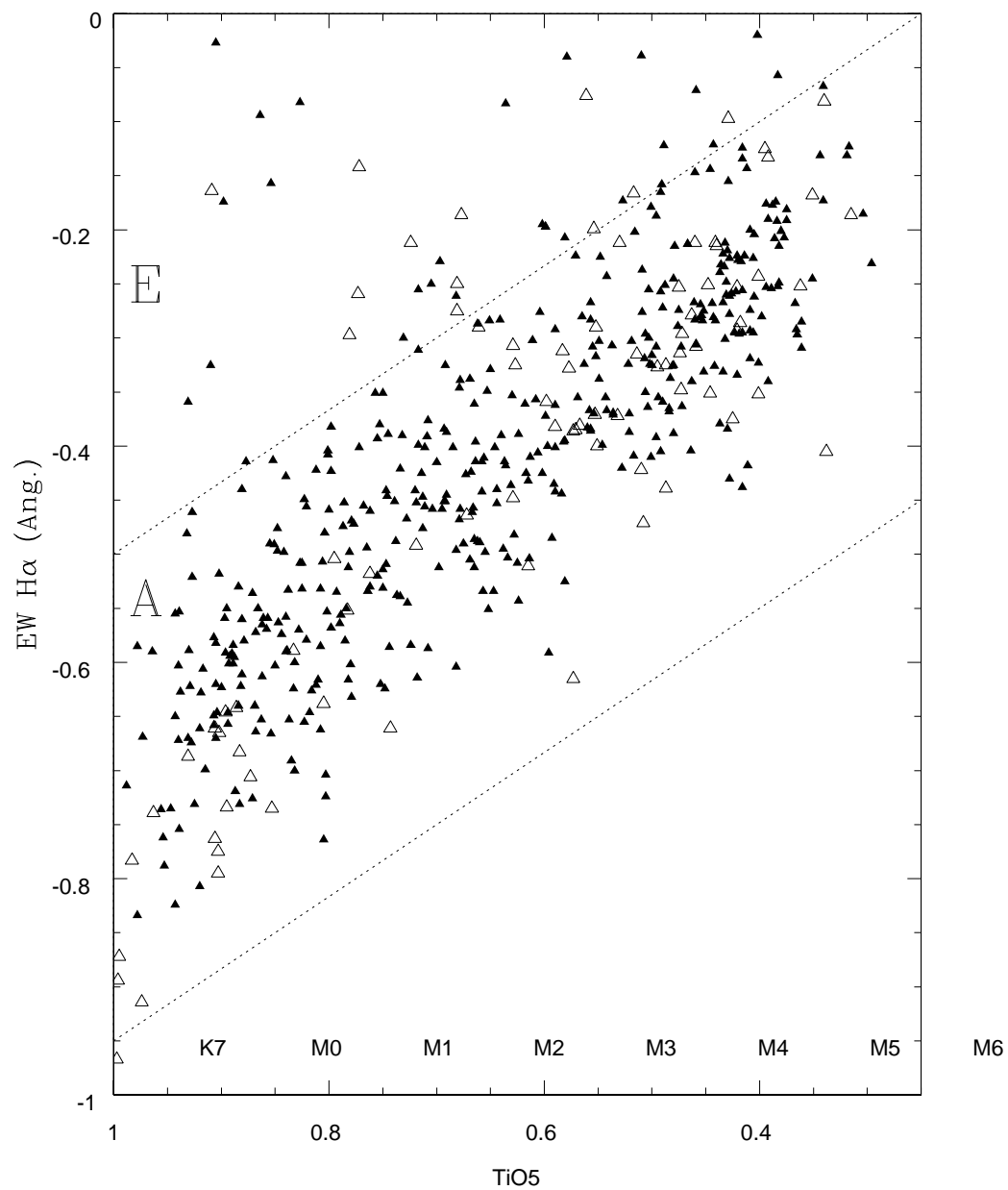


Fig. 6.— H α absorption as a function of TiO5 (spectral type). Symbols are as in Figure 5.

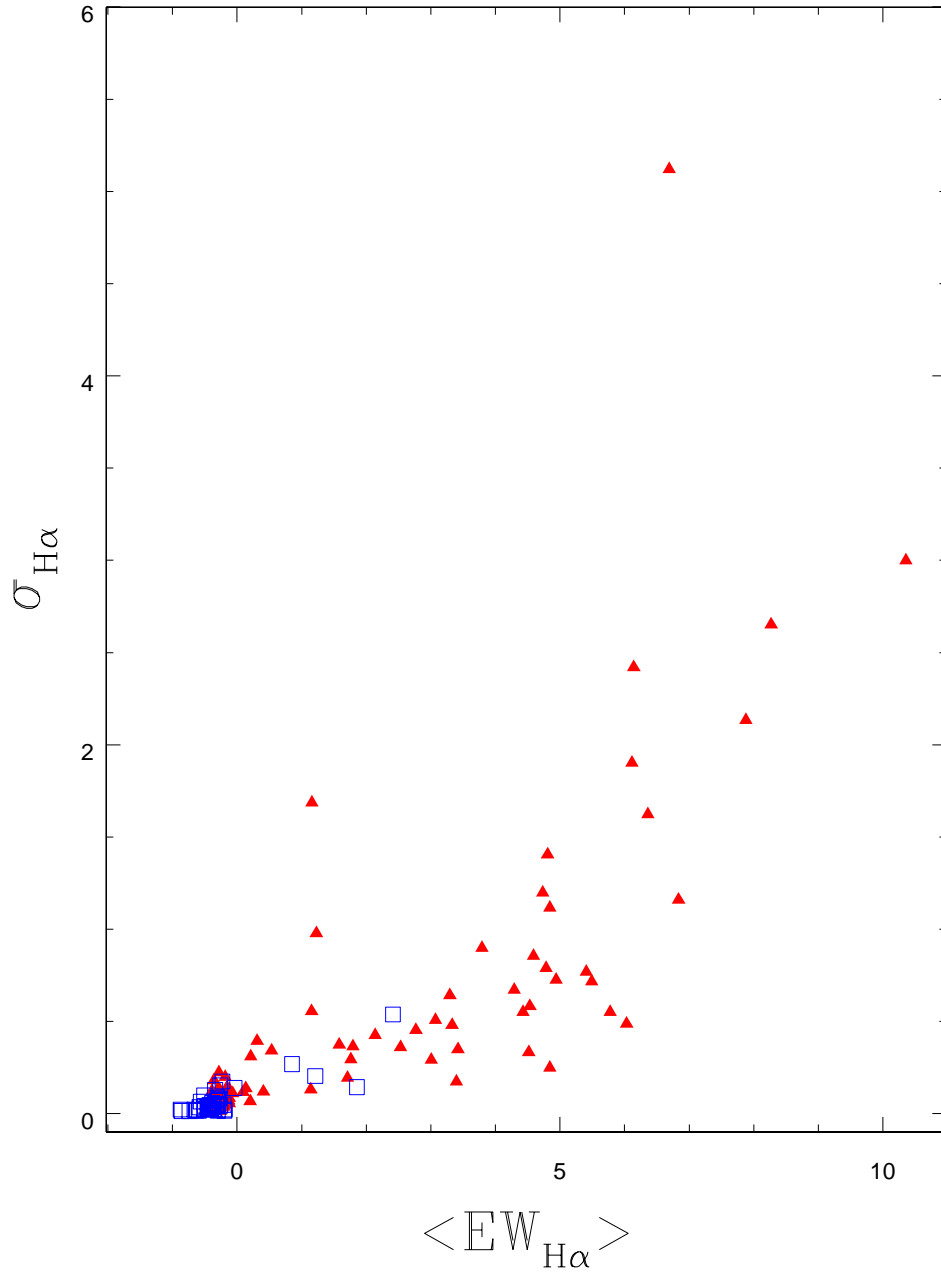


Fig. 7.— The observed standard deviation ($\sigma_{H\alpha}$) in the H α equivalent width as a function of $EW_{H\alpha}$ for dMe stars with at least 4 measurements. Stars with $EW_{H\alpha} > 5\text{\AA}$ exhibit significantly larger scatter.

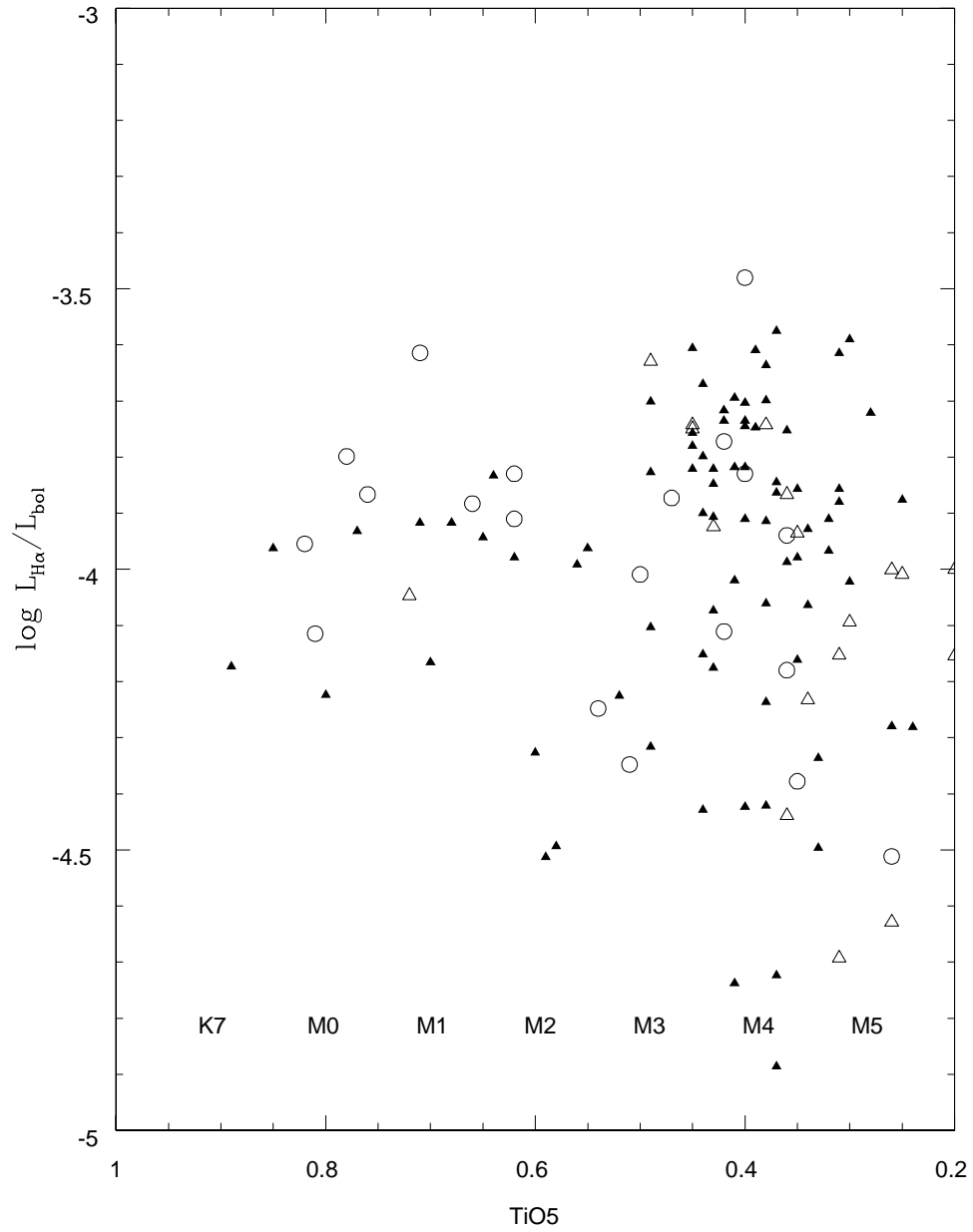


Fig. 8.— The chromospheric activity level expressed as the ratio of the H α luminosity to the bolometric luminosity. Symbols are as in Figure 5.

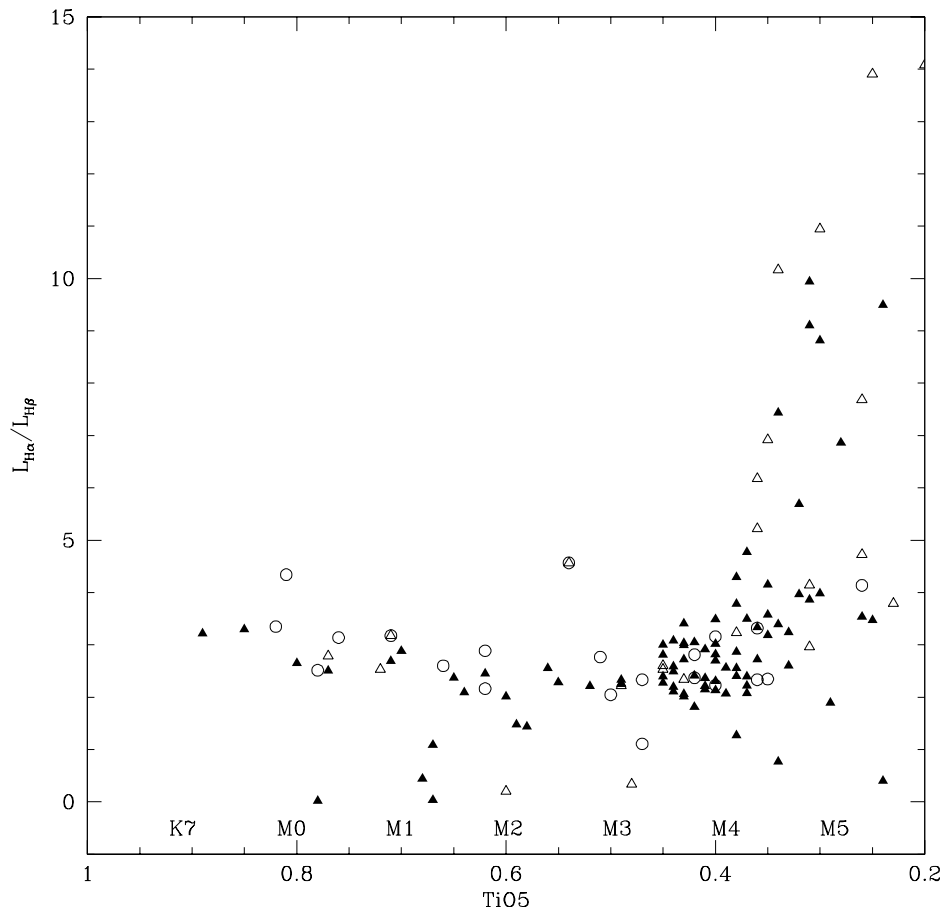


Fig. 9.— The ratio of the H α to H β emission. Symbols are as in Figure 5.

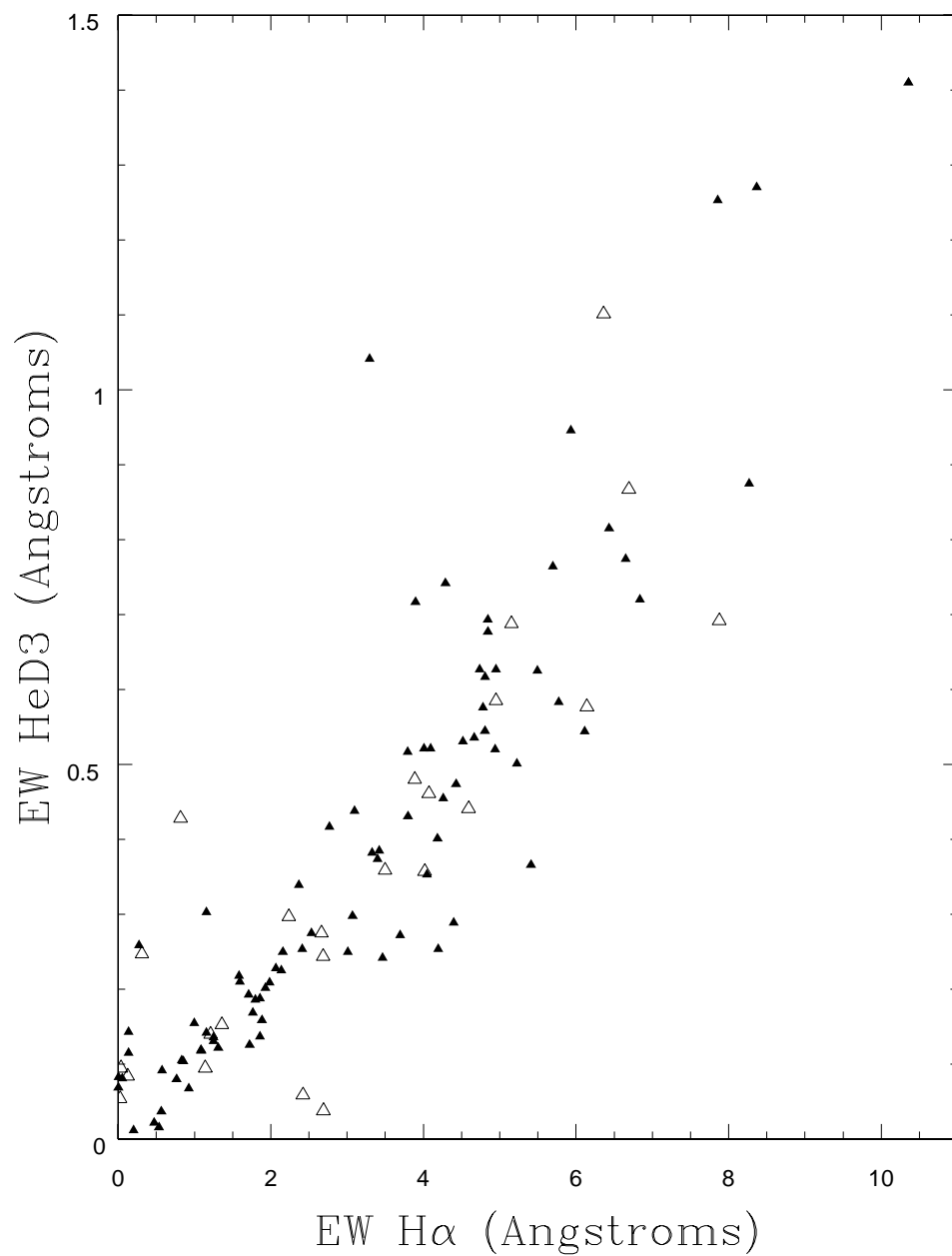


Fig. 10.— He D3 emission as a function of H α emission. Symbols are as in Figure 5.

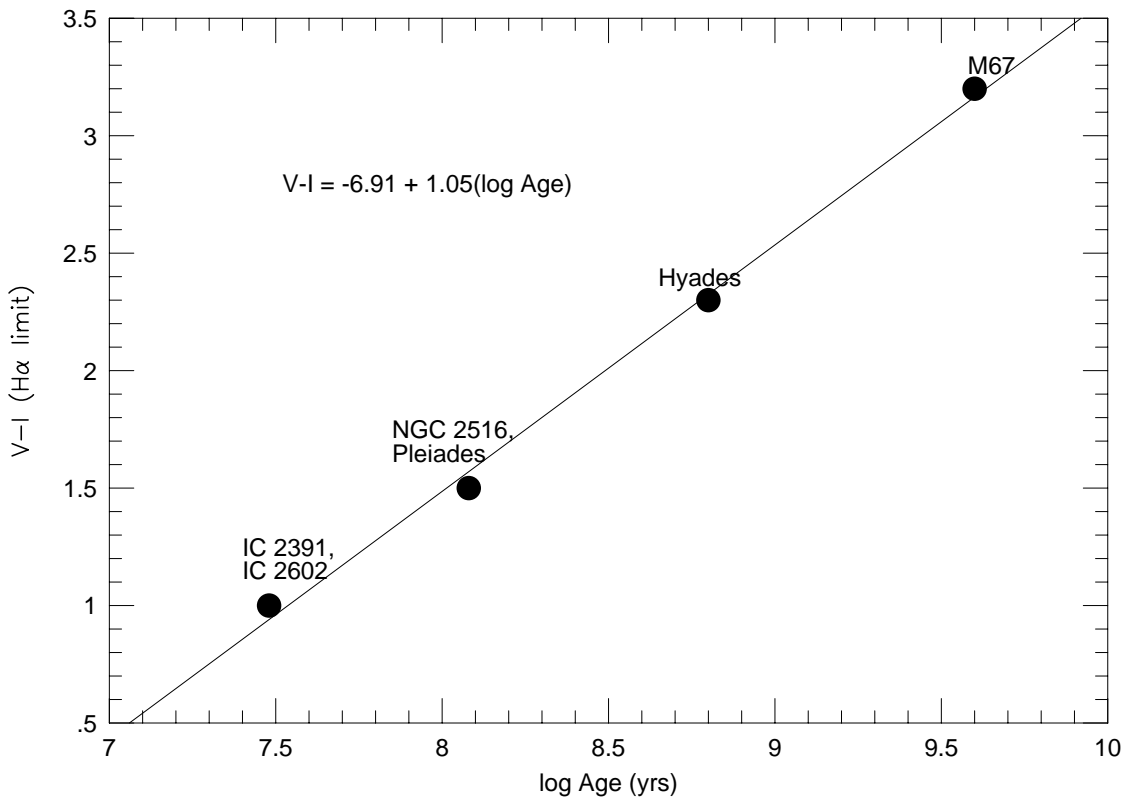


Fig. 11.— Calibration of $V-I_C$ at the $H\alpha$ limit as a function of cluster age, from Hawley et al. (1999). See text for discussion.

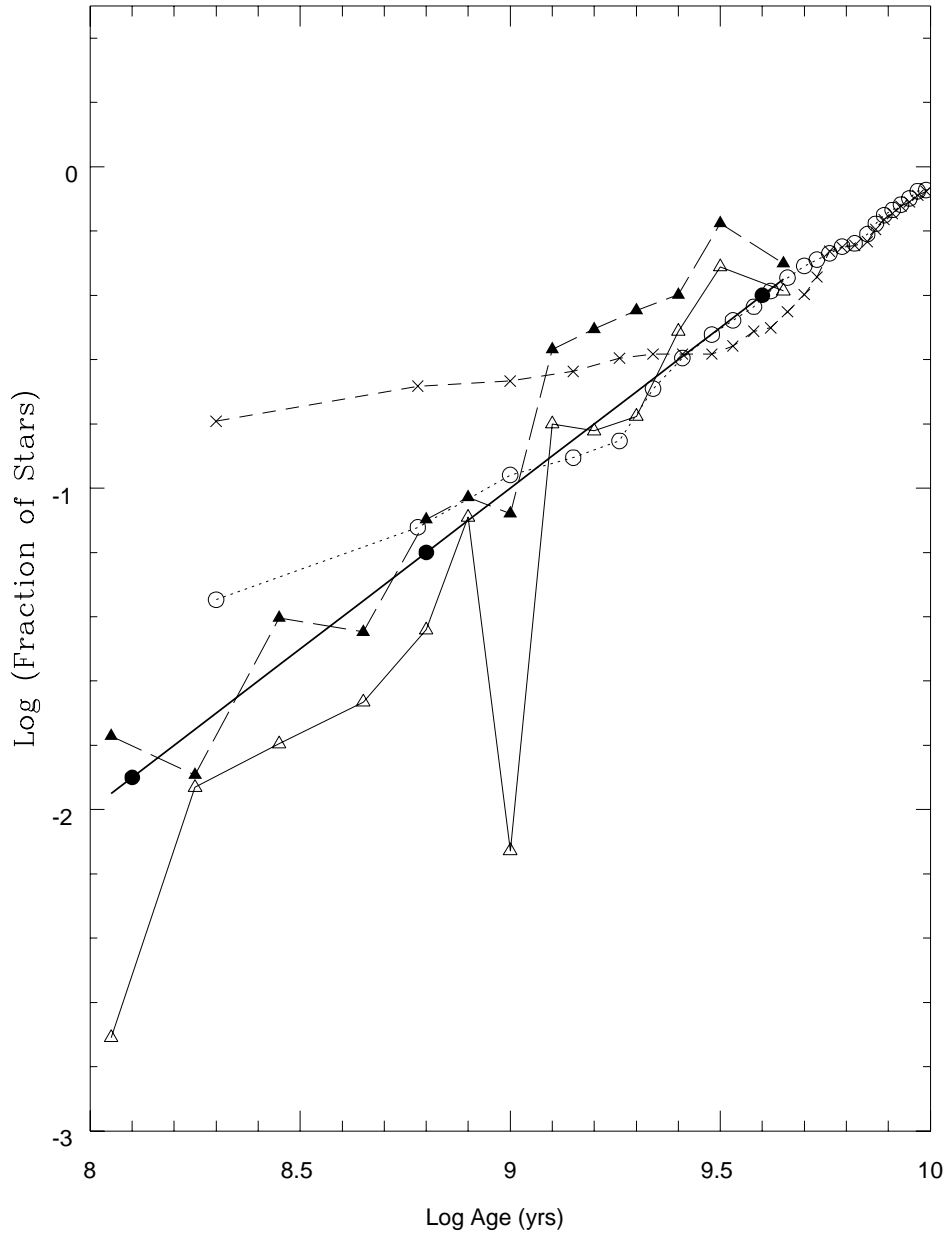


Fig. 12.— The star formation history of the Solar Neighbourhood (assuming a Galactic disk age of 10 Gyr). Our M dwarf results are shown for the W-weighted (solid line, open triangles) and unweighted (long-dashed line, filled triangles) analyses. The thick solid line, slope unity, illustrates the expected distribution for a constant star formation rate. The closed circles on this line mark the ages of the calibrating open clusters. Barry's (1988) G dwarf results (short-dashed line, crosses) are also shown together with the results from the Rocha-Pinto et al. (2000) G dwarf analysis (dotted line, open circles). The M dwarf results do not show the excess of young stars suggested by the former analysis and also fail to match the details of the latter.